WADC TR 52-307, Part I

FATIGUE PROPERTIES OF ALUMINUM ALLOYS AT VARIOUS DIRECT STRESS RATIOS

Part I - Rolled Alloys

B. J. LAZAN
AND A. A. BLATHERWICK
UNIVERSITY OF MINNESOTA

DECEMBER 1952

Materials Laboratory
Contract No. AF 33(038)-20840

RDO No. R 614 - 16

Wright Air Development Center
Air Research and Development Command
United States Air Force
Wright-Patterson Air Force Base, Ohio

FOREWORD

This report was prepared by the University of Minnesota under Contract No. AF 33(038)-20840 with the Wright Air Development Center, Wright-Patterson Air Force Base, Ohio, identified by the Expenditure Order No. R 614-16. It was administered under the direction of the Materials Laboratory, Wright Air Development Center, with Mr. W. J. Trapp acting as project engineer.

ABSTRACT

Newly developed equipment for axial stress fatigue testing in the tension-compression range is described. Fatigue data on 14S-T6, 24S-T4, and 75S-T6 aluminum alloys are presented as S - N curves and stress range diagrams to illustrate and analyze the effects of: (a) stress ratios in the range from static tension to reversed axial stress, (b) stress magnitude which causes failure in the range from 10^3 to 10^7 cycles, and (c) severity of circumferential notches having four different theoretical stress concentration factors in the range between 1.0 and 3.4. The extreme flatness of the stress range diagrams for severely notched specimens at long life is discussed in terms of the large reduction in mean load carrying capacity resulting from the addition of relatively small alternating stress. Unitless stress range diagrams are presented which indicate how material, life, and specimen type affect the combinations of alternating and mean stress which cause failure in a specified number of cycles. Data on the reduction in fatigue strength caused by notches are diagrammed to clarify the significance of mean stress, alternating stress, stress ratio, and cycles to failure as factors in fatigue notch sensitivity. The fatigue properties determined in this program are compared with prior work. The low fatigue strengths observed for 75S-T6 are briefly discussed.

PUBLICATION REVIEW

Manuscript copy of this report has been reviewed and found satisfactory for publication.

FOR THE COMMANDING GENERAL:

L. A. WHITMORE
for M. E. SORTE
Colonel, USAF
Chief, Materials Laboratory
Directorate of Research

TABLE OF CONTENTS

FATIGUE PROPERTIES OF UNNOTCHED AND NOTCHED ALUMINUM ALLOYS AT VARIOUS DIRECT STRESS RATIOS

I. INTRODUCTION

The inadequacy of fatigue data for structural aluminum alloys under various stress ranges has necessitated the use of rather broad assumptions in the design of aircraft structures. The strength data procured in this program at various stress ratios from static tension to reversed stress fatigue should help to alleviate this situation.

The strength potential of aircraft materials are frequently not fully realized because of stress concentration effects. The notches generally present in aircraft structures necessitate, in the absence of adequate data and a basic understanding, a rather cautious approach and the inefficiency of overdesign is frequently the result. Underdesign, even after large factors of safety have been applied, is also a serious threat. Notch sensitivity data procured in this work extend the range of stress ratios and fatigue lives covered in previous studies and provide improved prospective for structural designers.

II. PRIOR WORK

Much of the prior work on fatigue properties of notched and unnotched aluminum alloys has been under reversed bending conditions (1)* (2) (3) (4) (5), in which the alternating to mean stress ratio A** is infinity. The trend during recent years has been towards increased emphasis on axial load fatigue tests and consideration of other stress ratios. Although there have been several investigations on the unnotched and notched fatigue strength of aluminum alloys (6) (2) (3) it was not until very recently (7) (8) (9) that a reasonably wide range of stress ratios and notch effects were covered.

---

*Numbers in parenthesis refer to references in the bibliography.
**See Appendix A for definition of terms and symbols.

III. TEST PROGRAM

All tests were conducted at room temperature under axial (tensile or compressive) stress. Stress magnitudes which caused failure in from 10^3 to **2** x 10^7 cycles and in some cases to 10^8 cycles, were studied.

In order to cover as uniformly as possible the stress ratios ranging from static tension to reversed stress fatigue, selected steps of alternating to mean stress ratios (10) were used rather than selected steps of mean stress. The alternating stress to static mean stress ratios A originally selected for this work were A = O (static tension), 0.37, 0.89, 2.16, and ∞ (reversed stress). As the project progressed, it was observed that in many cases small magnitude of alternating stress seriously decreased the allowable mean stress, and therefore in such cases additional data were procured at stress ratios A of 0.15 and 0.08.

One single filleted unnotched type and three different notched types of specimens, as described in Section V, were used in this program to provide a range of stress concentration effects of value in service analysis.

IV. TEST MATERIALS

4.1 Specifications for Test Materials

The three aluminum alloys used in this program were: 14S-T6 (spec. QQ-A-266), 24S-T4 (spec. QQ-A-268), and 75S-T6 (spec. QQ-A-282) in rolled bar stock form. The results of tests on rolled stock only are given in this part. Data on extruded alloys are to be presented in Part II of this report to be issued in the near future.

4.2 Processing

Each of the three test materials, furnished by the Aluminum Company of America in the final heat-treated form, was received as rolled bars 20 feet long by 1 1/8" in diameter.

All bars of each material were fabricated from one ingot, each ingot was made into several blooms, and the identification of the blooms from which bars were rolled was recorded. Each bar was stamped at the Alcoa mill and each specimen was given a number to indicate its location in the original rolled bar. This attention to location details was undertaken so that if serious scatter in data were observed, the inhomogeneity of the material and its association with location could be evaluated. This precaution was apparently unnecessary since tests to date indicate the material to be reasonably uniform.

Alcoa's fabrication procedures from bloom to final rod are indicated below for each material.

14S-T6: Reheat 6" bloom, hot roll to 1.812", anneal, draw to 1.25", partially anneal, draw to 1.13", solution heat treat (940°F), roll straighten to 1.125", and artificially age 18 hours at 320°F.

24S-T4: Reheat 6" x 6" bloom, hot roll to 1.812", anneal, draw to 1.375", partially anneal, draw to 1.13", solution heat treat (915°F), and roll straighten to 1.125".

75S-T6: Reheat 6" x 6" bloom, hot roll to 1.452", anneal, draw to to 1.129", solution heat treat (915°F), roll straighten to 1.125", and artificially age 24 hours at 250°F.

4.3 Chemical Analysis

The chemical composition, as furnished by Alcoa for samples taken from one rod from each bloom, is shown in Table I.

4.4 Metallographic Structure

The metallographic structure of the three tests materials are shown in Fig. 1. Although the structure of the three test materials appears to be reasonably normal, rather large insoluble constituents (see Fig. 1h), which are probably chromium bearing segregation, were found in the 75S-T6. Since the fatigue properties of this batch of 75S-T6 were lower than average, the Materials Laboratory of Wright Air Development Center and the Research Laboratories of the Aluminum Company of America both examined the material and reported (11) (18) the presence of chromium-bearing constitutents

larger than usually found in such rod. However, tests conducted by the Douglas Aircraft Company (19) indicate that chromium-bearing segregation of the type observed does not necessarily cause low fatigue strength.

V. TEST SPECIMENS

5.1 Design of Specimens

The four types of specimens used to obtain a range of stress concentration, illustrated in Fig. 2, are described below. All specimens tested have the same diameter (0.400") at the test section.

Type V Unnotched Specimen has a single fillet which is large enough to justify the assumption of zero concentration of stress (theoretical stress concentration factor K_t is one). In some of the early tests on this specimen, failures were experienced in the thread instead of in the test section. This difficulty was almost completely corrected by using a larger than standard radius at the root of the thread (the "Unified" thread is now used) and in some cases the thread root was also rolled. Also a stress relieving groove of 3/16" radius was machined near the inside edge of the thread in some cases.

Type W Notched Specimen has a 0.400" diameter test section at the root of a semicircular circumferential notch of radius 0.100". The theoretical stress concentration factor, as calculated from Neuber's charts (12), is 1.6.

Type AB Notched Specimen has a circumferential 60° V notch with a 0.032" root radius. The theoretical stress concentration factor for this specimen is 2.4.

Type X Notched Specimen has a 60° V notch with a 0.010 inch root radius. The theoretical stress concentration factor for this specimen is 3.4.

5.2 Preparation of Test Specimens

All fatigue specimens were prepared completely by the John Stulen Company of Gibsonia, Pennsylvania (except for the polishing of type W and

AB specimens, which was done at Minnesota). Since machining and polishing techniques may greatly affect fatigue properties, the procedures used in specimen preparation are described below in detail.

5.2.1. Unnotched Specimens, Type V. The specimen was rough machined, threaded and lathe turned with a 60° tool bit having a 1/32" radius at the nose. Initial cuts of 0.050" were made at a speed of 1100 rpm and feed of .010 per revolution until the diameter was 0.050" larger than the final size. The specimens were then finish machined to .005" over final size in three cuts having successive depths of .010", .005", and .002", and feed of .006" per revolution. The lathe tool was always kept sharp during final cuts, and sulphurized cutting oil was used on these finishing cuts to produce freer cutting action.

During polishing the specimen was revolved at 600 rpm. An arm containing a 150 foot roll of 1/2" wide cloth abrasive tape was passed around a rubber disc in contact with the specimen. This arm was reciprocated at 180 cycles per minute in a direction parallel to the axis of the specimen. The abrasive tape passed around this rubber disc and over the specimen at a rate of 6" per minute. A constant pressure of 3 lbs was maintained between the tape and the specimen. The area of contact between the tape and the specimen was about 1/2" x 1/4", or 1/8 square inch.

The first polishing operation was done with 180 mesh tape of aluminum oxide abrasive grain. Stock was removed at a rate of .004" per minute. The tape was saturated with sperm oil to free the abrasive grain of cuttings and give a faster cutting action. With the specimen revolving at 600 rpm and the tape reciprocating longitudinally across the specimen, a cross hatching cutting action was produced at the center of the specimen. This operation was continued until the specimen was within 0.0005" of final size. The second polishing operation was similar to the first except that a 400 mesh aluminum oxide abrasive tape was used for 30 seconds. This was followed by 20 second polish with the specimen turning at 3 rpm to produce a longitudinal finish. The final polish was performed in the same manner with 900 mesh aluminum oxide abrasive grain tape. The surface finish thus produced was better than 10 micro-inches.

5.2.2 Machining and Grinding of Notched Specimens. The notch contour was cut in the specimens in two successive operations, rough machining to within 0.016" in diameter of final size, followed by finish grinding. Maching was done with sharp tools, cutting oil, and slow feed. The final grinding was done with a Carborundum Company wheel No. V80-V2-BT, which is 6" diameter and 1/4" wide. During final grinding the specimen was revolved at 900 rpm and metal was removed at a rate of .001" per 67 revolutions. A 5% sulphur base oil cut with 1 part kerosene and 3 oil was used as a coolant. After grinding there was no visible loading or glazing of the wheel at 40X magnification.

The type X notch received no further preparation after final grinding, whereas types W and AB notches were polished as indicated below.

5.2.3 Polishing of Notched Specimens Types W and AB. In deciding whether or not to polish the notches after final grinding, the advantages of a smoother and perhaps more stress-free surface produced by polishing must be weighed against the possibility that polishing may distort the notch form. Since sharp notches, of the X type, are difficult to control dimensionally during polishing, it was decided to test the type X specimens as ground. However, the type W and AB specimens could be polished without affecting notch form accuracy and therefore preliminary tests were conducted on both polished and unpolished types W and AB specimens. It was found that the polished specimens displayed somewhat smaller scatter than the unpolished ones and gave fatigue strength 5 to 10% higher. Therefore, all types W and AB specimens used for this work were polished.

The polishing set-up is shown in Fig. 3. The specimen is rotated at approximately 30 rpm. A cylindrical copper rod P having a diameter slightly less than that of the notch was mounted in a chuck at right angles to the axis of the specimen and rotated by motor spindle M at about 600 rpm. A polishing compound was used consisting of one part of 600 grit Alumina in 5 parts of 10W lubricating oil and 2 parts kerosene. The pressure exerted by the polishing rod on the specimen was adjusted by positioning sliding weight W on arm A so as to produce the desired moment about hinge H which supports the motor spindle assembly M. A force of 0.5 pounds between the

lap and specimen was used in all cases. The specimen was polished until all circumferential scratches were removed (usually from 4 to 6 minutes) with about 0.0005" reduction in diameter. This operation produces a surface finish of about 10 micro-inches, as measured by Brush surface analyser and Fax film procedures.

The final dimensions of all notched and unnotched specimens were accurately determined in an optical comparator to an accuracy of 0.0002".

VI. TESTING EQUIPMENT AND PROCEDURES

6.1 Fatigue-testing Machines

Two different types of fatigue-testing machines were used to cover the range of axial stress required. The axial stress fatigue machine L1 was used for low and medium alternating force tests, whereas a Sonntag fatigue machine with an amplifying fixture was used for high alternating force tests. Overlapping tests were made so that data from the two machines could be compared directly and no significant difference in fatigue properties was found.

6.1.1 Axial Stress Fatigue Machine, Model L1. Machines of this type, see Fig. 4, were originally developed for dynamic creep and rupture tests at elevated temperatures (10). Alternating force up to $\pm$ 5000 pounds is produced by a 3600 rpm centrifugal force type of mechanical oscillator 0 and preload is applied by means of flexible calibrated springs P which are kept at a constant force during the test by an automatic follow-up system. The test specimen S is securely held between grips K and L which are described in Section 6.2.

In some of the low stress ratio tests, the preload capacity was found to be adequate and the preload amplifying fixture shown in Fig. 5 was used. In this fixture the force in the preload compression spring P, adjusted to the desired value with the aid of vernier scale V, is transmitted through lever A to the lower grip K. The universal joint type of fulcrum is located so as to produce a four-fold amplification in the 1000 pound force capacity of spring P. Provisions are included in this preload amplifying fixture to

manually maintain constant spring force, or constant preload, even though the creep in the test specimen may be large.

6.1.2 Sonntag Fatigue Machine with Amplifying Fixture. The capacity of the L1 machine described above, was not adequate for several of the short-life, high stress ratios fatigue tests. Therefore, a special eight-to-one amplifying fixture was constructed for use with the standard Sonntag SF-1U fatigue machine (13) or any other similar machine. In this device, shown in Fig. 6, the force produced by the fatigue machine is transmitted from its oscillating head K through flex-plate B to amplifying arm A. The arm is supported by flex-plates F and others not visible so as to increase the fatigue machine force by a factor of eight and transmit this force to vibrating cage C. Additional flex-plates, not visible in the photograph, restrict the motion of cage C to a vertical direction only so as to avoid bending stress. The force is transmitted directly from cage C to test specimen S gripped in the fixture as shown. The capacity of this machine is 8000 lbs. preload and $\pm$ 8000 lbs. alternating force. Although this machine operates at 1800 rpm as compared to the 3600 rpm of the L1 machines, this difference in fatigue stress frequency is not considered significant.

6.2 Grips

The production and maintenance of a uniform stress distribution in direct stress fatigue specimens constitute a most important task. Very small errors in alignment in the specimen-grip assembly may frequently result in large extraneous bending stress, which may seriously reduce the observed fatigue strengths. As a result of these observations, particular emphasis was placed on procuring and maintaining uniform stress distribution in the specimen during: (a) clamping of specimen-grip assembly in fatigue machine, (b) application of preload, and (c) application of alternating force.

Stress distribution in specimens held in commercially manufactured grips was not satisfactory, so new types of grips were developed. Fig. 7 shows the assembled specimen-grip combination. In order to align the grips, the specimen S, nuts J, plate H, cap K, and screws A are assembled

as shown and placed between centers. Screws A are then preferentially tightened until the ground outer faces of H and K are perpendicular to the axis of the specimen. The specimen assembly so aligned is then placed in the machine and the bolts securing cap K to cage B are tightened. The three positioning screws D, preloaded with springs to avoid backlash difficulties, are then set with the aid of electrical contacts so that the plane of their lower ends is parallel to plate H. Bolts C are then tightened uniformly (using a torque wrench) and plate H is securely locked between ring R and screws D.

Calibration tests briefly described below indicate that this method of gripping effectively eliminated significant bending stress during both the specimen gripping operation and the application of the static and alternating loads.

6.3 Calibration of Machines and Grips

A thorough calibration study of the average stress and stress distribution in the test specimen was undertaken at the outset of this testing program. Since these calibration tests have been described in detail in reference (14), details shall not be given in this report.

Dynamic calibration of the forces applied to the specimen of one machine was accomplished in three independent ways: (a) direct measurement of strain using SR-4 strain gages cemented to the specimen, (b) measurement of force on a proving ring inserted in place of the specimen, and (c) calculation of force produced by the rotating eccentric. After taking into account the inertial forces of the vibrating parts these three methods checked each other within 1-1/2%. After this initial calibration, subsequent calibrations were made by the strain gage and theoretical methods only.

Bending stresses were measured with SR-4 gages cemented 120° apart around the periphery of the specimen. With the gripping procedure described in Section 6.2, the bending stress was generally less than 3%.

6.4 Test Procedure at High Mean Stress

During fatigue tests at high mean stress (in which the crest stress exceeds the yield strength of the material) the creep in the specimen was

found to be large in some cases. This creep may significantly reduce the preload imposed by the springs before the follow-up system could respond adequately. Since these tests were generally of short duration, and a reduced preload could not be tolerated for even a short period, some of the early tests were in error. In all the tests reported herein, efforts were made to impose full stress conditions as soon as possible after the start of the test, and the stress-relaxation through creep is not considered significant.

VII. RESULTS AND DISCUSSION

7.1 Static Tensile and Hardness Properties

In order to evaluate the uniformity of the three materials and also to determine how closely their properties compare with accepted values, a series of tensile and hardness tests were undertaken. The tensile tests were performed in accordance with ASTM standards (0.505" specimen diameter by 2" gage length) and the hardness tests were of the Rockwell R_A type. Data procured from specimens cut from the center and two ends of each of the 20 foot bars used are listed in Tables II, III, and IV. Also given in these tables are the moduli of elasticity determined from autographic load-deflection curves. The results of these tests agree closely with published data on these materials (2).

Static tension tests were also undertaken on the unnotched and notched type fatigue specimens used in this program. This was done not only to establish the general effects of the various types of notches on the static tensile strength but also to determine the zero stress ratio points for the stress range fatigue diagrams to be presented later. The results of these tests, given in Tables II, III, and IV, indicate generally higher static strengths for the fatigue type specimens than for the ASTM tension specimens. This is shown graphically in the lower part of Fig. 8 in which is plotted the tensile strength of the various types of fatigue specimens as a function of the notch severity, specified in terms of the theoretical stress concentration factor K_t.

The K_t values for all of the fatigue specimens are indicated along the abscissa. Also shown in this figure are the average tensile strengths for the standard straight-sectioned ASTM test specimen.

Figure 8 shows that the tensile strength increases with increasing notch severity, reaching a maximum at some intermediate K_t value, beyond which it decreases. This general pattern has been observed previously. Although such factors as stress gradient, plasticity properties, and the state of stress (whether uniaxial, biaxial or triaxial) are important, this effect is partially explainable on the basis that a fillet or notch has two major effects:

a. Causes stress concentration which tends to reduce the strength of the specimen, and
b. Restricts the reduction in area ("necking-down" prior to failure) which tends to increase the strength.

Figure 8 shows that the strength of the type V specimen is larger in all cases than the ASTM specimen, and this may be explainable on the basis that factor (a) above is practically the same for both specimens whereas factor (b) favors the type V specimen. The peaked strength curve may similarly be explainable on the basis that factor (b) predominates up to a certain notch severity beyond which factor (a) becomes the more critical. Thus, a reduction in strength is observed for notch severities beyond that of type AB specimen.

The elongation data for the various types of fatigue specimens are plotted in the upper part of Fig. 8. Note that the peak in the strength curves occur at the stress concentration factor at which the elongation curves reach a horizontal asymptote. However, a quantitative analysis of the relationship of the elongation data and related ductility factors to the strength trends shown in Fig. 8 is beyond the scope of this paper.

7.2 Creep and Rupture Properties

In order to accurately establish the zero stress-ratio point for all lives in the stress range diagram to be discussed in the next section, a few exploratory tests were made to determine if the time at load significantly affects the static strength of the fatigue type specimens at room

temperature. The data for 24S-T6 are presented in Fig. 9 and 10. Referring first to the lower curve of Fig. 9, the load on a specimen having a $K_t = 1$ was gradually increased in the steps shown and maintained at each step for sufficient time to establish creep trends. At the lower stresses no measurable creep was observed even for periods of time as large as several days. However, at fairly high stresses, as for example region a-b at 63,700 psi, measurable creep was observed as shown in curve a-b of Fig. 10. After approximately 100 hours at stress a-b the stress on this specimen was increased to c-d (67,000 psi) and again measurable creep ensued. Since in practically all the fatigue tests reported in this paper cycles to failure were not carried beyond 2×10^7 cycles, which occurs in less than 100 hours, these static stress-rupture tests were not carried beyond 100 hours. On this basis it was found that the long-term static strength was not significantly lower than the short duration static strength as shown by Fig. 9. Therefore, in the stress range diagrams presented later, zero stress ratio values are shown as one point for all lives.

The $K_t = 3.4$ specimen displayed a similar behavior as shown in the upper part of Fig. 9 and the lower three curves of Fig. 10. Even though significant creep occurred at stresses considerably below the ultimate strength, nevertheless the 100 hour stress-rupture strength of the $K_t = 3.4$ specimen was not significantly lower than the static tensile strength.

Based on these and a few other stress rupture tests not reported, it may be concluded that the stress rupture diagram is so flat at room temperature that the 100 hour stress-rupture value is practically the same as the static strength of the material. Therefore, the zero stress ratio points in all stress range diagrams are determined from the static tests on the particular specimen type being diagrammed.

7.3 Effect of Stress Relief on Fatigue Properties of Notched and Unnotched Specimens

As indicated in Section 5.2, considerable attention was devoted to the details involved in specimen preparation so that, among other factors, significant internal stress would not be induced. Since the introduction of

internal stresses may seriously affect the fatigue properties, particularly of notched specimens, an attempt was made to determine if the relief of internal stress through a thermal stress-relief treatment significantly affects the fatigue properties.

The series of specimens used were heat treated for stress relief as indicated in Table V. The hardness before and after the stress relief treatment given in the table, indicates less than one point of Rockwell B decrease in 14S-T6. The fatigue strengths for the stress relief specimens, as indicated in Table V, are not greatly different before and after stress relief. The $K_t = 1$ specimens showed an average increase of 5% in fatigue strength at the same life (range from -3 to 13%), the $K_t = 1.6$ specimens showed an average decrease of 2% (range from -10 to 3), and the $K_t = 3.4$ specimens showed an average increase of 3% (range from -5% to 9%). The over-all change for all specimens averages 2.3% increase. Considering the scatter inherent in fatigue data, this difference is not considered significant. It may therefore be concluded that the internal stresses induced in machining and polishing the specimens are not significant insofar as the comparative strengths of these materials are concerned.

7.4 Fatigue Properties of 14S-T6

7.4.1 S-N Fatigue Diagrams. The S-N fatigue data procured for 14S-T6 are listed in Table VI and plotted in Figs. 11, 12, 13, and 14. The S-N fatigue diagrams shown in these figures are plotted on the basis of the logarithm of the maximum or crest stress S_c during the cycle versus the log of the number of cycles to failure. The crest stress S_c is used in these plots instead of the alternating stress S_a or mean stress S_m in order to improve the curve separation and clarity. The logarithmic scale was used because of its constant percent spread feature, a 10% spread at any ordinate location being indicated to provide a measure of the scatter in the fatigue data.

Each stress ratio A is plotted as a separate S-N curve in accordance with the point and line code shown. In general, it may be observed that the lower the stress ratio the smaller the slope of the S-N curve. The zero

stress ratio curve is not shown but as discussed previously, the static stress-rupture data indicates practically a horizontal line.

Referring to Fig. 11, and others to be discussed later, it may be observed that the crest stress S_c may slightly exceed the static ultimate strength, S_u, for the same type specimen during a low stress-ratio fatigue test. Since this difference is generally small (only about 5% above the static ultimate strength) and since it occurs at high stress where the life is quite short, the data cannot be considered conclusive. Nevertheless, several tests have produced this same result on various materials and specimen types. It is believed to be possible for the crest stress to exceed the static ultimate strength, since strain rate and time at peak load may be important variables.

Since the scatter in fatigue strength data at long life is generally larger than at short life, it is generally rather difficult to establish the existence or non-existence of a horizontal asymptote or fatigue limit. Although the data presented in these figures and in subsequent diagrams do not appear to approach the asymptote up to 10^7 cycles nothing conclusive can be said on this matter.

In some cases the specimens which did not fail at a low stress level were retested at a higher stress level. The S-N fatigue points procured on specimens with such a previous stress history are marked by an asterisk in the S-N diagram. With only one or two exceptions the previous stress history does not appear to significantly affect the fatigue strength at a higher stress level. Since the effect of understressing is uncertain, these data are presented merely as a matter of interest.

If the slopes of the S-N curves in Figs. 11, 12, 13, and 14 are compared, it is seen that the higher the stress concentration factor the greater is the steepness of the short life part of the curves. This observation is as expected since the notched specimens display higher static strength, but lower long term fatigue strength, than do the unnotched specimens.

7.4.2 Stress Range Diagrams. The fatigue data diagrammed in Figs. 11, 12, 13, and 14 are replotted on a stress range basis in Figs. 15, 16, 17, and 18. The left ordinate indicates the alternating stress and the

bottom abscissa the mean stress. Each curve indicates the combinations of alternating and mean stress which results in failure in a definite number of cycles in the range from 10^3 to 10^7 cycles. The series of inclined lines which pass through zero indicate the stress ratios used. Also shown in this diagram is a straight dot-dash line to indicate the combination of alternating and mean stress whose total equals the ultimate strength, S_u, of the material for the specimen type under consideration. As pointed out previously, and as shown in Fig. 15, $S_a + S_m$ may exceed the ultimate strength of the material S_u at low stress ratios for short life. Figures 15, 16, 17, and 18 also include unitless scales in the upper abscissa and right hand ordinate. The unitless abscissa scale is the ratio of the mean stress on the specimen to the static ultimate strength of the material and the unitless ordinate is the ratio of the alternating test stress to the alternating stress which will cause failure in 10^7 cycles at a stress ratio of infinity.

Comparing Figs. 16, 17, and 18, it is apparent that the higher the stress concentration factor in the specimen the flatter are the stress range curves, particularly for long life. Also of significance is the observation that although the curves for the unnotched and mildly notched specimens are generally either concave downward or straight, the severely notched specimens display curves which are concave upward. As a result of these trends, relatively small alternating force may greatly reduce the allowable mean stress. For example, referring to the curve in Fig. 18 for a life of 10^7 cycles, the addition of an alternating stress of only 8 per cent decreases the allowable mean stress by 35% from 84,000 to 54,000, and an alternating stress of 15% of the preload reduces the allowable mean stress 68% from 85,000 psi to 27,000 psi. This observation is of considerable design significance since low magnitudes of alternating force are frequently encountered in service, and these are sometimes ignored on the assumption that they are insignificant.

It is desirable to determine if the stress range relationship is sufficiently consistent for all stress ratios to permit interpolation when only the reversed stress fatigue strengths and static strengths are known. In order to establish such a relationship, the stress range data of Figs. 15 to

18 are replotted on a completely unitless basis in Figs. 19 to 22. In these unitless diagrams both the maximum ordinate and maximum abscissa are arbitrarily made equal to one. This means that the ordinate scale is the ratio of the alternating stress for a given life (the various lives plotted are shown by the point and line code) to the alternating stress for the same life under reversed stress conditions ($A = \infty$). Even though each of the three families of curves fall within a band which can be approximated by a single curve, the general shape of the bands are quire different, particularly for the sharply notched specimens. Therefore, the stress range relationship cannot be defined by one equation for all fatigue lives and specimen types.

7.4.3 Notch Sensitivity Diagrams. It is apparent from the study of the foregoing stress range diagrams that the reduction in fatigue strength caused by a notch is a function of not only dimensions but also stress ratios and stress level or life. The relationship of the notch effect to these variables is clarified in the series of notch sensitivity diagrams shown in Figs. 23 to 28.

In these diagrams the harmful effect of the notch is specified in terms of the fatigue strength reduction factor K_f, which is defined as the ratio of the fatigue strength of the unnotched specimen to the fatigue strength (based on nominal stress calculations) of the notched specimen for the same life and same stress ratio. Since all data were procured and analysed on the basis of a fixed stress ratio (rather than fixed alternating stress and variable mean stress or fixed mean stress under variable alternating stress) and the ratios of $(S_c)_{unnotched}$ to $(S_c)_{notched}$ is the same as the corresponding S_a and S_m ratios, thus it is not necessary in an analysis based on fixed stress ratios to specify which stress (S_c, S_a, or S_m) was used to compute K_f.

The first of the notch sensitivity diagrams, shown in Fig. 23b, is constructed by first drawing "profile" curves of the type shown in Fig. 23a. Each of the profile curves covers a different stress ratio and each point represents the ratio of the fatigue strength of the unnotched specimen for a given life (determined from Fig. 11) to the fatigue strength of the notched specimen for the same life and same stress ratio (determined from Fig. 14).

The resultant K_f values are plotted against the alternating stress in the unnotched specimen.

The "profile" curves shown in Fig. 23a are projected to within the S_a versus S_m coordinate system shown in Fig. 23b to establish the K_f contour curves shown. For example, to determine the location of the K_f 2.2 point for the ratio A of 0.89, a dashed line is drawn vertically along the 2.2 K_f value in Fig. 23a until it intersects the A = 0.89 curve, at which alternating stress a horizontal projection line is constructed to intersect the 0.89 stress ratio line in Fig. 23b. Similarly, other contour line points for A = 0.89 and other stress ratios may be located and the contour curves shown in Fig. 23b may be constructed to show the K_f surface.

Because of the inherent scatter in fatigue data and in order to avoid complicated contour curves which might be difficult to interpret, some liberties were taken in plotting the K_f surface in Fig. 23b. All the contour points are located according to the actual S-N curves shown in Figs. 11-14, but the contour lines do not always pass through these points. However, in no case does the contour line deviate by more than 10%* from the plotted contour points, and only in a very few cases is the deviation this large. The regions of the contour curve shown in Fig. 23 in which the interpolation or extrapolation are rather uncertain are shown in dashed lines.

Similar K_f data for the other notches, (K_t = 2.4 and 1.6) are diagrammed in Fig. 24 and 25. For conciseness, the "profile" curves are omitted in this and subsequent figures of this type.

The following observations may be made from Figs. 23, 24 and 25. If the fatigue reduction factor K_f were reasonably independent of mean stress and dependent only on alternating stress, then the contour lines would be horizontal; whereas if K_f were dependent on mean stress and not on alternating stress, these contour lines would be vertical. In general, these contour lines are inclined indicating the dependence of K_f on both alternating and mean stress. However, in some regions the lines are essentially

*This limit of 10% deviation was established as follows: By inspection, the S-N point scatter may cause an error in the S-N curve of up to approximately 5%. Thus, since the K_f values are based on the ratio of two curves, an error up to 10% is possible.

horizontal whereas in other regions they are essentially vertical, indicating that either alternating or mean stress, respectively, may be the primary variable, depending on the conditions of test.

Referring again to Fig. 23, the highest K_f factor of 2.4 extends over a central region which includes stress ratio as low as 0.25. This observation that high K_f may exist at low ratios is intended to point out again how seriously even a small magnitude of alternating stress might affect parts with stress concentration. The maximum K_f observed (2.4) is considerably below the theoretical stress concentration factor of 3.4 for this specimen type.

For the other two notched specimens, diagrammed in Figs. 24 and 25, the same general trends may be observed. In general, the more severe the notch, the more the high K_f plateau extends toward the low stress-ratio region. In the case of the intermediate notch (K_t = 2.4), the maximum K_f is 1.8, while for the mild notch (K_t = 1.6) the maximum K_f is 1.35.

In order to clarify the role of length of fatigue life, a second type of notch sensitivity diagram is shown in Fig. 26. The contour lines shown in Fig. 26c for the K_f surface are constructed within stress ratio versus life N coordinates by projecting the sets of profile curves shown in Figs. 26a and 26b. The experimental points shown in Fig. 26a were determined from the ratio of the fatigue strengths for the same fatigue life for the unnotched and notched specimens diagrammed in Figs. 11 and 14. The points shown in Fig. 26b were determined from the ratios of the fatigue strengths determined from Figs. 11 and 14 for the same stress ratios, each curve in Fig. 26b representing a different life. The crest to trough stress ratio R is used in Fig. 26b and c instead of the alternating to mean stress ratio A, because the range in R values from -1.0 to +1.0 (reversed stress to static stress) is more easily diagrammed than the corresponding range of A values from zero to infinity. However, both scales are shown in these diagrams for completeness.

Referring to Fig. 26c it is possible to divide the K_f surface into characteristic regions E, F and G. In region E, in which the fatigue life is short and stress ratio A is large, the K_f contour lines are essentially vertical.

This indicates that K_f is essentially independent of stress ratio and primarily dependent on the fatigue life. In region G, however, where the fatigue life is comparatively long and the stress ratio A is small, the contour lines are essentially horizontal, indicating that stress ratio rather than life is most critical. Region F, the transition region between E and G, is one in which both the stress ratio and fatigue life are important.

The large slope in the K_f surface in region G, as indicated by the density of the K_f contour lines, again indicates that adding relatively little alternating stress in a notched member may greatly decrease the allowable preload.

Here again, there is a gradual transition in going from the severely notched specimen (Fig. 26c) to the mildly notched specimens (Fig. 28), the three regions discussed previously being least apparent in the case of the mild notch. Also, the K_f peak occurs at higher stress ratio A and at somewhat shorter life in the case of the mild notch. It is therefore apparent that K_f varies significantly with both stress ratio and life and that the pattern of variation is dependent on the severity of the notch.

Several attempts have been made in the past (15) (16) to analyse the over-all fatigue reduction factor K_f in terms of two more basic quantities: (a) the theoretical stress concentration factor K_t determined from the geometry of the notch, and (b) a material factor. A quantity sometimes used to represent the material fcctor is the dimensionless quantity q given by the expression $q = \frac{K_f - 1}{K_t - 1}$. On the basis of this definition q would normally lie between 0 (for a material that is extremely notch insensitive) to 1 (for a material which is extremely notch sensitive).

It is unlikely that a single material constant of the type q would adequately define the behavior of material at all stress ratios since both the static and fatigue properties may be involved to a varying degree. For similar reasons q is likely to be dependent upon fatigue life. Past work (16) indicates that q does vary considerably with factors other than material. Nevertheless, in the absence of a better measure of the material factor the values of q are diagrammed in Fig. 29 within alternating and mean stress coordinates for the three type specimens K_t = 1.6, 2.4, and 3.4). Although

the general shapes of the q surfaces for these types of specimen are similar in some respects, the specific values for q are generally quite different even under given stress conditions. In general, the sharp notch displays the higher q factor over most of the stress range field.

7.4.4 Yield, Creep and Elongation During Fatigue Test. As discussed under Section VI, the test specimen yeilds and creeps during the fatigue tests conducted above its yield strength. This yield, measured with a micrometer, occurs almost entirely during the very early stages of the test.

Total elongation was also determined by measuring the total length of the specimen before and after the test, the broken specimens of course being carefully matched at the fracture before measurement. Total elongation measured by this method compared favorably with the elongation measured by the micrometer method, although some difference due to elongation during final separation was sometimes apparent.

The total elongation of the specimens as a function of maximum stress and stress ratio is shown in Fig. 63. Also included for comparison purposes is the elongation of an unnotched fatigue specimen of 24S-T4 broken under static loading (the standard straight section static specimen has a percent elongation of 21% per 2" gage). In general, elongation does not become significant until the maximum stress exceeds the yield strength. Above this limit elongation decreases with increasing stress ratio, becoming negligible under reversed stress conditions.

7.4.5 General Observations Concerning Damping Capacity of Test Materials. No difficulty was experienced with specimen heating due to internal hysteresis damping. Even at the highest stress levels (frequency of loading 1800 rpm) no artificial cooling was required to keep the specimens at room temperature. This may be interpreted as a qualitative indication of the low damping capacity of these test materials.

7.5 Fatigue Properties of 24S-T4

The fatigue data procured on 24S-T4 are listed in Table VII and the corresponding S-N fatigue diagrams are shown in Figs. 30 to 33. The stress range diagrams of Figs. 34 to 41 and the notch sensitivity diagrams

of Figs. 42 to 48 display characteristics similar to those of 14S-T6 discussed in the previous section. The maximum K_f values are 1.35 for the mild notch (K_t = 1.6), 2.2 for the intermediate notch (K_t = 2.4), and 2.6 for the sharp notch (K_t = 3.4).

7.6 Fatigue Properties of 75S-T6

The fatigue data procured on specimens of 75S-T6 having K_t values of 1, 1.6, and 3.4 are listed in Table VIII and the corresponding S-N fatigue diagrams are shown in Figs. 49 to 51. The maximum K_f values are 1.2 for the mild notch (K_t = 1.6) and 2.1 for the severe notch (K_t = 3.4).

The stress range diagrams shown in Figs. 52 to 54 (also see Figs. 55 to 57) are similar in many respects to those discussed previously except that the unnotched specimen is abnormally flat.

VIII. COMPARISON AND ANALYSIS OF DATA

8.1 Fatigue Properties of Unnotched Specimens

A comparison of the stress range fatigue data obtained in this program on 14S-T6 and 24S-T4 with those of other sources is shown in Figs. 64 and 65, respectively. Also shown at vertical ordinate locations are rotating beam data (stress ratio of infinity) for these materials.* In general, the agreement is good although the Minnesota stress range data at high stress ratios is somewhat higher than the comparison data. Also, the rotating beam fatigue strengths are somewhat higher, in general, than the reversed axial stress strength, which is in agreement with general expectation. However, it should be noted from Fig. 65 that the Minnesota rotating beam data checks almost exactly the Minnesota reversed axial stress data (same batch of 24S-T4 used for both tests).

A comparison of 75S-T6 data from various sources, as shown in Fig. 66, reveals rather serious divergence. The Minnesota data is as much

*The points marked "B" in Fig. 64 designate the rotating beam fatigue strengths for a British alloy, B5562-1, having a chemical composition and static strength similar to 14S-T6.

as 50% below the comparison data at 10^5 cycles, and shows even a greater discrepancy at 10^7 cycles. However, tests conducted at the Aluminum Research Laboratories (18) on specimens from the same batch of material as tested in this program yield fatigue strengths significantly below average values. The ARL data, plotted as points "F" in Fig. 66, fall between Minnesota data and those from other sources. These comparative curves indicate that, though the static strengths are reasonably uniform, there is a wider variation in fatigue strengths of 75S-T6 than for the other aluminum alloys. A determination of how widespread this condition has been in the past and the probability of its occurrence in the future is beyond the scope of this report.

Fig. 67 shows a comparison of the fatigue strengths of 14S-T6, 24S-T4, and 75S-T6. In Fig. 67a, constant-life curves of 10^4 and 10^7 cycles are shown for unnotched specimens of the three materials. At the two lifetimes, the fatigue strengths for 14S-T6 and 24S-T4 are almost the same. The fatigue strength of 75S-T6, however, is much lower, especially at 10^7 cycles. The curves for 75S-T6 are much flatter in the low stress-ratio region, for long life, a fact which emphasizes, again, the serious effect that a small vibration stress may have on the allowable mean strength of this material.

In Fig. 67b, constant-life curves for 14S-T6 and 24S-T4 are diagrammed for specimens with an intermediate notch ($K_t = 2.4$). At 10^4 cycles, the fatigue strength of 14S-T6 is slightly lower than that of 24S-T4. However, at 10^7 cycles the strengths are almost identical. Fig. 67c shows the fatigue strengths of the three materials for the sharp notch ($K_t = 3.4$) specimens. Here the strength of 24S-T4 is the highest with 14S-T6 and 75S-T6 following in that order. At 10^7 cycles, the fatigue strengths of all three materials are practically the same. Since the fatigue strengths of the unnotched specimens of 75S-T6 were so much lower than those of 14S-T6 and 24S-T4 and yet the strengths of the sharp-notched specimens are practically the same, it seems reasonable to conclude that the stress concentration effects of the inhomogeneities in the 75S-T6 contribute to the low fatigue of this material.

8.2 Notch Sensitivity Properties

The data on fatigue strength reduction presented in Section VII for all three materials show clearly that the fatigue strength reduction factor K_f varies not only with the theoretical stress concentration factor K_t but also to a significant degree with stress ratio and stress magnitude (or life). In general, the notch sensitivity properties of 14S-T6 and 24S-T4 are quite similar except for minor differences. For these two materials the maximum K_f factor for the sharp type X notch is about 2.5 and it occurs under reversed stress conditions, as compared to a theoretical K_t factor of 3.4. The stress concentration properties of 75S-T6, however, are different from the other two materials. Not only is the general shape of the K_f surface quite different from the other two materials, but the maximum K_f of 2.1 is lower than for the other materials and it occurs at a higher stress or shorter life.

A comparison of the notch sensitivity properties determined in this work with those of sheet materials (7), (8), (9) is shown in Fig. 68. Values of K_f for the round specimens of 24S-T4 tested in this program are plotted in Fig. 68a against K_t for different lifetimes. The values of K_f for 24S-T3, sheet material (9) are also plotted on the same grid. Comparison of the two sets of data shows the K_f curves obtained at Minnesota to be lower throughout. However, a few points are shown plotted from data obtained at Ohio State (5) on round specimens in reversed bending and these points fall below Minnesota data. Although the magnitudes of K_f do not agree too closely, both show an increase in K_f with increasing K_t.

In Fig. 68b, similar curves are shown for 75S-T6. Here it is observed that the values of K_f reported herein are much lower than those on sheet material, indicated by dashed curves. This is in line with previous discussion. The Ohio State data (5), however, are still lower. A few K_f points reported by the Royal Aircraft Establishment (4) on DTD683, a British alloy similar to 75S-T6 are also generally lower than the Minnesota data.

An analysis of the significance of q or other measures of the material factors, and the possibility of separating such factors from the geometry factors, is beyond the scope of this report.

IX. SUMMARY AND CONCLUSIONS

A series of axial stress fatigue tests were undertaken on 14S-T6, 24S-T4 and 75S-T6 to determine the effect of various combinations of alternating and mean stress on fatigue life. The stress range from reversed stress (from tension to equal compression) to static tension was covered in several stress ratios. Four types of specimens were studied, an unnotched type and three circumferentially notched types having theoretical stress concentration factors of 1.6, 2.4, and 3.4. Stress combinations were varied to produce fatigue failure in the range from 10^3 to 10^8 cycles.

The basic fatigue data are presented in a series of S-N curves and stress range diagrams. Since the ratio of unnotched to notched fatigue strengths varied considerably with stress ratio and stress magnitude (or life), the fatigue strength reduction factor was plotted as a K_f surface within two coordinate systems: (a) alternating stress versus mean stress, and (b) stress ratio versus number of cycles to failure. Also the data was partially analysed to determine the validity of the notch sensitivity index q as an indication of the "material factor."

The fatigue data procured in this program was compared with published data on similar materials.

The following conclusions are based on the fatigue and notch sensitivity data presented in this report.

(a) Static tension tests performed on two types of unnotched specimens and three types of notched specimens indicate an approximately 25% increase in strength up to a theoretical notch severity of 2.5, beyond which a significant reduction occurs. This trend may be partially explainable on the basis of two opposing factors introduced by the notch: the weakening effect of stress concentrations versus the strengthening effect which the notch offers in resisting the confinement of reduction in area preceding fracture.

(b) Based on limited tests, the 100 hour stress-rupture strength of all specimen types at room temperature are approximately the same as the static tensile strength.

(c) The axial stress fatigue properties of unnotched and notched 14S-T6 and 24S-T4 are practically equal at all stress ratios from static tension to reversed stress. The properties determined in this program checked prior work within practical limits.

(d) Even though the static properties of the 75S-T6 used in this program are normal, the fatigue properties are abnormally low and significantly below those of 14S-T6 and 24S-T4. In general, there appears to be greater divergence in fatigue properties of different lots of 75S-T6 than in 14S-T4 and 24S-T4.

(e) The stress range diagrams (S_a versus S_m for fixed number of cycles to failure) display extreme flatness and upward concavity for notched specimens. In the sharply notched specimens, for example, adding only 15% alternating stress reduces the allowable mean load by an average of approximately 70%. Thus, small magnitude vibrations frequently encountered in service, and sometimes ignored as being insignificant, may affect greatly the mean load carrying capacity of notched parts exposed to a large number of fatigue cycles.

(f) Stress range data for 14S-T6 plotted on a completely unitless basis (ordinate and abscissa intercept arbitrarily made equal to one for all lives) fall within bands for each specimen type, and each band can be approximated by a single curve. For the unnotched and mildly notched specimen, a straight line joining the two unity values provides a reasonable approximation, which in most cases is somewhat conservative. In the sharply notched specimen, however, the band is "S-shaped" such that the data falls significantly below the straight-line relationship for high stress ratios and somewhat above for low stress ratios. The same general patterns are evident in the 24S-T4 data except the band width is somewhat larger. For 75S-T6 the band width for the data on unnotched specimens is still wider and the long life points fall considerably below the straight line relationship.

For all materials in a severely notched condition the data falls significantly below the straight line relationship at high stress ratios.

(g) The fatigue strength reduction factor K_f plotted as a surface within an alternating stress versus mean stress coordinate system reveals, in general, contour lines which are inclined. This means that, in general, both alternating and mean stress significantly affect K_f, although in some regions one type of stress may be more critical than the other.

(h) For the severely notched specimens at high stress ratios (A above 0.25), contour lines are reasonably straight and have an inclination with the horizontal between approximately 10 to 30 degrees. At low stress ratios in the fatigue failure region, the slope of the K_f surface is extremely sharp (contour lines close together), which indicates that adding relatively little alternating stress to a high mean load greatly increases notch sensitivity. The peak of the K_f surface extends over a narrow plateau, covering stress ratios from infinity to approximately 0.25. The maximum K_f values observed are 2.4, 2.6, and 2.0 for 14S-T6, 24S-T4, and 75S-T6, respectively, compared with a theoretical notch sensitivity factor for the severely notched specimens of 3.4.

(i) The specimens of 14S-T6 and 24S-T4 with the intermediate notch (K_t = 2.4) display approximately the same characteristics as those of the sharp notch, except that the effects are not so pronounced. The maximum K_f occurs along a plateau in the K_f surface extending from stress ratio ∞ toward a stress ratio of .15 at low stress magnitude. Maximum values of K_f are 1.8 for 14S-T6 and 2.2 for 24S-T4.

(j) The mildly notched specimens display approximately the same type of K_f surface except that the peak is confined to stress ratios near infinity. The maximum K_f values are 1.3 for both 14S-T6 and 24S-T4 and 1.2 for 75S-T6 compared to a theoretical value of 1.6.

(k) In order to more clearly reveal the effects of specimen life, the K_f surfaces were also plotted for each material within a stress ratio versus number of cycles to failure coordinate system. Here again the slopes of the K_f contour lines indicate that both stress ratio and life may be of critical importance, depending on the region.

(l) In the sharply notched specimens of 14S-T6 and 24S-T4, a circularly-shaped plateau appears in the K_f surface in the region of high stress ratio A and long life. For short fatigue lives the contour lines are essentially horizontal, indicating that stress ratio is considerably more critical than life. Thus, the addition of small alternating stress to a high mean load critically affects the stress concentration effect only at long fatigue life. For the sharply notched 75S-T6 specimens the K_f surface is similar, in general, to that of the other two materials except that the plateau is vertically oblong at a shorter life of 10^4 cycles.

(m) For the intermediate-notch specimens of 14S-T6, the contour curves have the same general characteristics as for the sharp notch, except that the effect of life in the short-life region is not so pronounced, and the maximum K_f extends over a much wider plateau. For 24S-T4, life has a greater effect on K_f in the longer-life region, and no definite plateau of maximum values occurs within the range of life covered by these data.

(n) The K_f surface for the mildly notched specimens of 14S-T6 and 24S-T4 reveals a small circularly-shape plateau at a stress ratio of infinity, with a rather uniform surrounding slope. For 75S-T6 the maximum K_f is at a stress ratio of infinity, but at a greater life than for 14S-T6 and 24S-T4.

(o) Plots were made of the notch sensitivity index "q" for the three types of notch specimens within a mean stress versus alternating stress coordinate system to determine if q is independent of notch geometry. As has been established in the past, q is greatly dependent on notch geometry and is not a true material factor even at a fixed stress ratio.

(p) The elongation of fractured specimens at various stress ratios plotted against maximum stress indicates that the elongation is generally small at all stress ratios if the crest stress is below the static yield strength. However, when the crest stress exceeds the yield strength, the elongation becomes increasingly large with increasing crest stress and decreasing stress ratio.

BIBLIOGRAPHY

1. T. J. Dolan, "Effects of Range of Stress and of Special Notches on Fatigue Properties of Aluminum Alloys", NACA TN852, 1942.
2. "Alcoa Aluminum and its Alloys", The Aluminum Co. of America, 1950.
3. "Strength of Metal Aircraft Elements", ANC-5, June, 1951.
4. W. J. Taylor and N. J. F. Gunn, "The Effect of Notches on the Fatigue Strength of Three Light Alloys", Royal Aircraft Establishment Report No. Met. 42, Aug., 1950.
5. J. W. Spretnak, M. G. Fontana, and H. E. Brooks, "Notched and Unnotched Tensile and Fatigue Properties of Two Engineering Alloys", Trans. ASM, v. 43, 1951.
6. W. C. Braeggeman, M. Mayer, Jr. and W. H. Smith, "Axial Fatigue Tests at Zero Mean Stress of 24S-T4 Aluminum Alloy Sheets With and Without a Circular Hole", NACA TN 955, 1944.
7. H. J. Grover, S. M. Bishop, and L. R. Jackson, "Fatigue Strengths of Aircraft Materials", NACA TN 2324, 1951.
8. H. J. Grover, S. M. Bishop, and L. R. Jackson, "Fatigue Strengths of Aircraft Materials", NACA TN 2389, June, 1951.
9. H. J. Grover, W. S. Hyler, and L. R. Jackson, "Fatigue Strengths of Aircraft Materials", NACA TN 2639, Feb., 1952.
10. B. J. Lazan, "Dynamic Creep and Rupture Properties of Temperature Resistant Materials Under Tensile Fatigue Stress", Proc. ASTM , v. 49, 1949.
11. Wright-Patterson Air Development Center, "Examination of 75S-T6 Rods", Report No. WCRTL-R52-11, Project E-604-307, Feb. 4, 1952.
12. H. Neuber, "Theory of Notch Stresses", Edwards Brothers, Ann Arbor, Mich., 1946.

13. B. J. Lazan, "Fatigue Testing Machine", Machine Design, May, 1947.

14. University of Minnesota, "Annual Report on Dynamic Mechanical Properties of Temperature Resistant Materials, Members, and Joints", Air Force Contract No. AF-33(038)-18903, March 1, 1952.

15. R. E. Peterson, "Stress Concentration Phenomena in the Fatigue of Metals", Trans. ASME, 1933.

16. C. S. Yen, T. J. Dolan, "A Critical Review of the Criteria for Notch-Sensitivity in Fatigue of Metals", Bul. No. 398, University of Illinois Engineering Experiment Station, March, 1952.

17. ASTM "Manual on Fatigue Testing", 1949.

18. The Aluminum Company of America, "Fatigue Properties of 75S-T6 Rolled-and-Drawn Rod Supplied to Professor Lazan", June 6, 1952.

19. The Douglas Aircraft Company, "Fatigue Strength of 75S-T, Effect of Chromium Segregation", August 20, 1952.

APPENDIX A

DEFINITIONS OF TERMS AND SYMBOLS

The terms and symbols used in this report are defined below. In general, they are the same notation as used in the ASTM Manual on Fatigue Testing (17) with a few minor deviations and some extensions.

S_u -- Static Ultimate Strength.

S -- Instantaneous Principal Stress (tensile stresses considered positive, compressive negative.)

S_c -- Crest Stress - the highest algebraic value of stress in the stress cycle = $S_m + S_a$.

S_t -- Trough Stress - the lowest algebraic stress in the stress cycle = $S_m - S_a$.

S_a -- Alternating Stress - the amplitude of the cyclic stress = $\frac{S_c - S_t}{2}$.

S_m -- Mean Stress - the algebraic mean of the maximum and minimum stresses = $\frac{S_c + S_t}{2}$.

A -- Alternating Stress Ratio - the ratio of the alternating to the mean stress = S_a/S_m.

R -- Trough Stress Ratio - the ratio of the trough stress to the crest stress = S_t/S_c.

N -- Fatigue Life - the number of cycles of stress which may be endured without failure for a given test condition.

S_{cn} -- Crest Fatigue Strength - the highest crest stress that may be endured for a specified number of alternating stress cycles at a given stress ratio without failure.

S_{an} -- Alternating Fatigue Strength - the highest alternating stress that may be endured for a specified number of cycles at a given stress ratio without failure.

S_{mn} -- Mean Fatigue Strength - the highest mean stress that may be imposed at a given stress ratio for a specified number of alternating stress cycles without failure.

K_t -- Theoretical Stress Concentration Factor - the ratio of the true maximum stress based on the geometry of a notch to the nominal stress.

K_f -- Fatigue Strength Reduction Factor - the ratio of the Fatigue Strength of an unnotched specimen or member to that of a notched specimen or member at the same life and stress ratio.

q -- Notch Sensitivity Index - a measure of the degree of agreement between K_f and K_t for a particular specimen or member of given size and material = $K_f - 1/K_t - 1$.

TABLE I. CHEMICAL ANALYSES OF THE THREE TEST MATERIALS

Alloy	Sample	Cu-%	Fe-%	Si-%	Mn-%	Mg-%	Zn-%	Cr-%	Ti-%
14S-T6	Rod #1	4.20	.50	.83	.76	.40	.00	.00	.05
	Rod #6	4.19	.51	.81	.78	.40	.01	.00	.05
	Rod #11	4.22	.50	.83	.78	.41	.01	.00	.05
24S-T4	Rod #2	4.25	.30	.13	.63	1.42	.07	.01	.02
	Rod #7	4.20	.30	.14	.63	1.46	.07	.02	.02
	Rod #13	4.17	.30	.13	.63	1.49	.07	.02	.02
75S-T6	Rod #1	*1.59	*.32	.15	.03	2.35	*5.60	.26	.05
	Rod #6	*1.55	*.32	.15	.03	2.40	*5.52	.26	.05
	Rod #11	*1.63	*.34	.15	.03	2.32	*5.51	.26	.05

*Determinations made chemically. All others made spectrographically.

TABLE II. STATIC PROPERTIES OF 14S-T6

Specimen No. and Type	Hardness R_A	Mod. E 10^6 (psi)	Tensile Strength (ksi)	.2% Offset Yield Str. (ksi)	Elong.
H 1*	51.5	10.6			14 %/2"
H 15*	50.0	10.	71.7	63.7	14 %/2"
H 29*	51.5	10.5	71.9	64.4	14 %/2"
I 1*	51.5	10.7	71.1	62.4	14 %/2"
I 15*	51.5	10.6	71.9	63.5	14 %/2"
I 29*	51.0	10.5	72.2	63.6	13 %/2"
J 1*	52.5	10.4	71.4	63.1	13 %/2"
J 15*	52.0	10.6	71.6	63.6	13 %/2"
J 29*	51.5	10.5	72.4	63.7	13 %/2"
K 1*	51.0	10.6	71.3	63.4	13 %/2"
K 15*	51.5	10.3	71.7	63.7	13 %/2"
K 29*	52.0	10.7	71.8	63.4	14 %/2"
L 1*	51.0	10.5	71.2	63.4	12 %/2"
L 15*	51.5	10.5	71.6	63.4	12 %/2"
L 29*	51.0	10.6	71.9	62.9	14 %/2"
M 1*	51.0	10.5	71.8	63.5	13 %/2"
M 15*	52.0	10.5	71.8	63.0	14 %/2"
M 29*	50.0	10.5	71.6	62.4	14 %/2"
N 1*	51.5	11.0	70.6	63.1	
N 15*	51.0	10.8	71.7	63.4	12 %/2"
N 29*	51.5	10.5	71.6	63.4	12 %/2"
Avg.*	51.3	10.5	71.6	63.5	13.6 %/2"
N23-V			73.9	68.3***	0.056"
I25-W**			87.2		0.044"
Q1484AB			97.4		0.024"
Q1459AB			96.6		0.020"
Average for Type AB Specimens			97.0		0.022"
M3-X			84.2		0.016"
N10-X			84.8		0.021"
Average for Type X Specimens			84.5		0.018"

*Standard ASTM specimen and test.

**Previous stress history of 2.5×10^7 cycles at S_c = 30,000 psi and A = 0.89.

***This is based on an equivalent straight length for the type V specimen determined by an integration method.

TABLE III. STATIC PROPERTIES OF 24S-T4

Specimen No. and Type	Hardness R_A	Mod. E 10^6 (psi)	Tensile Strength (ksi)	.2% Offset Yield Str. (ksi)	Elong.
A 1*	47		73.6	48.5	22 %/2"
A 15*	48	10.7	73.1	48.8	21 %/2"
A 29*	49.5	10.3	73.7	49.2	21 %/2"
B 1*	47	10.7	72.9	48.6	22 %/2"
B 15*	48.5	10.7	72.8	48.7	21 %/2"
B 29*	48	10.7	73.6	49.2	22 %/2"
C 1*	48.5	10.5	72.4	49.1	21 %/2"
C 15*	49	10.7	72.1	48.5	21 %/2"
C 29*	49	10.6	73.0	49.2	22 %/2"
D 1*	49	10.7	73.6	48.9	22 %/2"
D 5*	48.5	10.7	72.3	48.5	21 %/2"
D 29*	49.5	10.6	73.1	49.2	21 %/2"
E 1*	49	10.7	72.7	49.0	21 %/2"
E 15*	48.5	10.5	72.2	48.3	22 %/2"
E 29*	49.5	10.4	72.9	48.5	22 %/2"
F 1*	47.5	10.8	72.3	47.7	20 %/2"
F 15*	49	10.6	72.8	47.6	22 %/2"
F 29*	49	10.7	72.3	48.1	22 %/2"
G 1*	49	10.7	72.5	48.5	22 %/2"
G 15*	48	10.7	72.5	48.5	22 %/2"
G 29*	49	10.7	73.1	49.2	21 %/2"
Avg.*	48.5	10.6	72.8	48.6	21.4 %/2"
A9-V			74.6	53.6	0.162"
G5-V			74.4	51.3	
P475-V			73.8		
Average for Type V Spec.			74.3	52.5	
F3-W			76.3		
P1425-AB			87.0		0.028"
P1439-AB			86.0		0.024"
Average for Type AB Spec.			86.5		0.026"
B4-X			73.2		
F13-X			72.6		
D17-X			75.2		
A10-X			74.8		0.027"
G17-X			75.0		0.032"
Average for Type X Spec.			74.2		0.029"

*Standard ASTM specimen and test, 0.505" diameter, 2" gage length.

TABLE IV. STATIC PROPERTIES OF 75S-T6

Specimen No. and Type	Hardness R_A	Mod. E 10^6 (psi)	Tensile Strength (ksi)	.2% Offset Yield Str. (ksi)	Elong.
O 1*	55.5	10.5	82.8	72.1	16 %/2"
O 15*	56.5	10.3	82.7	71.2	17 %/2"
O 29*	56.0	10.3	82.3	70.5	16 %/2"
P 1*	57.0	10.4			16 %/2"
P 15*	55.5	10.4	82.3	70.3	16 %/2"
P 29*	57.5	10.3	81.7	70.3	16 %/2"
Q 1*	56.0	10.3	82.1	70.1	17 %/2"
Q 15*	56.0	10.5	82.3	70.5	16 %/2"
Q 29*	56.0	10.4	82.1	71.6	17 %/2"
R 1*	56.0	10.3	82.7	71.3	17 %/2"
R 15*	56.0	10.4	83.0	71.2	17 %/2"
R 29*	56.0	10.4	82.2	71.0	17 %/2"
S 1*	56.0	10.4	82.8	70.7	17 %/2"
S 15*	56.5	10.3	82.9	71.0	16 %/2"
S 29*	56.0	10.4	82.6	71.8	17 %/2"
T 1*	55.5	10.4	82.2	70.5	17 %/2"
T 15*	55.5	10.4	82.6	70.3	17 %/2"
T 29*	56.0	10.4	81.8	70.8	16 %/2"
U 1*	56.0	9.7	82.3	70.8	16 %/2"
U 15*	56.0	10.4	82.3	71.1	16.5 %/2"
U 29*	56.0	10.5	81.8	70.8	16.5 %/2"
Avg.*	56.0	10.4	82.3	70.9	16.5 %/2"
Q12-V			85.2	75.2	
T23-V**			84.9	75.2	
R28-W			99.2		0.043"
T4-W			98.9		0.055"
Q24-X			96.5		0.023"
Q21-X			96.4		

*Standard ASTM specimen and test, 0.505" diameter, 2" gage length.

**Previous stress history of 3.6×10^7 cycles at S_c 20,300 psi and A = 0.85.

TABLE V. EFFECT OF STRESS RELIEF ON HARDNESS AND FATIGUE PROPERTIES

Material and Heat Treatment	Specimen No. and Type	Rockwell B Before H. T.	Rockwell B After H. T.	Fatigue Test Stress Ratio A	Fatigue Test S_c (ksi)	Fatigue Test N to Fail Kilocycles	Per Cent** Change in S_c for Same N Due to H. T.
ALUMINUM ALLOY 14S-T6 STRESS RELIEVED 4 HOURS AT 350°F	N16-V	83.5	84.4	1.11	68.0	31.6	+ 13
	N12-V	84.0	83.5	2.16	31.0	77.8*	0
	J16-V	84.1	85.3	∞	36.0	158	+ 3
						Average	+ 5
	K14-W	81.4	76.2	0.37	50.0	158	- 10
	L8 -W	81.3	81.4	0.89	67.0	7.75	- 4
	K25-W	81.3	78.5	2.16	40.0	18.7	0
						Average	- 5
	L17-X	81.5	81.4	0.15	31.0	24,300*	+ 3
	I10-X	81.9	83.4	0.37	49.0	13.6	+ 9
	H7 -X	81.5	80.8	0.89	21.0	140	+ 8
	Average	82.3	81.6			Average	+ 7
ALUMINUM ALLOY 24S-T4 STRESS RELIEVED 1 HOUR AT 375°F	P495-V	77.5	74.5	0.89	70.0	13.6	+ 6
	P494-V	77.3	75.1	0.89	39.0	11,700*	+ 3
	P481-V	77.5	74.5	∞	39.0	153	+ 8
						Average	+ 6
	A14-W	75.6	75.6	0.37	48.0	440	0
	B19-W	76.0	77.5	0.89	37.0	766	+ 3
	A19-W	75.9	75.0	∞	39.0	12.5	0
						Average	+ 1
	B7 -X	76.7	73.3	0.89	41.0	8.54	- 5
	G10-X	76.4	75.5	4.04	10.0	24,700*	0
	C21-X	76.4	77.0	∞	16.3	274	+ 8
	Average	76.6	75.3	∞		Average	+ 1
ALUMINUM ALLOY 75S-T6 STRESS RELIEVED 4 HOURS AT 250°F	U5 -V	92.2	92.7	0.37	32.0	447	- 3
	R16-V	91.2	91.7	0.89	66.0	10.8	+ 3
	S16 -V	93.7	93.7	2.16	26.0	300	+ 13
						Average	+ 4
	Q3 -V	89.9	91.4	0.37	44.0	10.9	0
	U17-V	90.9	92.7	0.37	25.0	100	+ 2
	Q10-V	91.0	92.6	2.16	13.0	210	- 4
	Average	91.3	92.5			Average	- 1
						OVERALL AVERAGE	+ 2.3

*Test stopped before fracture.

**This percentage represents the change in fatigue strength of the specimen after heat treatment compared to the average fatigue strength at the same life N before heat treatment.

TABLE VI. FATIGUE DATA FOR 14S - T6

Specimen Type V - K_t = 1.0				Specimen Type W - K_t = 1.6				Specimen Type AB - K_t = 2.4				Specimen Type X - K_t = 3.4			
Spec. No.	Stress Ratio A	Crest Stress S_c (ksi)	Kilocycles to Failure	Spec. No.	Stress Ratio A	Crest Stress S_c (ksi)	Kilocycles to Failure	Spec. No.	Stress Ratio A	Crest Stress S_c (ksi)	Kilocycles to Failure	Spec. No.	Stress Ratio A	Crest Stress S_c (ksi)	Kilocycles to Failure
Q1006V	0.15	77.0	1.2	Q1329W	0.15	68.0	356.	Q1659AB	0.15	88.0	26.6	Q 973X	0.08	65.0	100.
Q1001V	0.15	75.0	265.					Q1456AB	0.15	75.0	30.3	Q 936X	0.08	55.0	21,700. *
Q 999V	0.15	68.0	21,300. *	Q1309W	0.37	55.0	178.	Q1491AB	0.15	65.0	63.1				
				Q1349W	0.37	52.0	522.	Q1657AB	0.15	55.0	254.	Q 925X	0.15	46.0	118.
Q 753V	0.393	74.0	1.4	Q1314W	0.37	48.0	1,000	Q1658AB	0.15	52.0	1,240.	Q 929X	0.141	40.0	253.
Q 780V	0.389	73.2	24.		0.37	46.0	9,210	Q1477AB	0.15	50.0	162.	Q 923X	0.14	35.1	655.
Q 768V	0.380	67.6	50.5	Q1342W	0.36	44.5	11,700. *	Q1649AB	0.15	49.0	20,700. *	Q 941X	0.15	29.0	27,100. *
Q 751V	0.376	62.6	293.					Q1650AB	0.15	45.0	20,400. *				
Q 783V	0.378	62.4	163.	Q1317W	0.89	70.0	7.9	Q1475AB	0.15	43.0	21,000. *	Q 950X	0.37	55.0	6.3
Q 776V	0.372	59.0	296.	Q1318W	0.842	61.9	19.9					Q 951X	0.37	45.0	14.1
Q 758V	0.372	54.6	675.	Q1351W	0.825	52.1	60.6	Q1482AB	0.37	75.0	4.20	Q 963X	0.37	35.0	37.3
Q 469V	0.37	52.1	4,890.	Q1338W	0.89	44.0	248.	Q1455AB	0.37	60.0	10.9	Q 957X	0.37	27.0	108.
Q 466V	0.37	49.0	9,170. *	Q1311W	0.89	40.0	575.	Q1466AB	0.37	40.0	68.4	Q 962X	0.37	27.0	108.
				Q1337W	0.89	37.0	550.	Q1463AB	0.37	34.0	352.	Q 968X	0.37	23.0	810.
Q 765V	0.93	72.8	3.5	Q1353W	0.806	36.9	5,110.	Q1653AB	0.37	32.0	140.	Q 922X	0.37	22.5	400.
Q 747V	0.914	66.2	12.2	Q1343W	0.89	33.0	11,300.	Q1644AB	0.37	32.0	16,700. *	Q 928X	0.37	22.0	270.
Q 759V	0.88	59.8	23.		0.89	30.0	24,600. *	Q1465AB	0.37	30.0	20,900. *	Q 944X	0.37	22.0	302.
Q 757V	0.903	55.2	57.1					Q1473AB	0.37	27.0	27,000. *	Q 962X	0.37	21.5	30,700. *
Q 777V	0.896	47.4	173.	Q1323W	2.16	58.0	6.5								
Q1000V	0.89	42.0	734.	Q1331W	2.09	50.5	23.1	Q1647AB	0.89	65.0	2.70	Q 972X	0.90	53.2	2.1
Q 998V	0.89	42.0	2,640.	Q1327W	1.90	46.9	42.3	Q1486AB	0.89	55.0	3.36	Q 973X	0.90	45.6	3.6
Q 997V	0.815	39.9	2,290.	Q1350W	2.16	40.0	116.	Q1460AB	0.89	40.0	27.2	Q 974X	0.90	34.2	10.3
Q 470V	0.89	40.0	3,490.	Q1332W	2.16	37.0	132.	Q1457AB	0.89	30.0	108.	Q 970X	0.90	26.6	33.2
Q1004V	0.89	37.0	6,260.	Q1315W	2.16	32.0	187.	Q1652AB	0.89	26.0	156.	Q 973X	0.90	22.8	61.0
				Q1320W	1.80	31.8	182.	Q1452AB	0.89	25.0	1,840.	Q 959X	0.89	20.0	173.
Q 767V	2.27	66.4	1.2	Q1354W	1.78	29.8	401.	Q1472AB	0.89	23.0	1,120.				
Q 752V	2.17	66.0	2.5	Q1328W	2.16	26.0	3,270.	Q1458AB	0.89	21.0	6,870.	Q 960X	2.16	50.0	1.3
Q 778V	2.19	60.2	11.3					Q1654AB	0.89	20.0	9,270.	Q 956X	2.16	37.0	5.9
Q 750V	2.17	56.4	21.	Q1322W	∞	40.0	13.3	Q1643AB	0.89	19.0	8,680.	Q 952X	2.16	30.0	11.1
Q 781V	2.15	50.1	50.4	Q1346W	∞	35.0	24.8	Q1648AB	0.89	18.0	31,200. *	Q 955X	2.16	23.0	45.3
Q 779V	2.18	36.6	308.	Q1348W	∞	33.0	38.2					Q 967X	2.16	20.0	63.0
Q 467V	2.16	32.0	637.	Q1324W	∞	30.0	121.	Q1453AB	2.16	50.0	1.92	Q 961X	2.16	16.0	292.
Q 472V	2.16	29.0	5,470.	Q1326W	∞	29.0	195.	Q1479AB	2.16	35.0	19.1	Q 921X	2.16	14.0	1,280.
Q1002V	2.16	28.0	7,260.	Q1341W	∞	27.0	184.	Q1655AB	2.16	28.0	42.5	Q 947X	2.16	13.0	2,560.
				Q1321W	∞	25.0	510.	Q1469AB	2.16	26.0	43.4	Q 938X	2.16	12.0	3,820.
Q 762V	∞	57.3	1.8	Q1313W	∞	23.0	1,310. *	Q1483AB	2.16	26.0	183.	Q 935X	2.16	11.0	20,800. *
Q 763V	∞	48.7	16.3	Q1345W	∞	23.0	2,190.	Q1642AB	2.16	24.0	180.	Q 932X	2.16	10.5	103,000. *
Q 772V	∞	37.2	82.7	Q1319W	∞	21.0	3,040.	Q1462AB	2.16	22.0	68.4				
Q 473V	∞	31.9	281.	Q1325W	∞	20.0	2,520.	Q1489AB	2.16	21.0	420.	Q 964X	∞	35.0	3.6
Q 787V	∞	25.8	1,130.					Q1480AB	2.16	19.0	3,870.	Q 969X	∞	25.0	18.0
Q 464V	∞	25.0	3,490.					Q1645AB	2.16	18.0	6,600.	Q 958X	∞	19.0	38.2
Q 468V	∞	24.0	4,660. *					Q1646AB	2.16	16.0	10,500.				
								Q1656AB	2.16	15.5	18,900.	Q 949X	∞	15.0	97.2
												Q 965X	∞	13.0	421.
								Q1464AB	∞	38.0	2.10	Q 919X	∞	12.0	659.
								Q1474AB	∞	29.0	13.3	Q 939X	∞	11.0	4,450.
								Q1471AB	∞	20.0	137.	Q 920X	∞	10.0	7,830.
								Q1470AB	∞	18.0	661.	Q 924X	∞	9.0	10,000.
								Q1454AB	∞	16.0	1,670.	Q 931X	∞	8.0	20,200. *
								Q1490AB	∞	14.5	2,420.				
								Q1488AB	∞	12.0	17,200.				
								Q1651AB	∞	11.5	27,600.				

*Specimen did not fracture.

TABLE VII. FATIGUE DATA FOR 24S - T4

Specimen Type V - K_t = 1.0				Specimen Type W - K_t = 1.6				Specimen Type AB - K_t = 2.4				Specimen Type X - K_t = 3.4			
Spec. No.	Stress Ratio A	Crest Stress S_c (ksi)	Kilocycles to Failure	Spec. No.	Stress Ratio A	Crest Stress S_c (ksi)	Kilocycles to Failure	Spec. No.	Stress Ratio A	Crest Stress S_c (ksi)	Kilocycles to Failure	Spec. No.	Stress Ratio A	Crest Stress S_c (ksi)	Kilocycles to Failure
P 483V	0.15	75.0	205.	P1295W	0.37	55.0	119.	P1417AB	0.15	80.0	15.1	P1021X	0.08	70.0	40.0
P 491V	0.15	66.0	6,800.	P1016W	0.369	48.6	216.	P1428AB	0.15	65.0	80.0	P1035X	0.08	65.0	84.3
P 489V	0.15	60.0	20,000.	P1294W	0.37	48.0	281.	P1436AB	0.15	55.0	246.	P1039X	0.08	55.0	3,220.
				P1304W	0.37	45.0	4,000.	P1415AB	0.15	47.0	575.				
P 694V	0.412	79.2	18.5	P1287W	0.37	45.0	11,700.	P1638AB	0.15	44.0	30,800. *	P1027X	0.15	58.0	53.4
P 710V	0.412	73.9	30.0	P1287W	0.37	43.5	22,800. *	P1449AB	0.15	40.0	20,600. *	P1037X	0.15	40.0	432.
P 696V	0.400	66.7	87.0	P1295W	0.37	42.0	35,200. *					P1032X	0.15	35.0	1,200.
P 714V	0.39	60.5	101.					P1445AB	0.37	75.0	1.65	P1025X	0.15	31.0	2,730.
P 708V	0.39	55.6	140.	P1278W	0.89	45.0	197.	P1430AB	0.37	60.0	13.2	P1029X	0.15	28.0	20,000.
P 500V	0.37	54.0	259.	P1012W	0.885	42.5	115.	P1424AB	0.37	40.0	105.				
P 500V	0.37	46.0	107,000. *	P1290W	0.89	38.0	122.	P1434AB	0.37	35.0	270.	P1024X	0.37	55.0	10.4
				P1307W	0.89	38.0	464.	P1421AB	0.37	30.0	585. *	P 890X	0.365	44.2	32.4
P 706V	0.98	67.3	11.4	P1010W	0.887	37.7	292.	P1633AB	0.37	28.5	20,400. *	P 905X	0.365	33.8	64.8
P 698V	0.95	64.8	15.5	P1289W	0.92	34.5	7,980. *	P1432AB	0.37	27.0	20,400. *	P 913X	0.367	29.1	112.
P 711V	0.94	59.0	26.0	P1306W	0.89	33.0	6,480. *					P 918X	0.37	29.1	144.
P 718V	0.98	56.4	46.0	P1298W	0.89	33.0	12,700.	P1433AB	0.89	60.0	1.26	P 898X	0.29	25.8	470.
P 697V	0.90	47.5	414.0	P1283W	0.89	32.0	25,300.	P1423AB	0.89	50.0	13.4	P1023X	0.37	23.0	524.
P 727V	0.90	38.0	9,100.					P1422AB	0.89	40.0	35.2	P1044X	0.37	21.0	864.
P 480V	0.89	35.0	29,400.	P1269W	2.16	55.0	4.6	P1637AB	0.89	32.0	163.	P 918X	0.37	20.0	10,200. *
				P1279W	2.16	45.0	22.7	P1435AB	0.89	29.0	93.5	P 918X	0.37	18.0	35,000. *
P 700V	2.40	71.4	1.1	P1285W	2.16	45.0	38.7	P1418AB	0.89	27.0	378.	P1023X	0.37	17.0	9,500. *
P 712V	2.27	64.9	5.0	P1291W	2.16	37.0	75.6	P1437AB	0.89	25.0	3,260.				
P 702V	2.24	57.0	13.0	P1014W	2.14	36.8	108.	P1640AB	0.89	24.5	573.		1.00	50.0	3.3
P 705V	2.17	50.5	30.0	P1266W	2.16	32.0	670.	P1412AB	0.89	23.0	3,450.	P1030X	0.89	45.0	5.7
P 713V	2.17	43.5	140.	P1267W	2.16	32.0	1,750. *	P1450AB	0.89	21.5	18,700.	P 909X	0.887	34.9	25.2
P 724V	2.16	39.4	517.	P1009W	2.17	30.6	568.					P 891X	0.884	23.5	115.
P 498V	2.16	36.0	3,160.	P1296W	2.18	29.0	2,470.	P1427AB	2.16	50.0	3.30	P1042X	0.89	19.0	330.
P 501V	2.16	33.0	4,700.	P1288W	2.16	28.0	4,180.	P1447AB	2.16	40.0	9.80	P1033X	0.89	19.0	466.
P 478V	2.16	31.0	9,660.	P1282W	2.16	27.0	5,950.	P1440AB	2.16	30.0	72.0	P1033X	0.89	14.0	20,100. *
				P1271W	2.16	25.0	13,500.	P1448AB	2.16	27.0	180.				
P 731V	∞	57.0	1.0	P1265W	2.16	24.0	18,200.	P1420AB	2.16	22.0	655.		2.41	45.0	1.8
P 735V	∞	52.9	9.0					P1413AB	2.16	20.0	1,170.	P1019X	2.16	37.0	4.6
P 726V	∞	51.6	10.1	P1017W	∞	38.5	10.8	P1441AB	2.16	18.0	5,230.	P 902X	2.25	35.7	6.3
P 720V	∞	45.8	23.8	P1275W	∞	35.0	29.0	P1636AB	2.16	16.0	14,400.	P 899X	2.16	30.0	9.6
P 482V	∞	35.0	676.	P1273W	∞	32.0	43.2						2.06	30.4	15.0
P 730V	∞	34.4	159.	P1308W	∞	30.0	41.3	P1431AB	∞	38.0	1.74	P 911X	2.15	26.1	43.2
P 497V	∞	32.0	839.	P1300W	∞	30.0	57.0	P1444AB	∞	29.0	21.9	P1031X	2.16	22.0	99.4
P 485V	∞	29.0	1,560.	P1270W	∞	28.0	119.	P1416AB	∞	23.0	106.	P 892X	2.15	19.7	259.
P 477V	∞	28.8	2,250.	P1264W	∞	27.5	274.	P1451AB	∞	20.0	443.		2.16	14.0	1,550.
P 499V	∞	27.0	3,290.	P1015W	∞	30.0	292.	P1419AB	∞	18.0	482.	P 916X	2.41	12.5	15,100.
P 488V	∞	26.0	3,300.	P1305W	∞	25.0	508.	P1443AB	∞	15.0	998.				
P 490V	∞	25.0	6,340.	P1018W	∞	25.0	529.	P1426AB	∞	13.0	3,350.	P 893X	∞	39.8	1.8
								P1635AB	∞	12.0	8,440. *	P 482X	∞	33.5	7.2
				P1268W	∞	21.5	904.	P1639AB	∞	11.0	20,600. *	P1026X	∞	27.5	18.4
				P1299W	∞	20.0	1,980.					P 894X	∞	22.0	43.2
				P1303W	∞	18.0	12,100.					P1020X	∞	22.3	86.5
				P1275W	∞	16.5	36,100. *					P 897X	∞	17.7	216.
												P 914X	∞	13.1	497.
												P 907X	∞	13.1	520.
												P 908X	∞	11.6	1,470.
												P 914X	∞	10.0	20,300. *

*Specimen did not fracture.

TABLE VIII. FATIGUE DATA FOR 75S - T6

Specimen Type V - K_t = 1.0				Specimen Type W - K_t = 1.6				Specimen Type AB - K_t = 2.4				Specimen Type X - K_t = 3.4			
Spec. No.	Stress Ratio A	Crest Stress S_c (ksi)	Kilocycles to Failure	Spec. No.	Stress Ratio A	Crest Stress S_c (ksi)	Kilocycles to Failure	Spec. No.	Stress Ratio A	Crest Stress S_c (ksi)	Kilocycles to Failure	Spec. No.	Stress Ratio A	Crest Stress S_c (ksi)	Kilocycles to Failure
R 789V	0.373	85.8	2.8	R1369W	0.15	88.0	42.0					R1081X	0.37	18.0	626.
R 796V	0.373	80.6	8.7	R1372W	0.15	70.0	63.4					R1051X	0.37	18.0	640.
R 792V	0.373	73.7	16.5	R1361W	0.15	60.0	115.					R1078X	0.37	17.0	21,600. *
R 809V	0.37	65.5	30.3	R1377W	0.15	57.0	422.					R1077X	0.37	17.0	105,000. *
R 791V	0.37	65.5	25.7	R1378W	0.15	55.0	6,780.					R1057X	0.37	16.5	20,000. *
R 798V	0.36	48.0	118.									R1071X	0.37	15.0	24,900. *
R 794V	0.36	38.8	198.	R1360W	0.37	87.0	7.20								
R 818V	0.365	29.9	831.	R1384W	0.37	70.0	15.9						0.89	50.0	2.0
R 820V	0.365	27.3	11,200.	R1358W	0.37	50.0	82.6					R1052X	0.89	40.0	4.4
R 523V	0.36	27.3	45,000. *	R1397W	0.37	45.0	56.6					R1073X	0.89	28.0	13.2
				R1362W	0.37	40.0	233.					R1066X	0.89	20.0	65.7
R 790V	0.898	81.2	1.4	R1376W	0.37	33.0	133.					R1055X	0.89	20.0	101.
R 814V	0.901	76.4	3.5	R1386W	0.37	32.0	485.					R1053X	0.89	17.0	140.
R 812V	0.899	66.5	9.3	R1379W	0.37	31.0	281.					R1059X	0.89	17.0	259.
R 799V	0.895	56.9	18.4	R1392W	0.37	30.0	406.					R1072X	0.89	15.0	285.
R 793V	0.897	47.4	32.6	R1371W	0.37	27.0	22,300. *					R1079X	0.89	15.0	335.
R 808V	0.895	34.3	74.7									R1092X	0.89	14.0	456.
R 802V	0.852	34.2	86.4	R1383W	0.89	60.0	10.5					R1067X	0.89	13.5	443.
R 817V	0.845	28.1	129.	R1395W	0.89	43.0	27.0					R1075X	0.89	13.5	24,400. *
R 803V	0.892	24.2	281.	R1367W	0.89	30.0	95.5					R1079X	0.89	13.0	31,300. *
R 813V	0.899	22.8	3,160.	R1356W	0.89	25.0	360.					R1055X	0.89	12.5	20,000. *
R 825V	0.845	20.3	36,200.	R1373W	0.89	22.0	1,340.								
				R1393W	0.89	20.0	3,250.					R1082X	2.16	42.0	2.2
R 795V	2.18	76.0	1.0	R1359W	0.89	18.0	20,800.					R1062X	2.16	35.0	3.0
R 797V	2.16	69.6	4.7									R1058X	2.16	23.0	16.2
R 807V	2.18	63.2	5.9	R1398W	2.16	58.0	6.59					R1069X	2.16	18.5	25.2
R 800V	2.16	50.3	19.5	R1387W	2.16	40.0	27.6					R1085X	2.16	18.0	62.1
R 811V	2.17	31.7	60.9	R1363W	2.16	27.0	79.2					R1054X	2.16	17.0	90.0
R 977V	2.16	25.0	173.	R1366W	2.16	25.0	146.					R1061X	2.16	15.0	126.
R 981V	2.16	21.6	324.	R1364W	2.16	25.0	637.					R1096X	2.16	15.0	281.
R 822V	2.08	21.4	929.	R1355W	2.16	18.0	756.					R1064X	2.16	12.0	734.
R 981V	2.16	20.0	21,200. *	R1375W	2.16	15.0	21,000. *					R1070X	2.16	11.0	553.
												R1076X	2.16	11.0	9,010.
R 819V	∞	57.4	4.0	R1368W	∞	39.0	14.4					R1096X	2.16	11.0	34,400. *
R 805V	∞	45.8	13.9	R1374W	∞	25.0	96.9					R1061X	2.16	10.0	9,040. *
R 816V	∞	34.4	42.9	R1365W	∞	18.0	216.								
R 975V	∞	32.0	37.8	R1381W	∞	15.0	2,850.					R1056X	∞	30.0	3.5
R 806V	∞	28.6	60.5	R1394W	∞	13.0	20,900. *					R1065X	∞	22.0	13.3
R 976V	∞	28.0	72.									R1060X	∞	20.0	24.5
R 978V	∞	24.0	124.									R1046X	∞	15.0	61.2
R 986V	∞	22.0	330.									R1049X	∞	12.0	216.
R 980V	∞	19.0	227.									R1099X	∞	11.0	356.
R 979V	∞	18.5	22,400.									R1068X	∞	10.0	10,600.
R 976V	∞	17.0	21,600. *									R1090X	∞	9.0	1,770.

No specimens of this type tested.

Specimen Type X - K_t = 3.4			
Spec. No.	Stress Ratio A	Crest Stress S_c (ksi)	Kilocycles to Failure
R1098X	0.08	49.0	860.
R1097X	0.08	45.0	25,400. *
R1094X	0.15	42.0	238.
R1100X	0.37	55.0	5.2
R1074X	0.37	51.0	7.2
R1047X	0.37	45.0	9.0
R1048X	0.37	35.0	25.2
R1050X	0.37	25.0	97.2
R1078X	0.37	25.0	166.
R1063X	0.37	20.0	277.
R1057X	0.37	20.0	311.
R1095X	0.37	18.0	400.

*Specimen did not fracture.

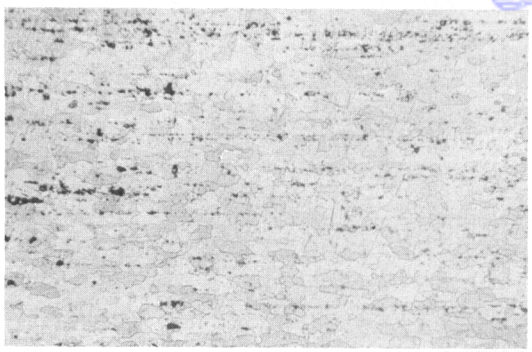

a. 14S-T6 Longitudinal Section 100X

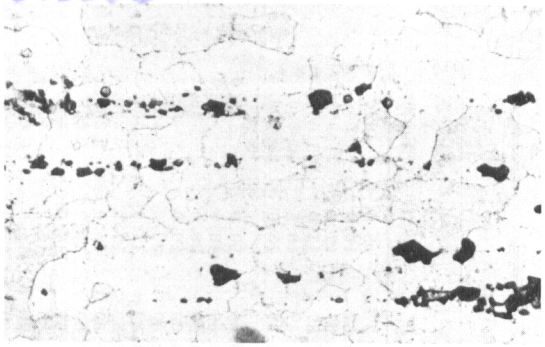

e. 14S-T6 Longitudinal Section 500X

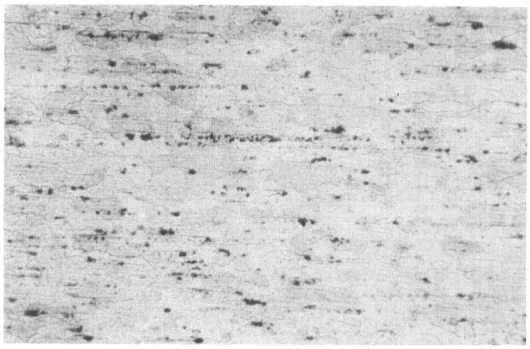

b. 24S-T4 Longitudinal Section 100X

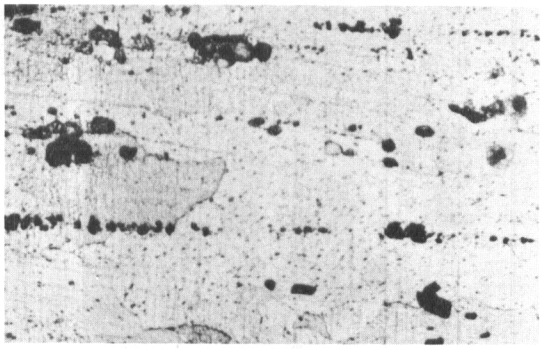

f. 24S-T4 Longitudinal Section 500X

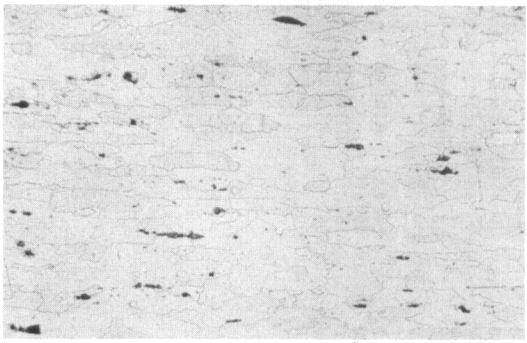

c. 75S-T6 Longitudinal Section 100X

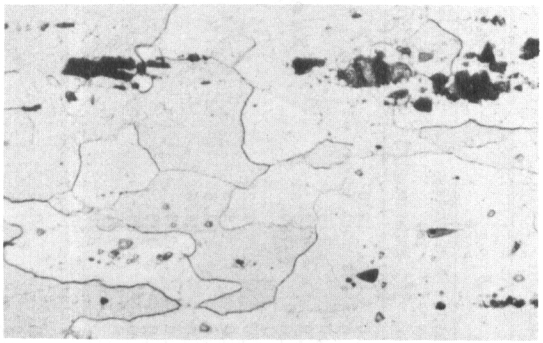

g. 75S-T6 Longitudinal Section 500X

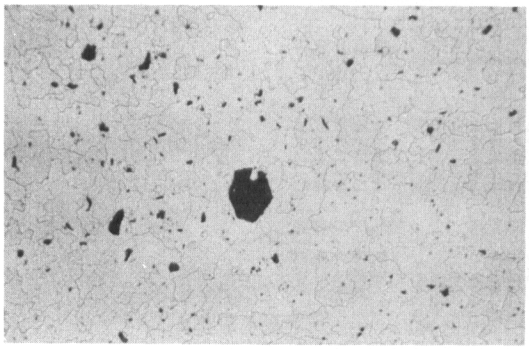

d. 75S-T6 Transverse Section 100X

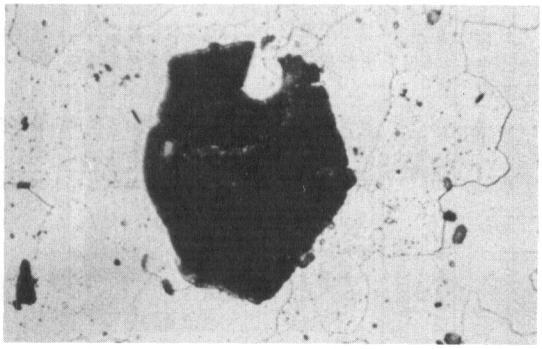

h. 75S-T6 Cross Section of Chrome Bearing Constituent. Transverse Section 500X

Etchant: Keller's Etch

FIG. 1. MICROSTRUCTURE OF 14S-T6, 24S-T4, & 75S-T6 ALUMINUM ALLOYS IN "AS RECEIVED" CONDITION

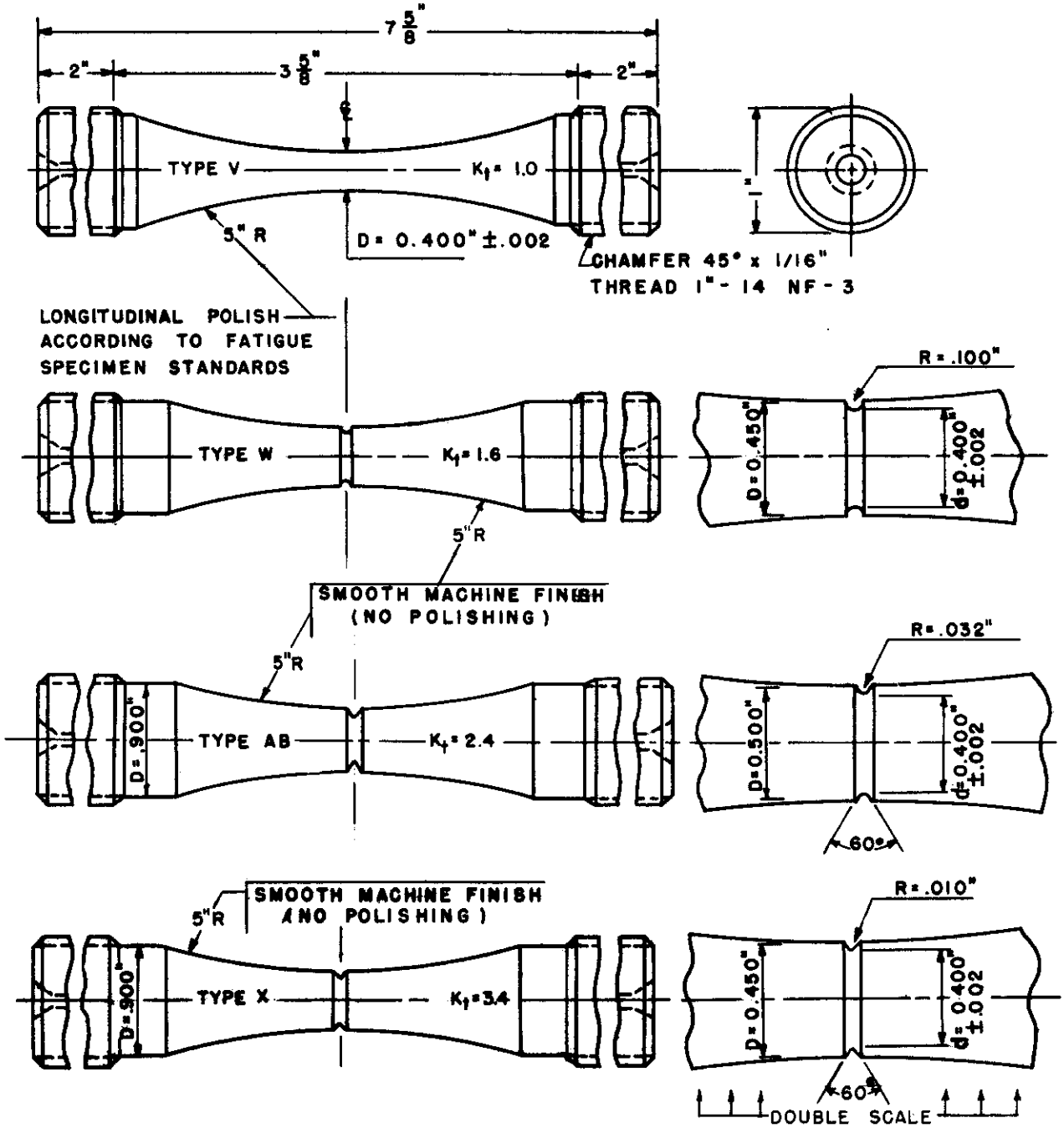

NOTCHES TO BE CYL. GROUND WITH VERY LOW FINISHING SPEED.

ETCH IDENTIFICATION MARKS ON BOTH ENDS.

SMOOTH MACHINE FINISH ALL OVER.

DIAMETER MUST BE CONCENTRIC WITH THREAD END WITHIN 0.002" TOTAL INDICATOR READING.

FIG. 2. UNNOTCHED AND NOTCHED FATIGUE SPECIMENS TYPES V, W, AB, AND X.

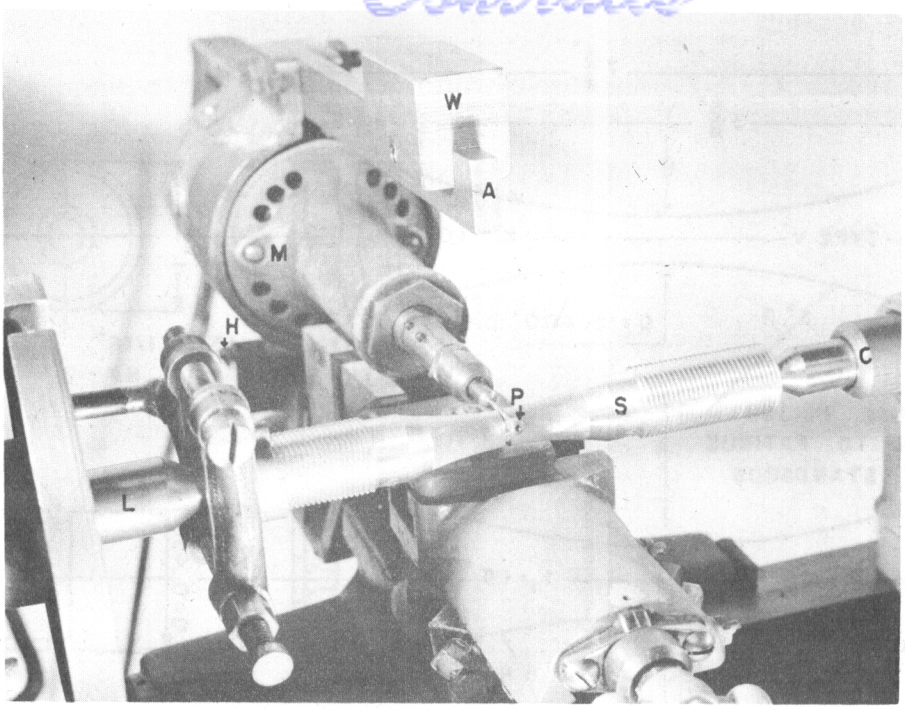

FIG. 3. SPECIMEN NOTCH POLISHING SET-UP

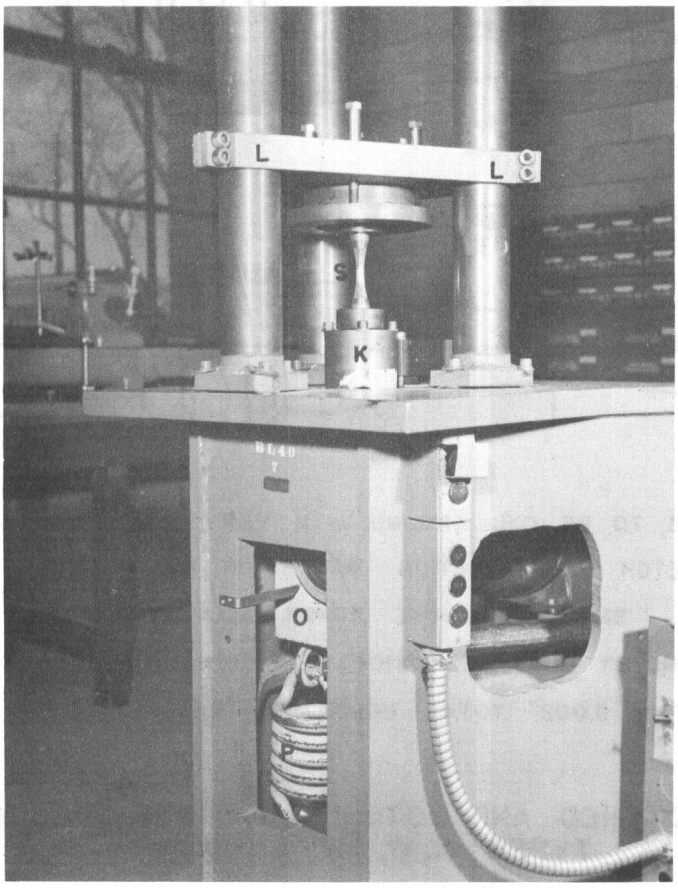

FIG. 4. DIRECT STRESS FATIGUE MACHINE LI

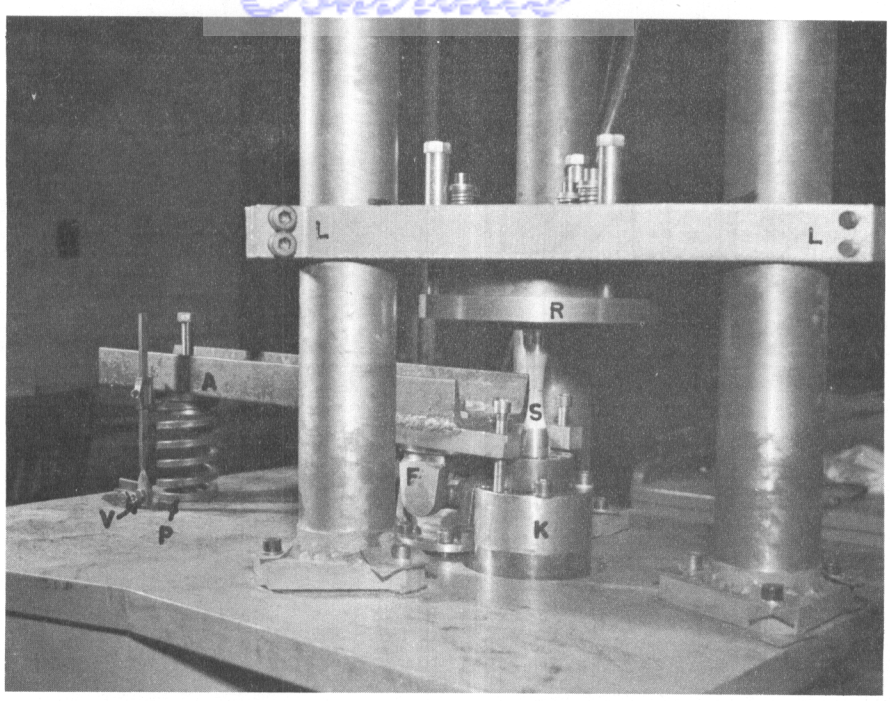

FIG. 5. PRELOAD AMPLIFYING FIXTURE FOR LI MACHINE

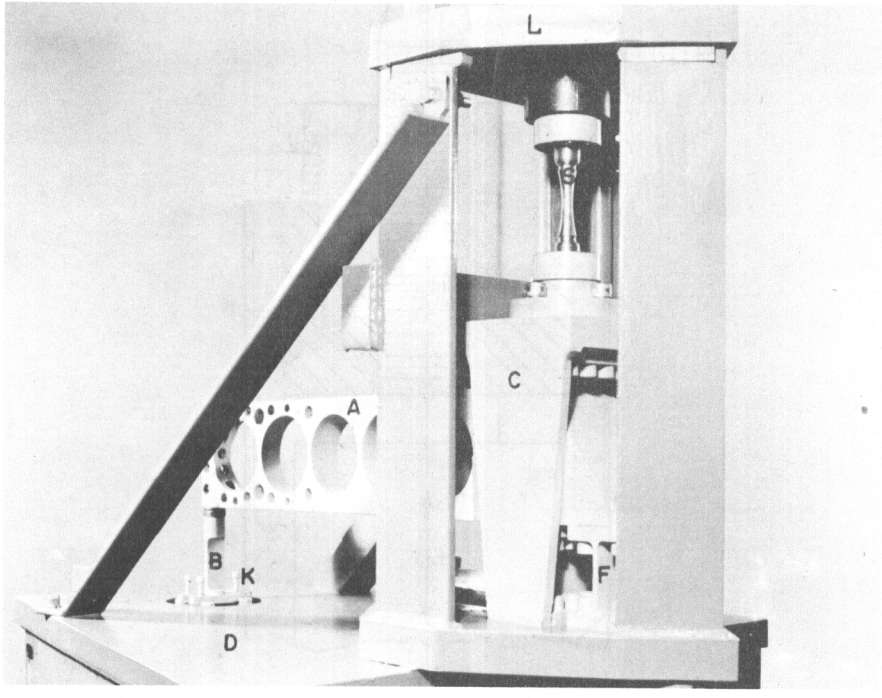

FIG. 6. EIGHT-TO-ONE FORCE AMPLIFYING FIXTURE

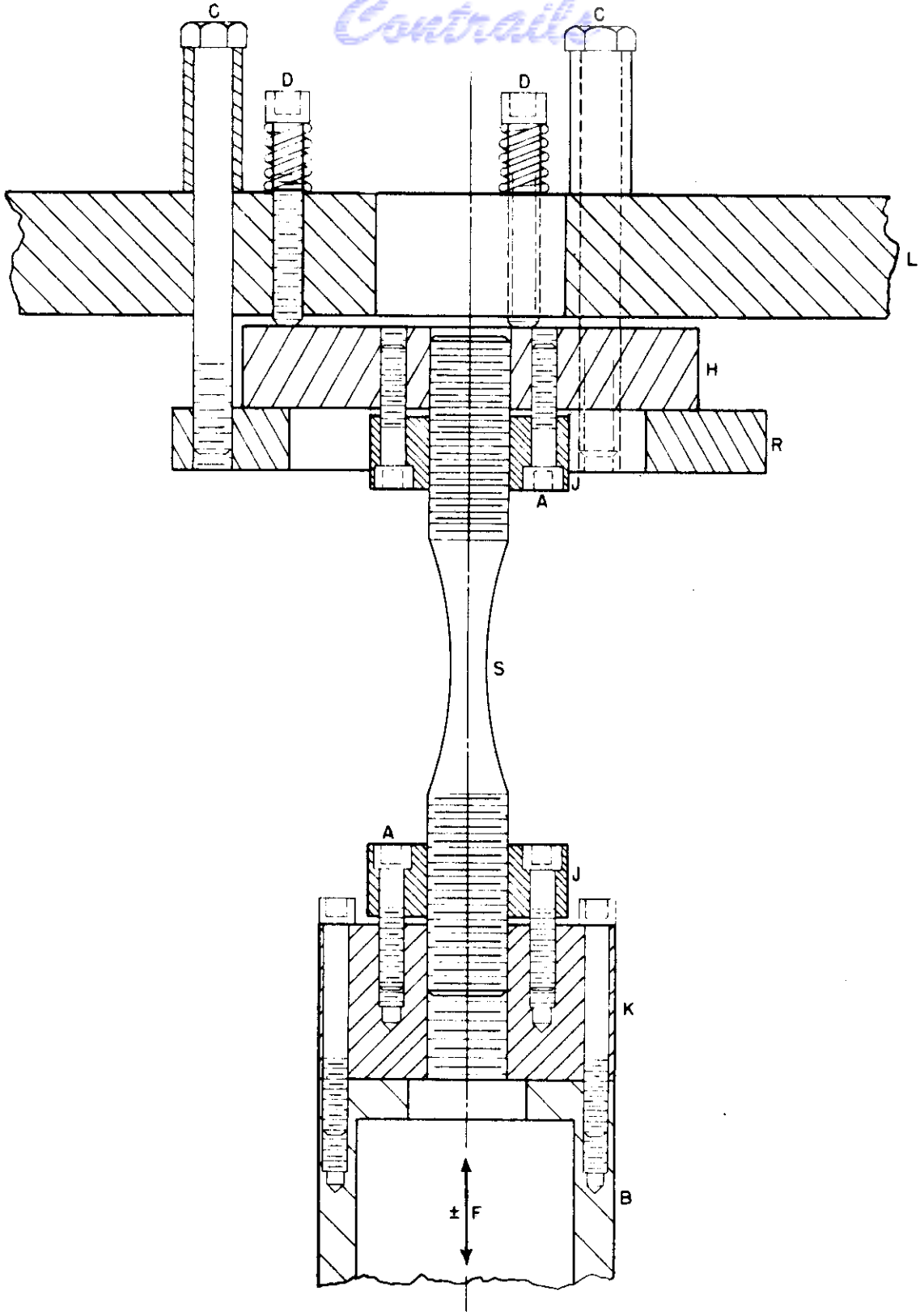

FIG. 7 DIRECT STRESS GRIPS FOR ROOM TEMPERATURE TESTS

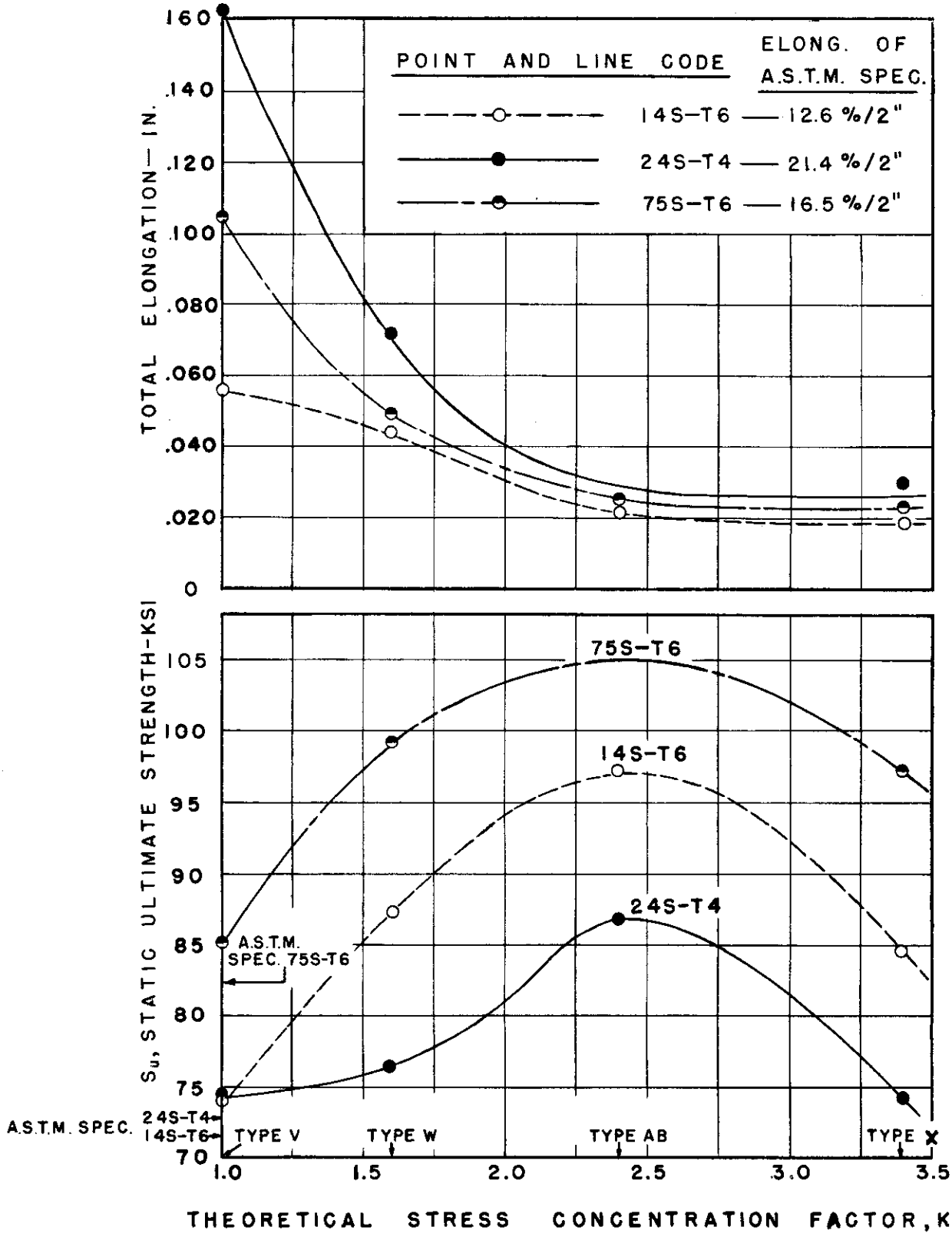

FIG. 8. VARIATION OF STATIC ULTIMATE STRENGTH AND TOTAL ELONGATION WITH TYPE OF SPECIMEN

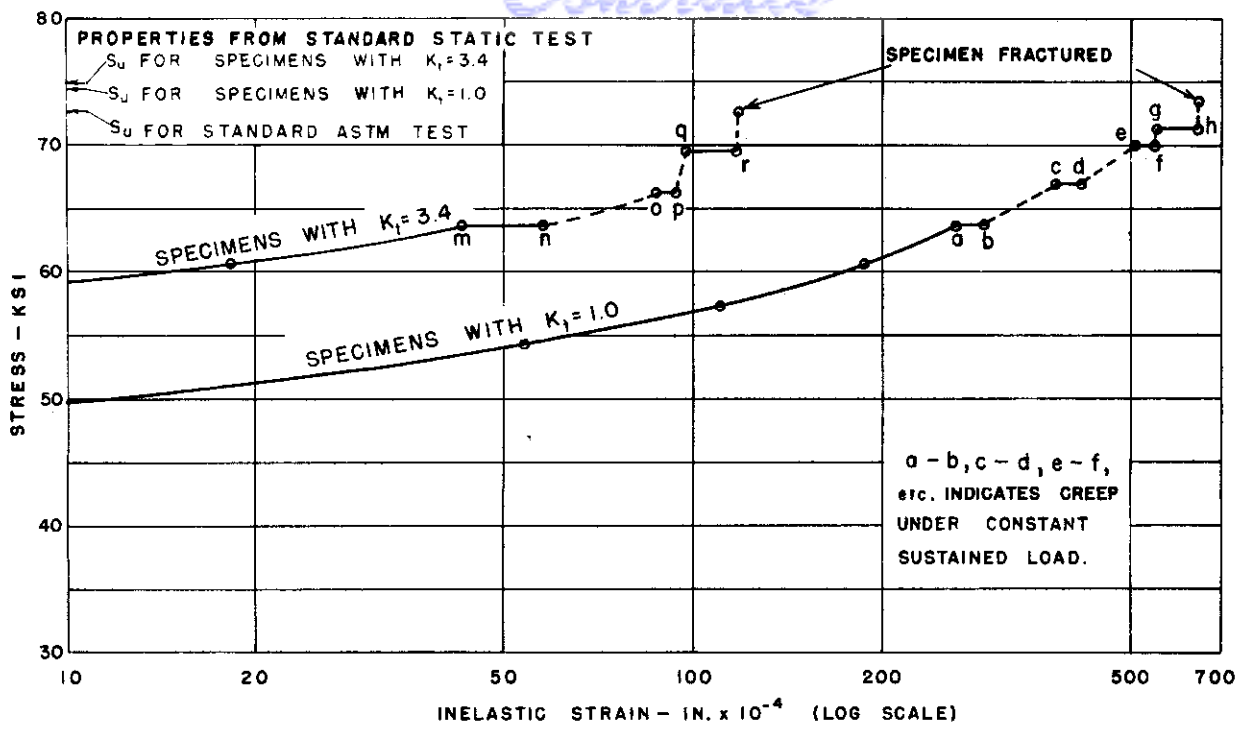

FIG. 9. STRESS - STRAIN CURVE FOR 24S-T4 ALUMINUM ALLOY, UNDER STEP LOADING IN THE INELASTIC RANGE.

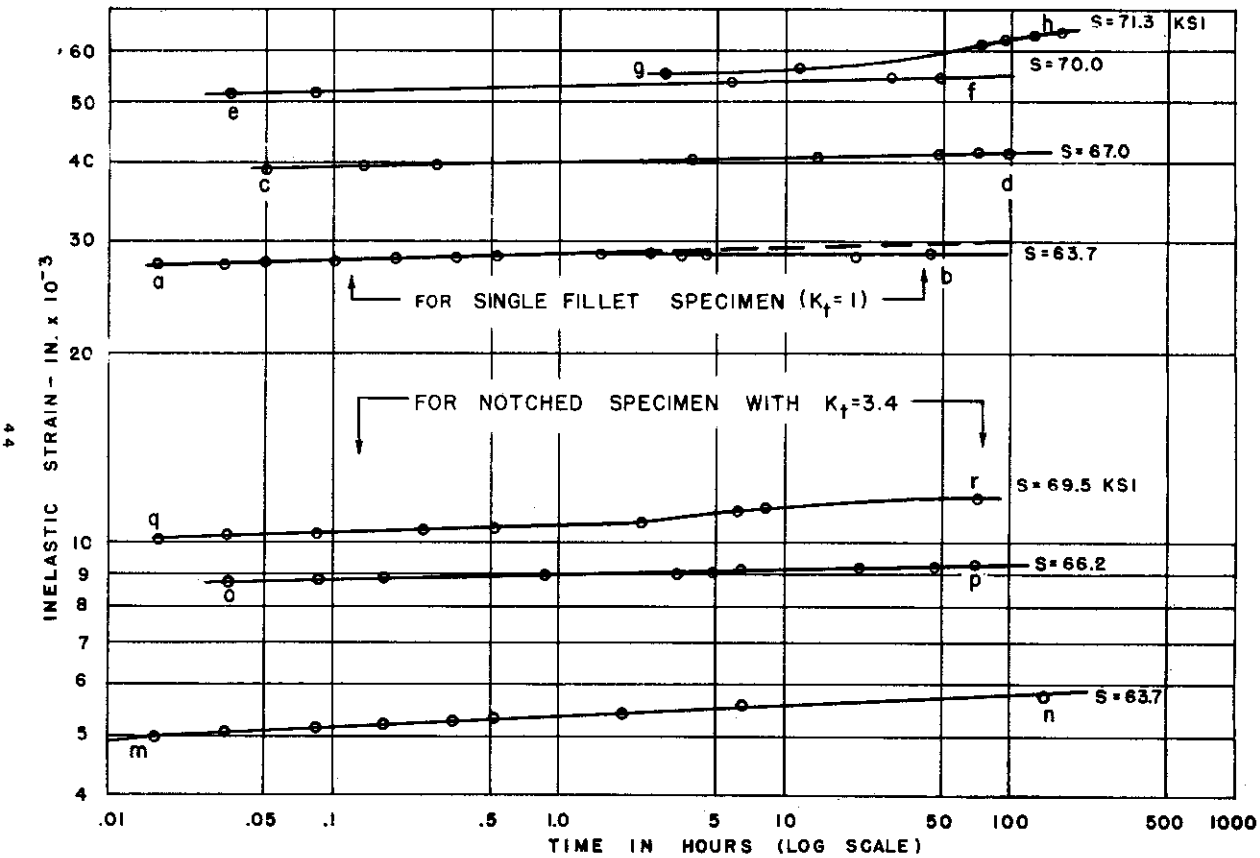

FIG. 10. CREEP-TIME CURVES FOR 24S-T4 AT HIGH STRESSES

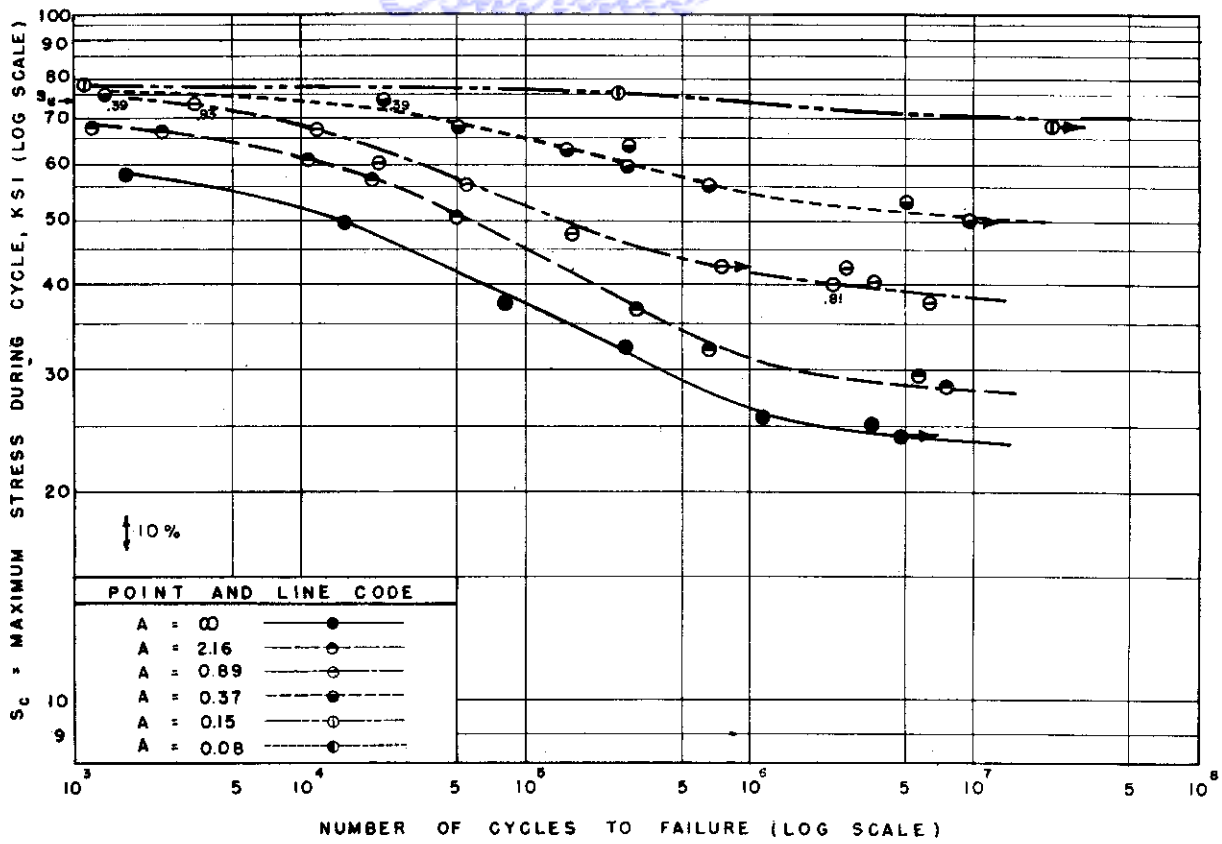

FIG. 11. S-N FATIGUE DIAGRAMS AT VARIOUS STRESS RATIOS FOR K_t = 1.0 SPECIMENS OF ALUMINUM ALLOY 14S-T6 .

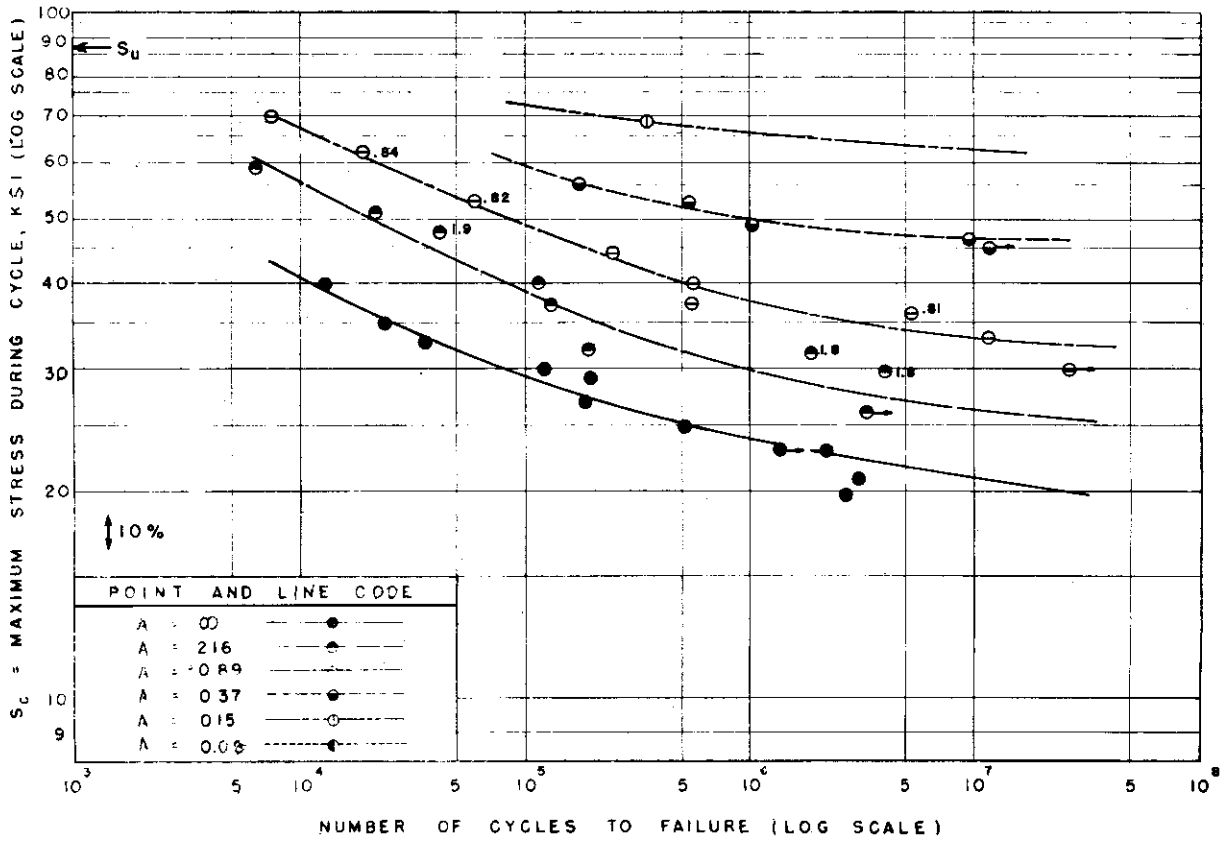

FIG. 12. S-N FATIGUE DIAGRAMS AT VARIOUS STRESS RATIOS FOR K_t = 1.6 SPECIMENS OF ALUMINUM ALLOY 14S-T6.

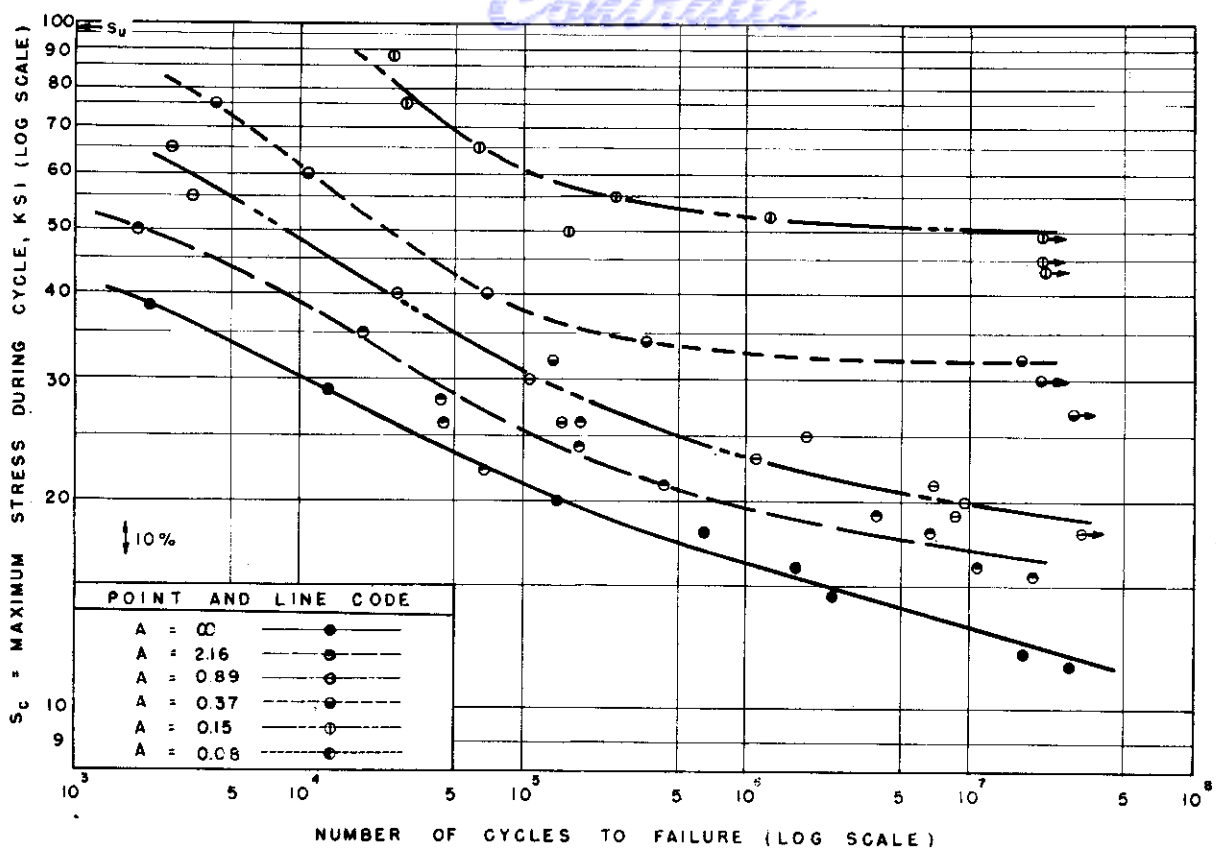

FIG.13. S-N FATIGUE DIAGRAMS AT VARIOUS STRESS RATIOS FOR $K_t = 2.4$ SPECIMENS OF ALUMINUM ALLOY 14S – T6

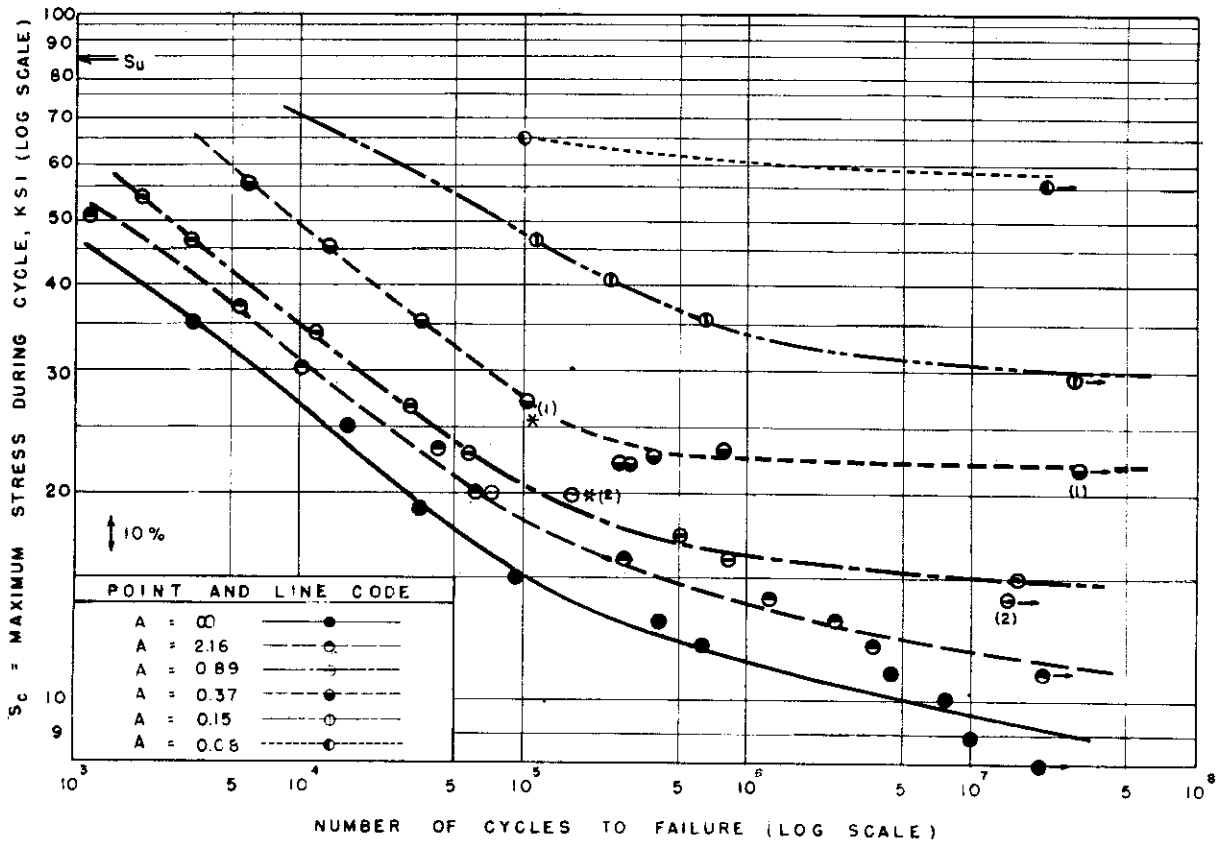

FIG.14. S-N FATIGUE DIAGRAMS AT VARIOUS STRESS RATIOS FOR $K_t = 3.4$ SPECIMENS OF ALUMINUM ALLOY 14S-T6 .

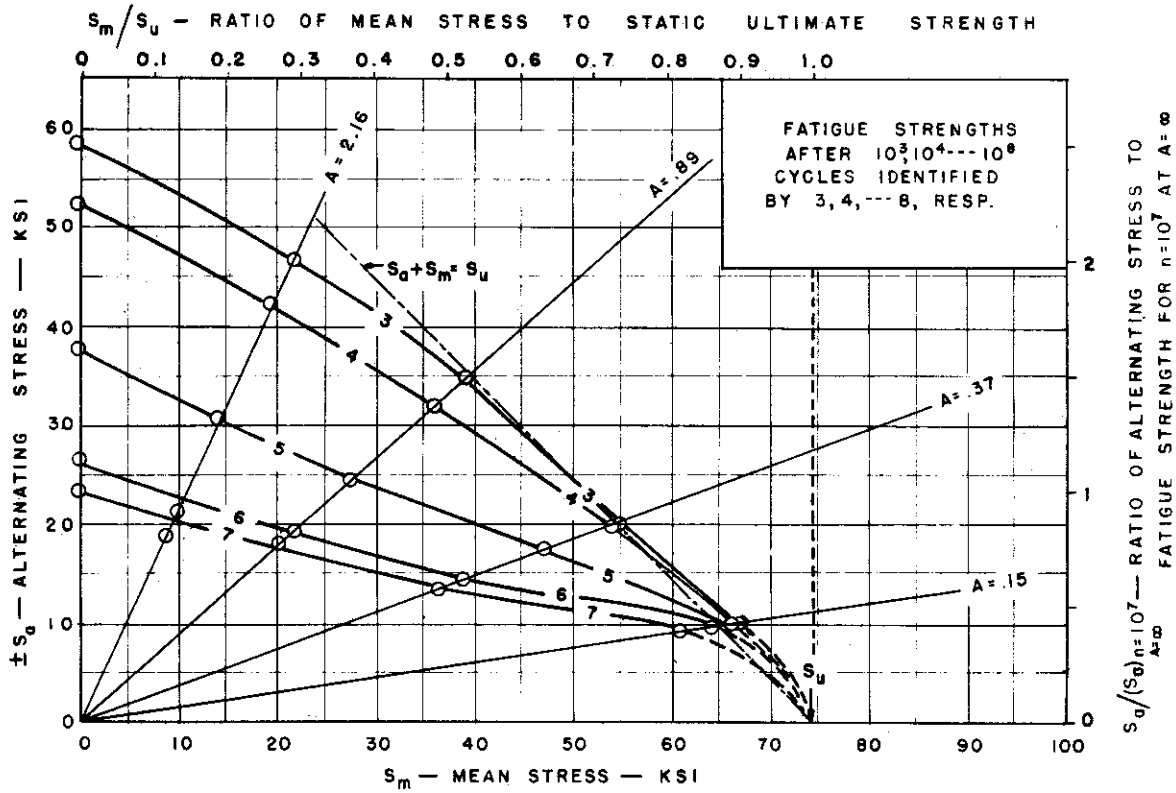

FIG. 15. — STRESS RANGE FATIGUE DIAGRAM FOR $K_t = 1.0$ SPECIMENS OF ALUMINUM ALLOY 14S-T6.

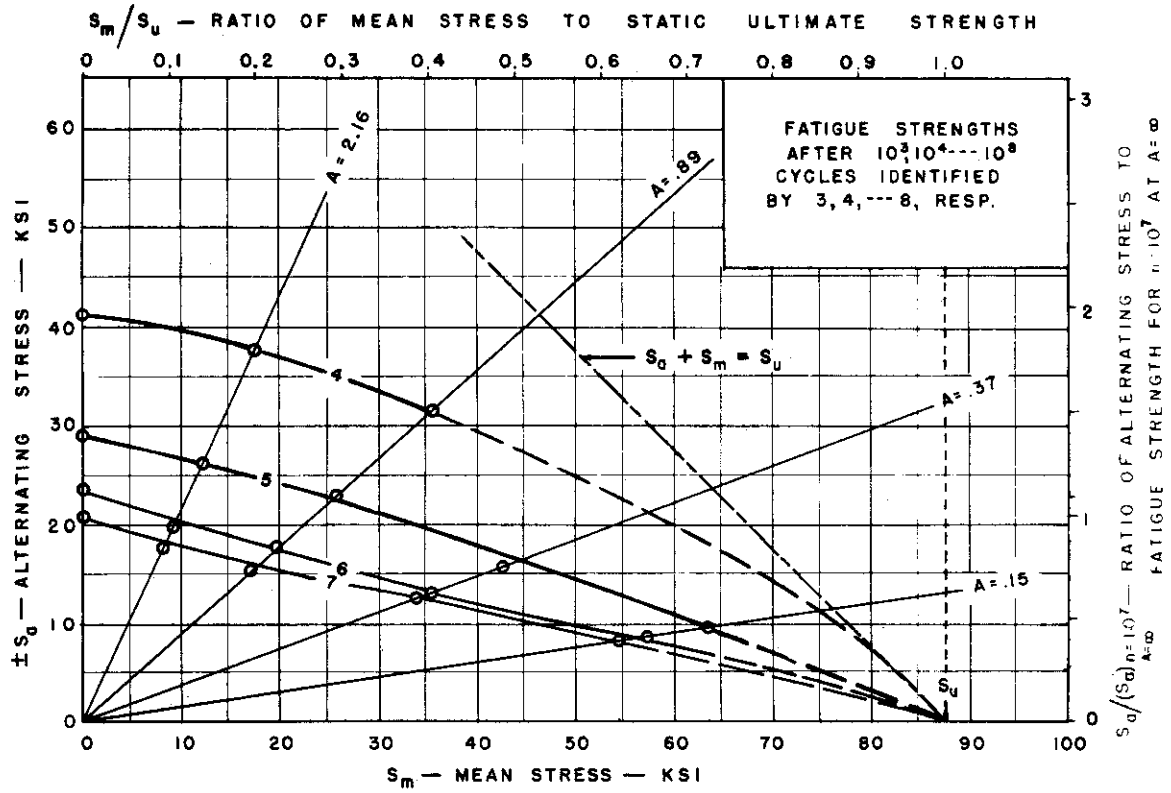

FIG. 16. — STRESS RANGE FATIGUE DIAGRAM FOR $K_t = 1.6$ SPECIMENS OF ALUMINUM ALLOY 14S-T6.

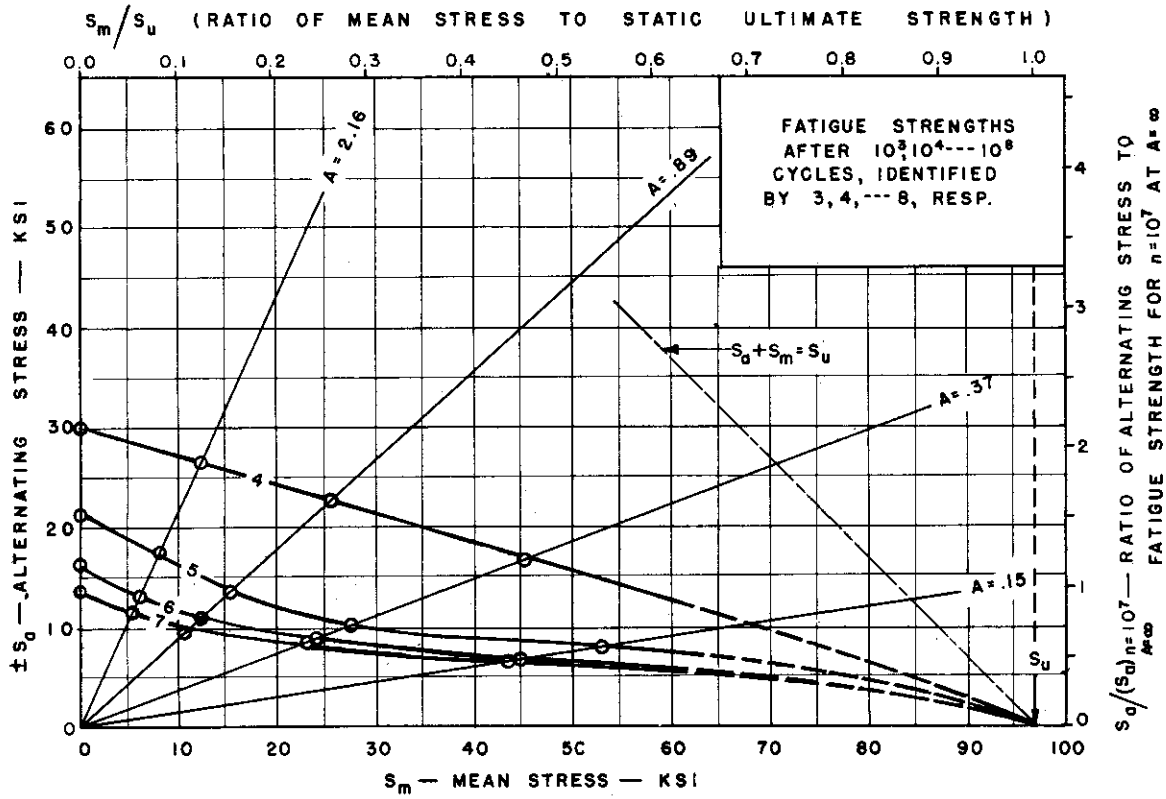

FIG. 17. — STRESS RANGE FATIGUE DIAGRAM FOR $K_t = 2.4$ SPECIMENS OF ALUMINUM ALLOY 14S – T6

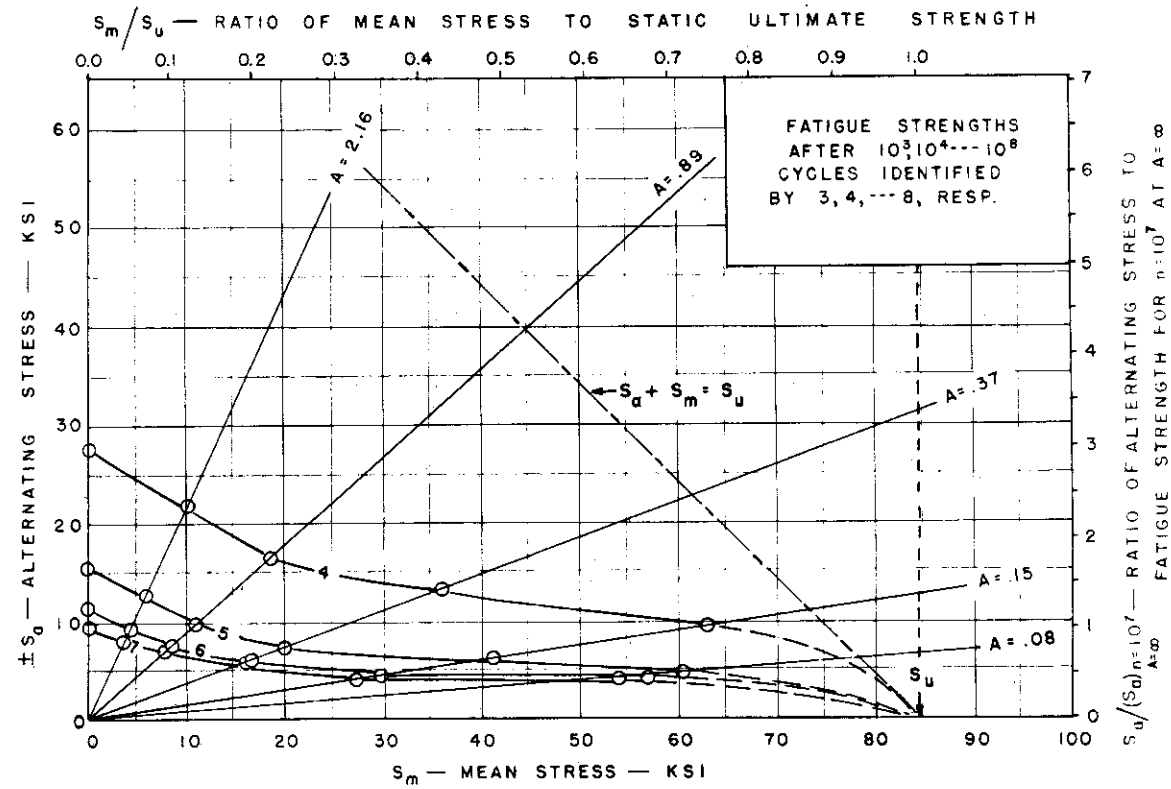

FIG. 18. — STRESS RANGE FATIGUE DIAGRAM FOR $K_t = 3.4$ SPECIMENS OF ALUMINUM ALLOY 14S – T6.

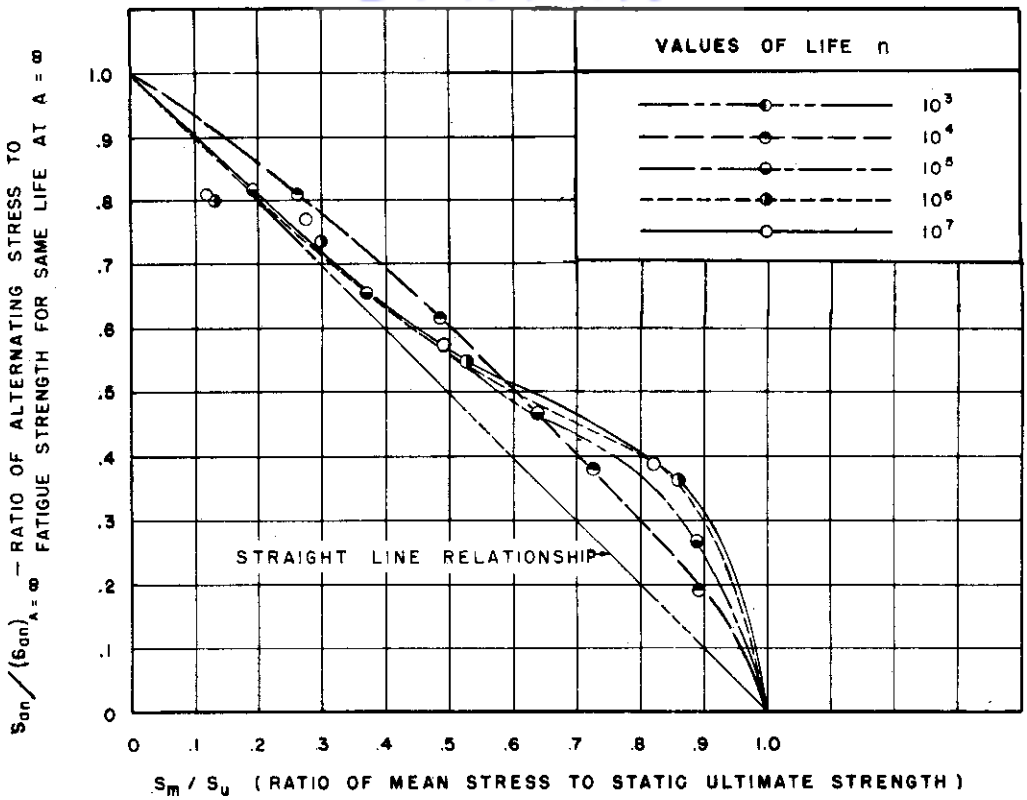

FIG. 19. STRESS RANGE CURVES FOR K_t=1.0 SPECIMENS OF 14S-T6 ALUMINUM ALLOY USING DIMENSIONLESS RATIOS

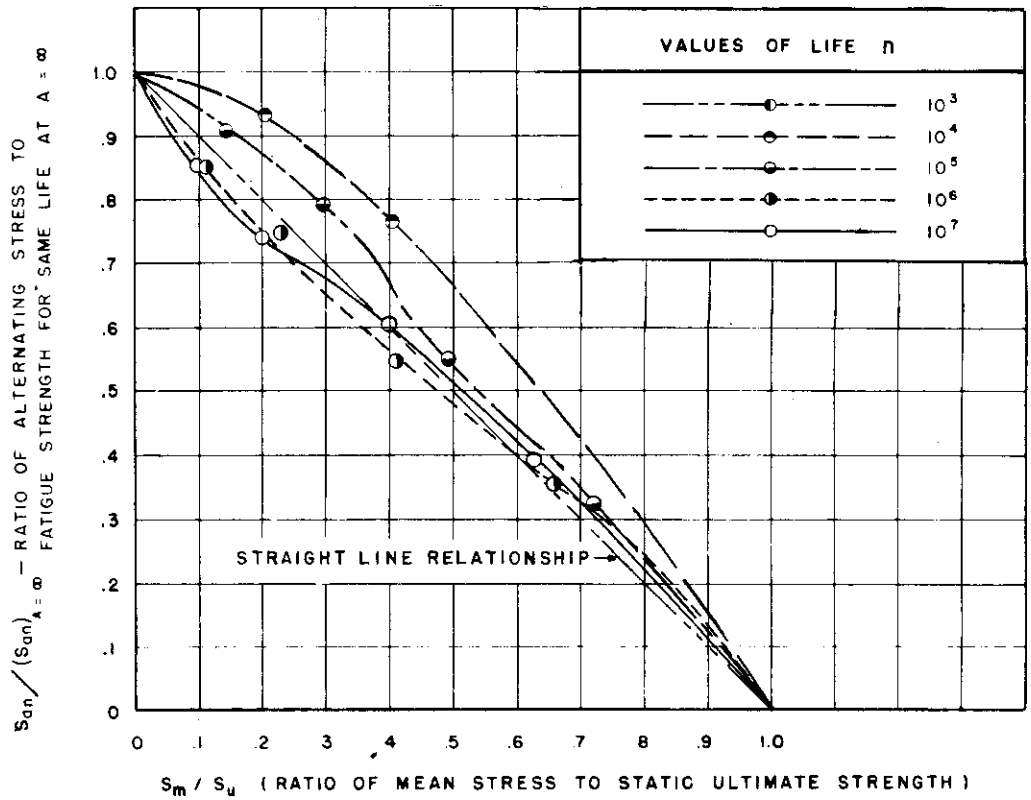

FIG. 20. STRESS RANGE CURVES FOR K_t=1.6 SPECIMENS OF 14S-T6 ALUMINUM ALLOY USING DIMENSIONLESS RATIOS

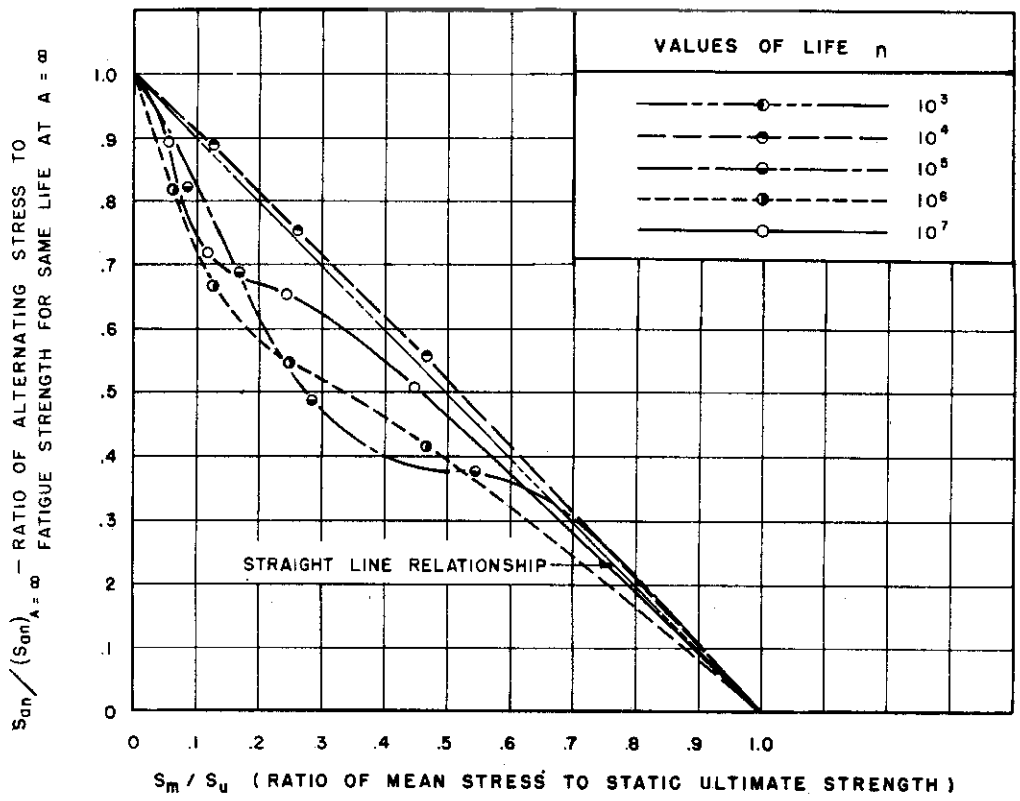

FIG. 21. STRESS RANGE CURVES FOR K_t=2.4 SPECIMENS OF 14S—T6 ALUMINUM ALLOY USING DIMENSIONLESS RATIOS

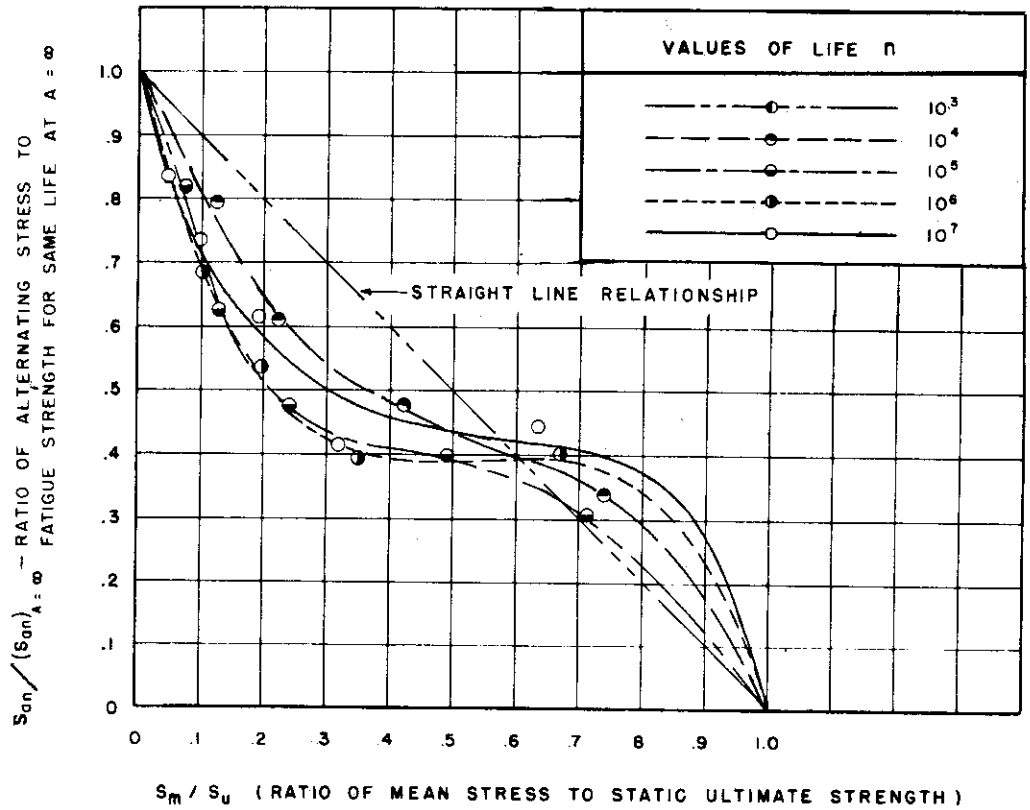

FIG. 22. STRESS RANGE CURVES FOR K_t=3.4 SPECIMENS OF 14S—T6 ALUMINUM ALLOY USING DIMENSIONLESS RATIOS

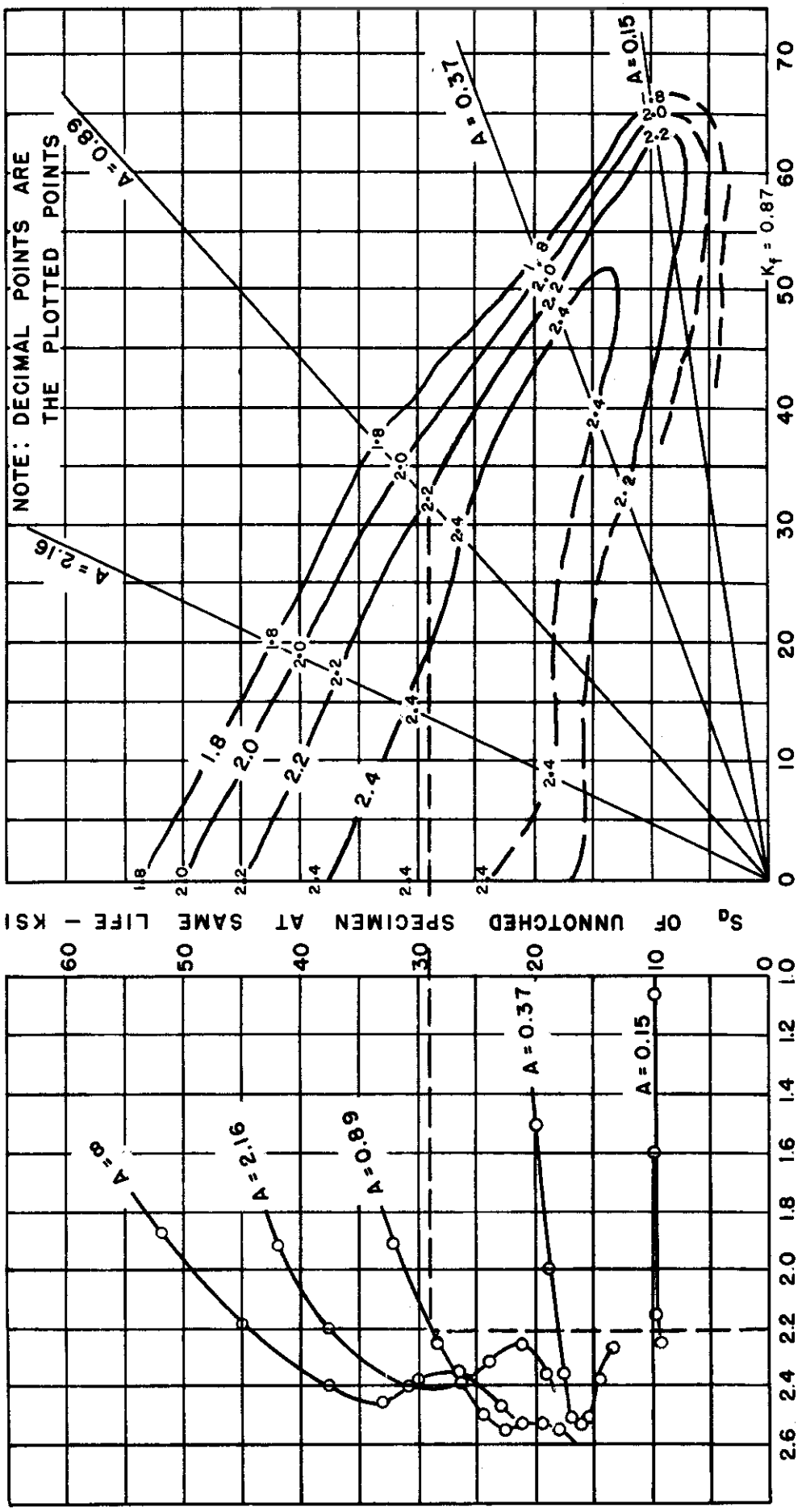

FIG.23(b) CONTOUR CURVES SHOWING K_f AS A FUNCTION OF S_a & S_m OF UNNOTCHED SPECIMEN FOR K_f=3.4 SPECIMENS OF ALUMINUM ALLOY 14S-T6

FIG 23(a) PROFILE CURVES OF K_f VS S_a OF UNNOTCHED SPECIMEN FOR K_f=3.4 SPECIMENS OF ALUMINUM ALLOY 14S-T6

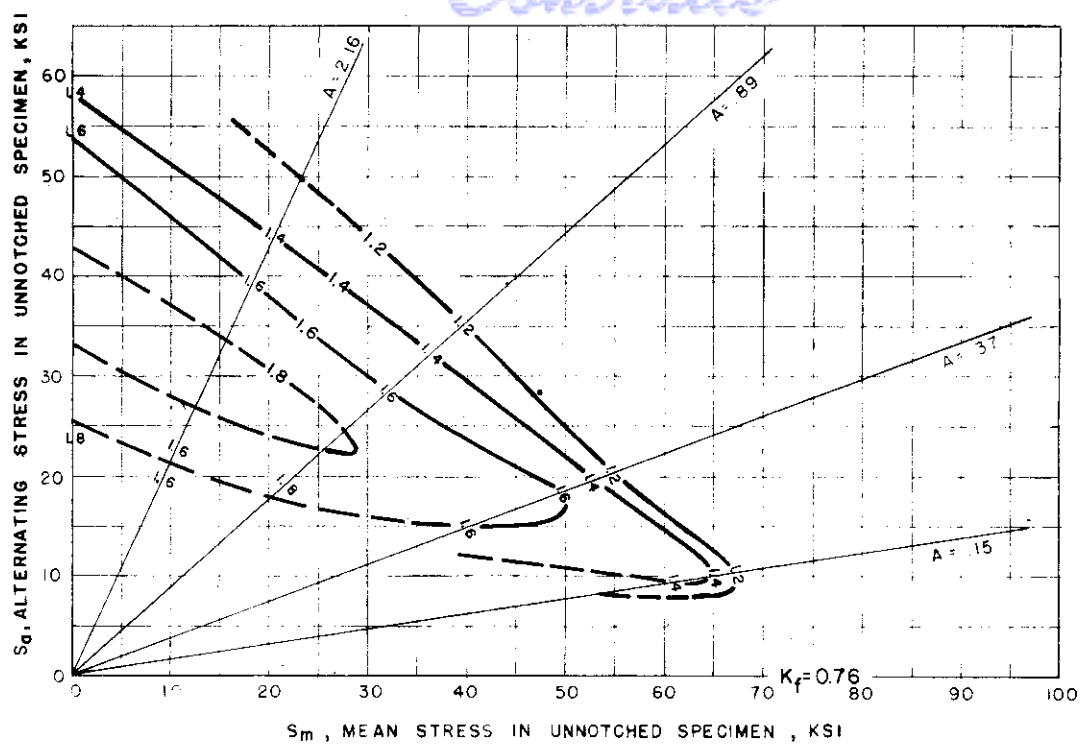

FIG. 24 FATIGUE STRENGTH - REDUCTION "CONTOUR" CURVES FOR K_t = 2.4 SPECIMENS OF ALUMINUM ALLOY 14S-T6 SHOWING K_f AS A FUNCTION OF S_a AND S_m OF THE UNNOTCHED SPECIMEN.

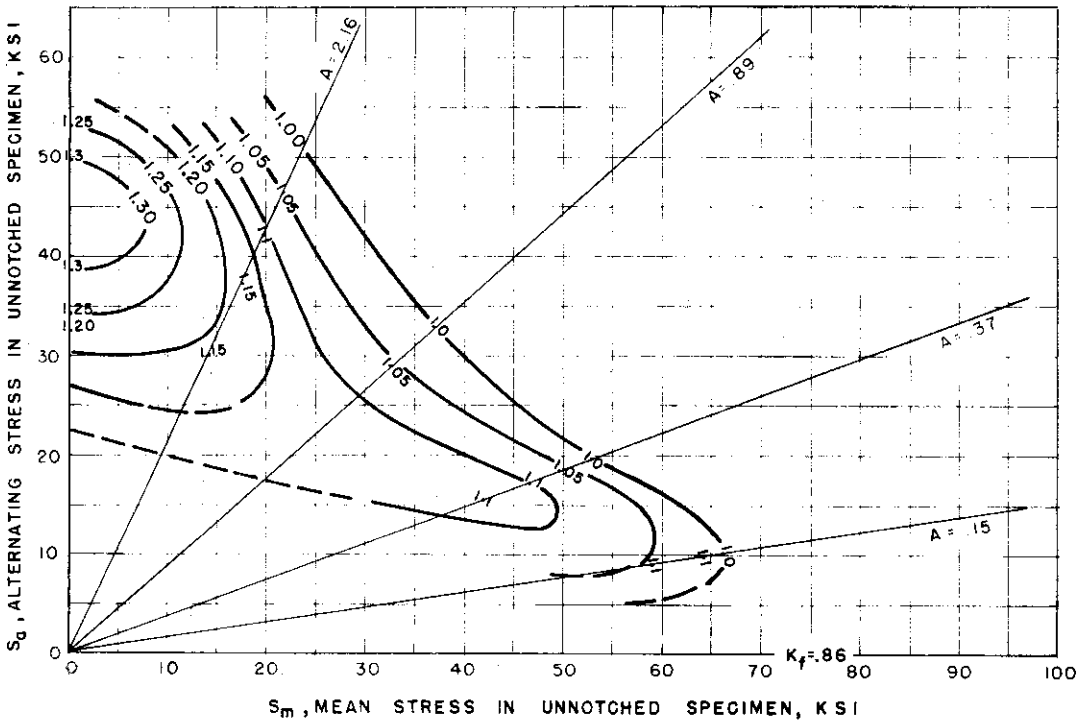

FIG. 25. FATIGUE STRENGTH - REDUCTION "CONTOUR" CURVES FOR K_t = 1.6 SPECIMENS OF ALUMINUM ALLOY 14S-T6 SHOWING K_f AS A FUNCTION OF S_a AND S_m OF THE UNNOTCHED SPECIMEN.

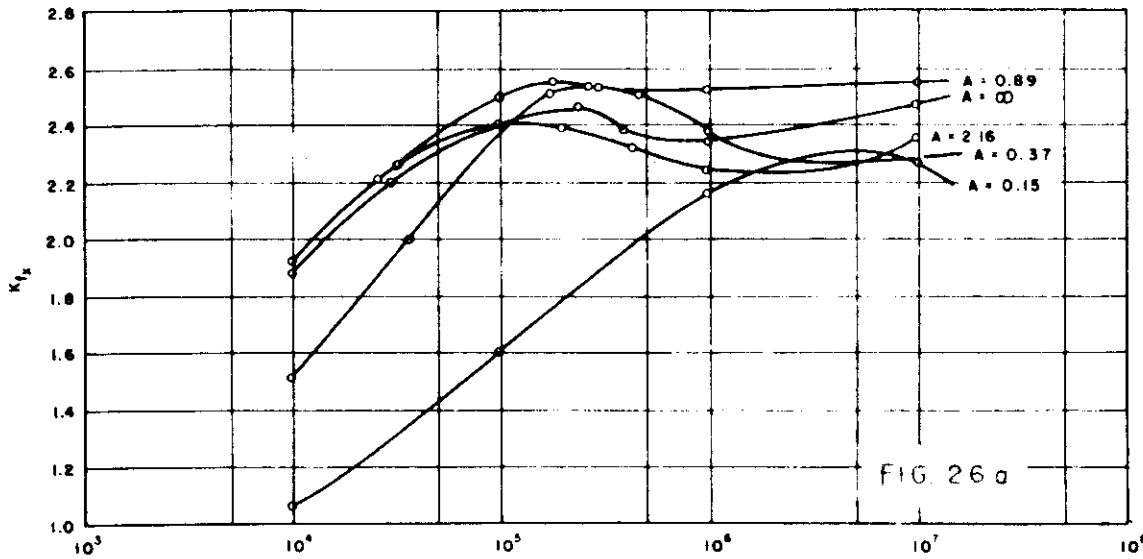

FIG 26a PROFILE CURVES OF K_f vs. N FOR $K_t = 3.4$ SPECIMENS OF ALUMINUM ALLOY 14S-T6

FIG 26b PROFILE CURVES OF K_f vs. STRESS RATIO R FOR $K_t = 3.4$ SPECIMENS OF ALUMINUM ALLOY 14S-T6

FIG 26c CONTOUR CURVES SHOWING K_f AS A FUNTION OF STRESS RATIO AND NUMBER OF CYCLES FOR $K_t = 3.4$ SPECIMENS OF ALUMINUM ALLOY 14S-T6.

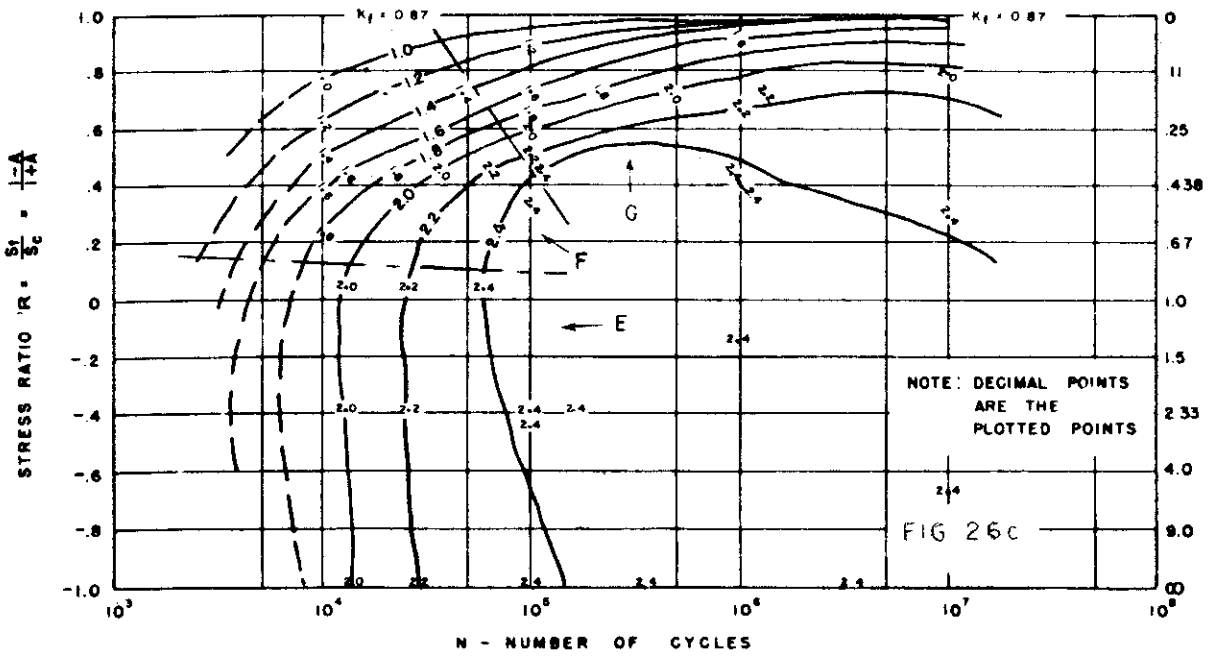

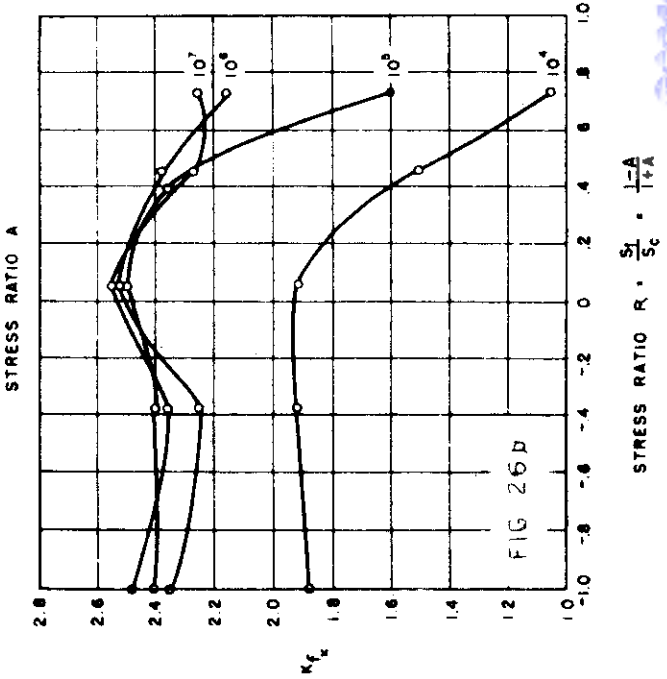

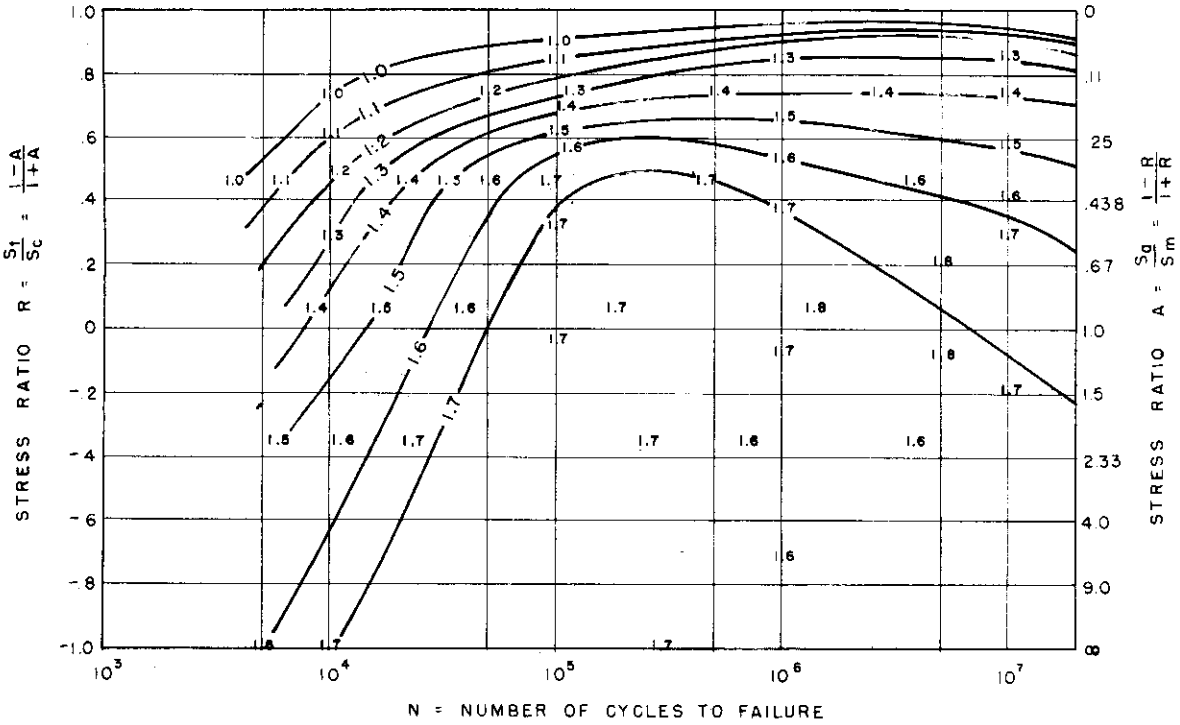

FIG. 27 FATIGUE STRENGTH REDUCTION "CONTOUR" CURVES FOR $K_t = 2.4$ SPECIMENS OF ALUMINUM ALLOY 14S-T6 SHOWING K_f AS A FUNCTION OF N AND STRESS RATIO R

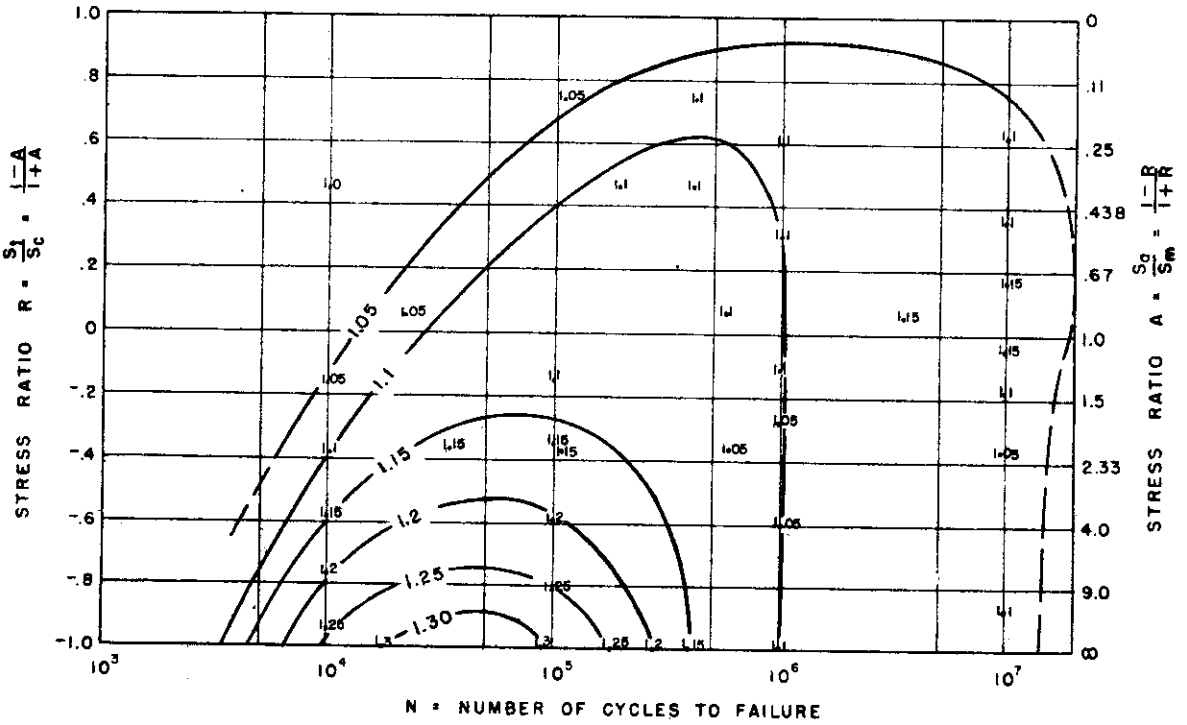

FIG. 28. FATIGUE STRENGTH - REDUCTION "CONTOUR" CURVES FOR $K_t = 1.6$ SPECIMENS OF ALUMINUM ALLOY 14S-T6 SHOWING K_f AS A FUNCTION OF N AND STRESS RATIO R

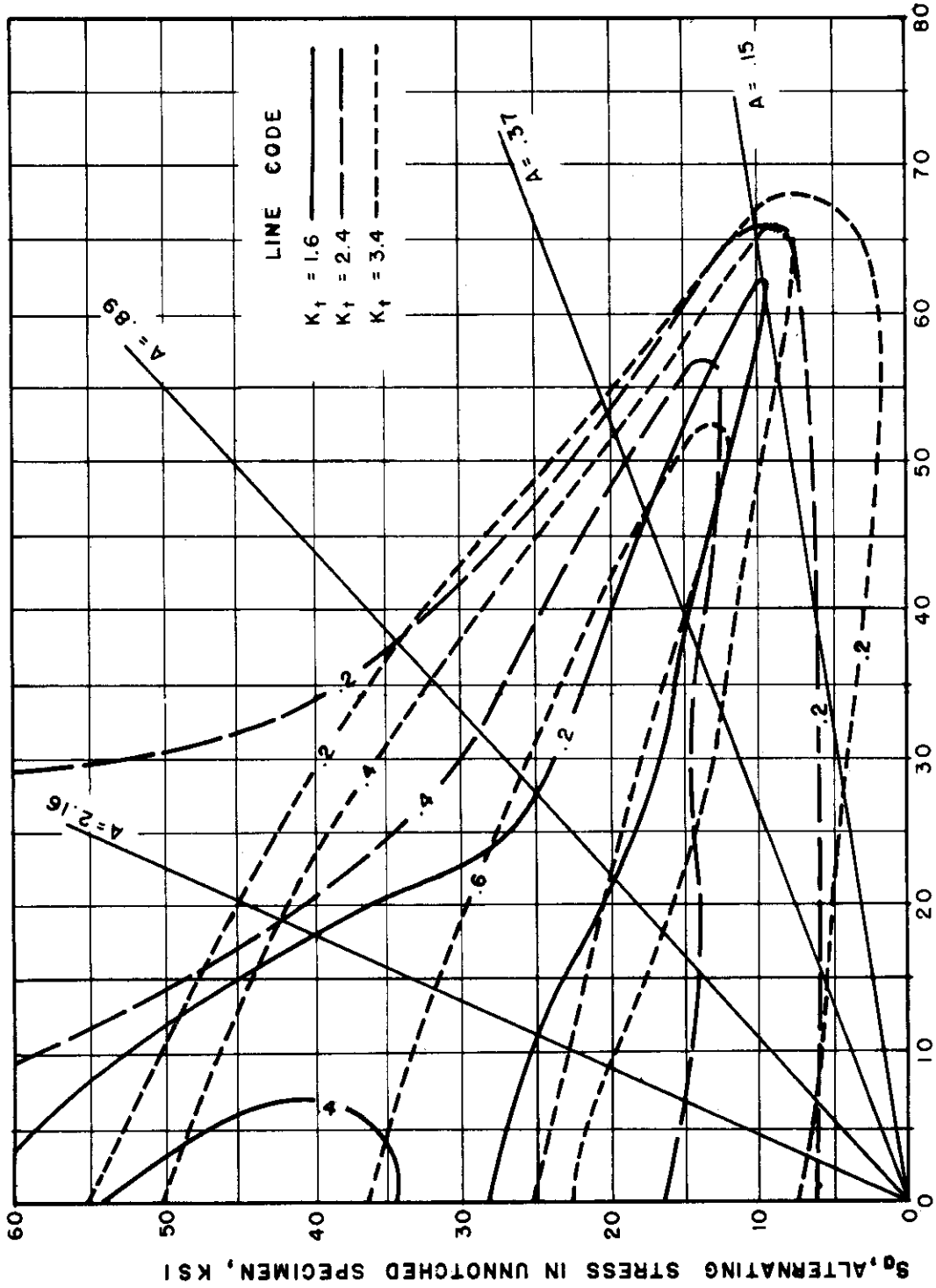

FIG. 29 NOTCH SENSITIVITY INDEX CURVES FOR K_t = 1.6, 2.4, AND 3.4 SPECIMENS OF ALUMINUM ALLOY 14S-T6 SHOWING q AS A FUNCTION OF S_a AND S_m OF THE UNNOTCHED SPECIMEN

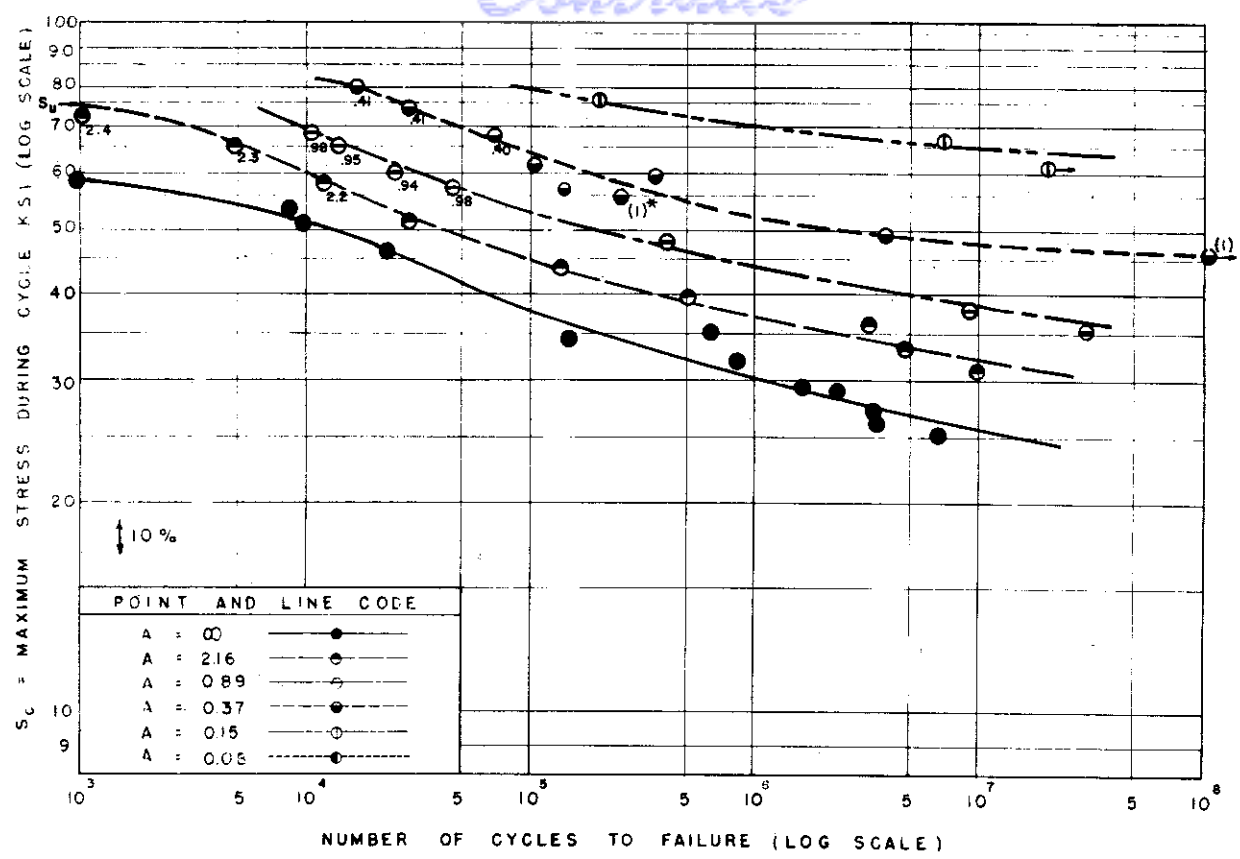

FIG. 30 S-N FATIGUE DIAGRAMS AT VARIOUS STRESS RATIOS FOR K_t = 1.0 SPECIMENS OF ALUMINUM ALLOY 24S-T4.

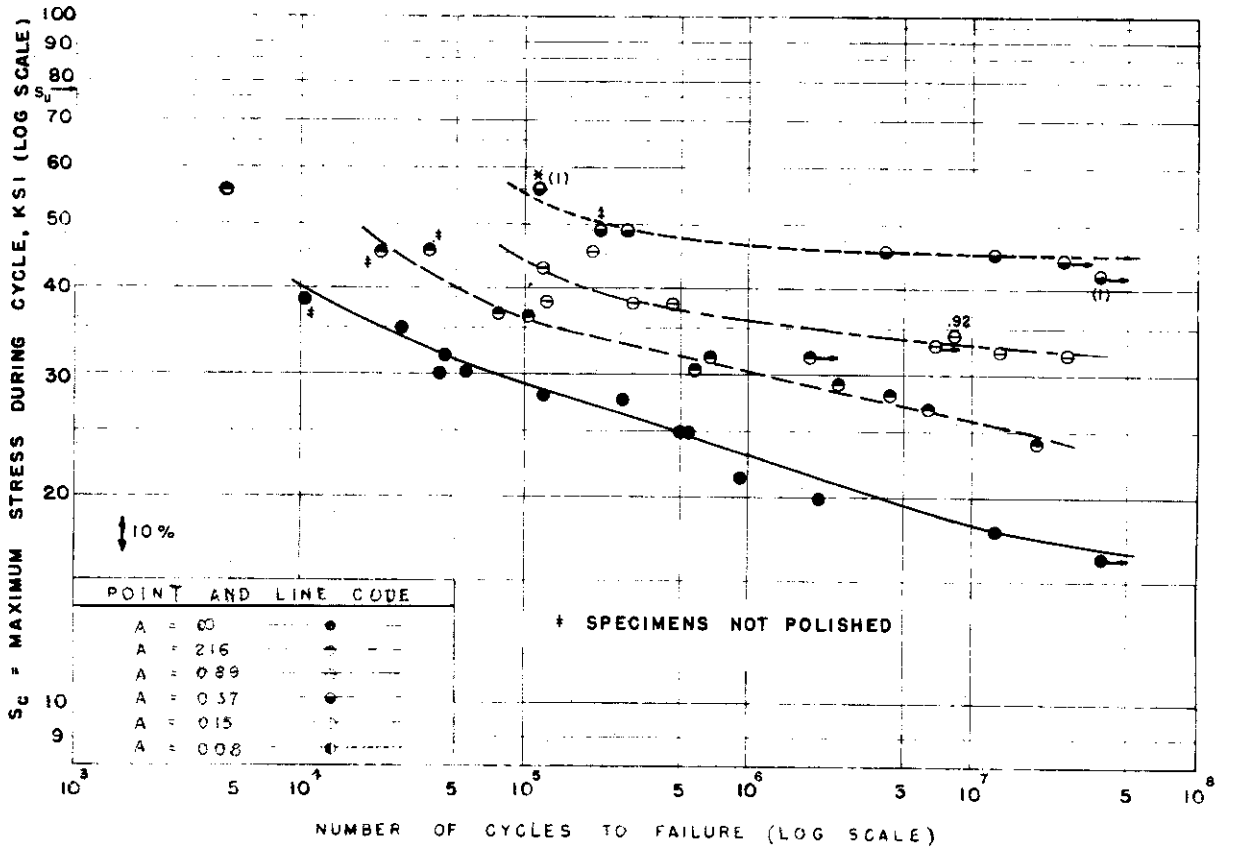

FIG. 31 S-N FATIGUE DIAGRAMS AT VARIOUS STRESS RATIOS FOR K_t = 1.0 SPECIMENS OF ALUMINUM ALLOY 24S-T4

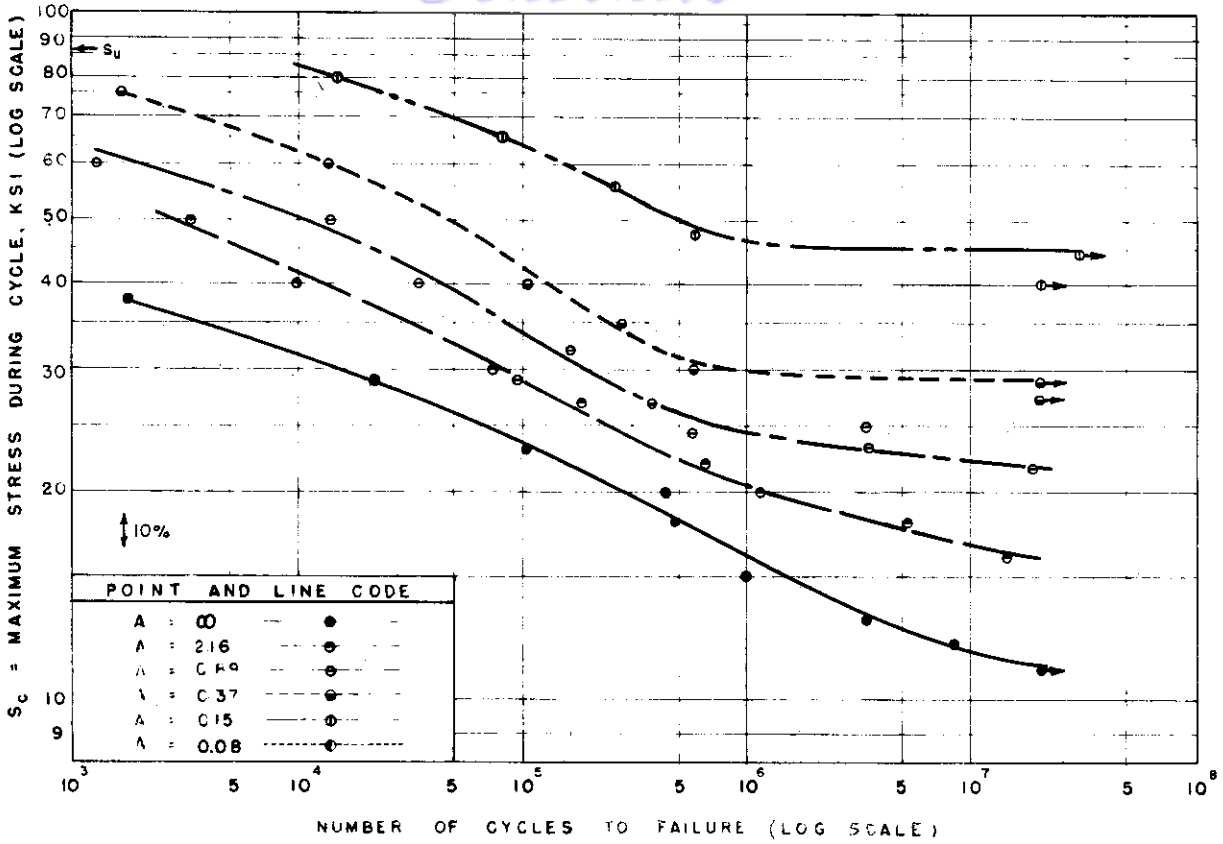

FIG.32 S-N FATIGUE DIAGRAMS AT VARIOUS STRESS RATIOS FOR $K_t = 2.4$ SPECIMENS OF ALUMINUM ALLOY 24S T4

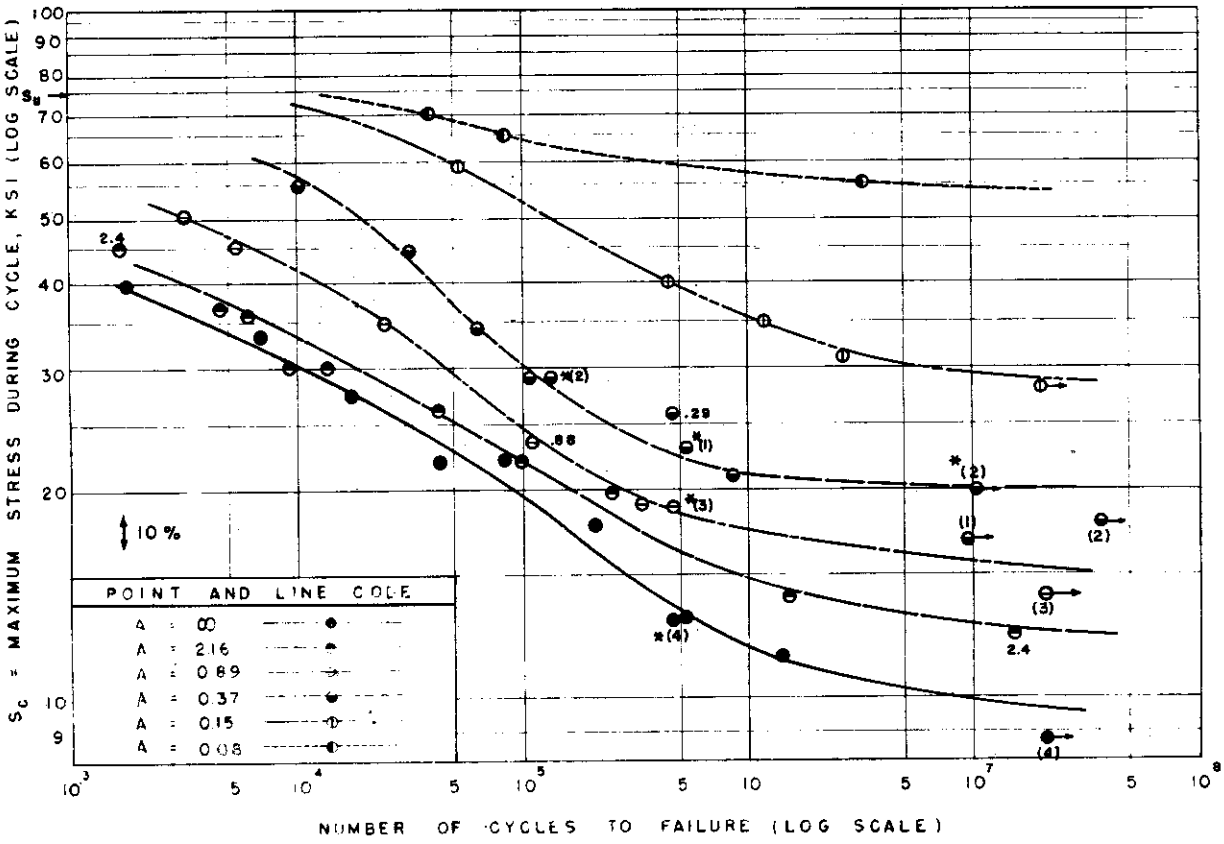

FIG.33 S-N FATIGUE DIAGRAMS AT VARIOUS STRESS RATIOS FOR $K_t = 3.4$ SPECIMENS OF ALUMINUM ALLOY 24S-T4.

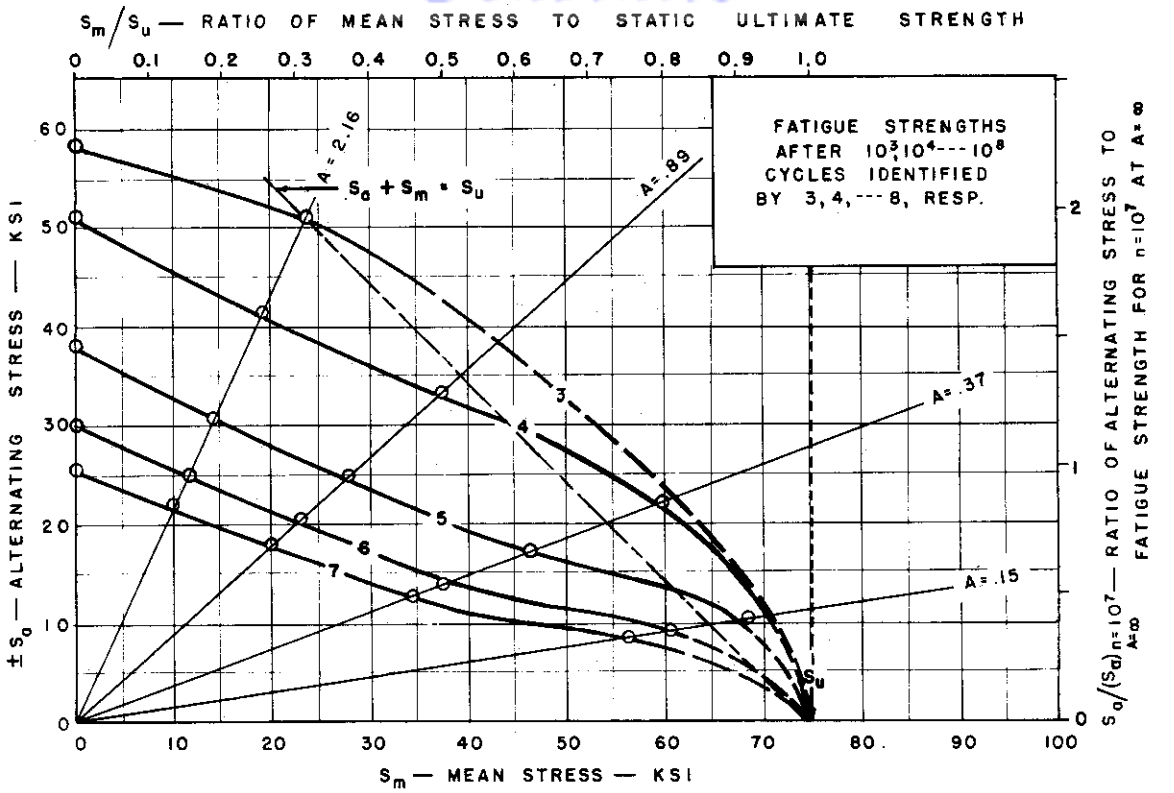

FIG.34. — STRESS RANGE FATIGUE DIAGRAM FOR K_t=1.0 SPECIMENS OF ALUMINUM ALLOY 24S-T4

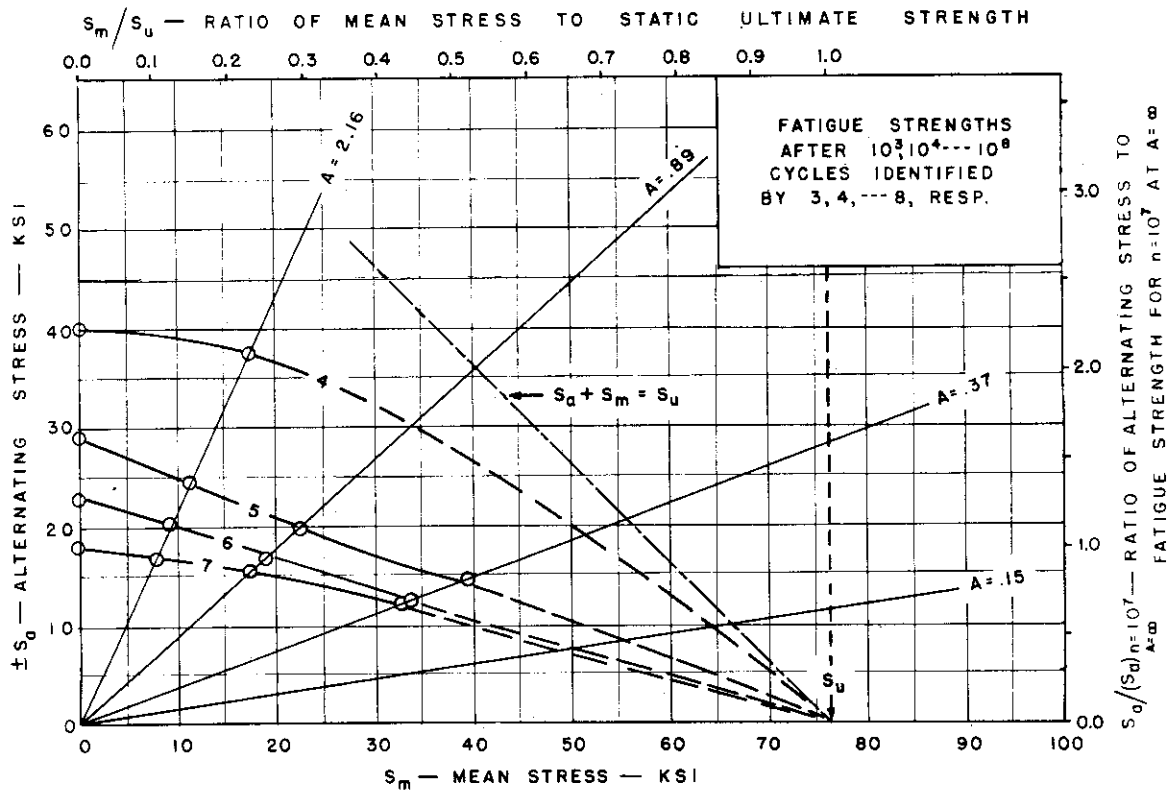

FIG. 35. — STRESS RANGE FATIGUE DIAGRAM FOR K_t=1.6 SPECIMENS OF ALUMINUM ALLOY 24S-T4.

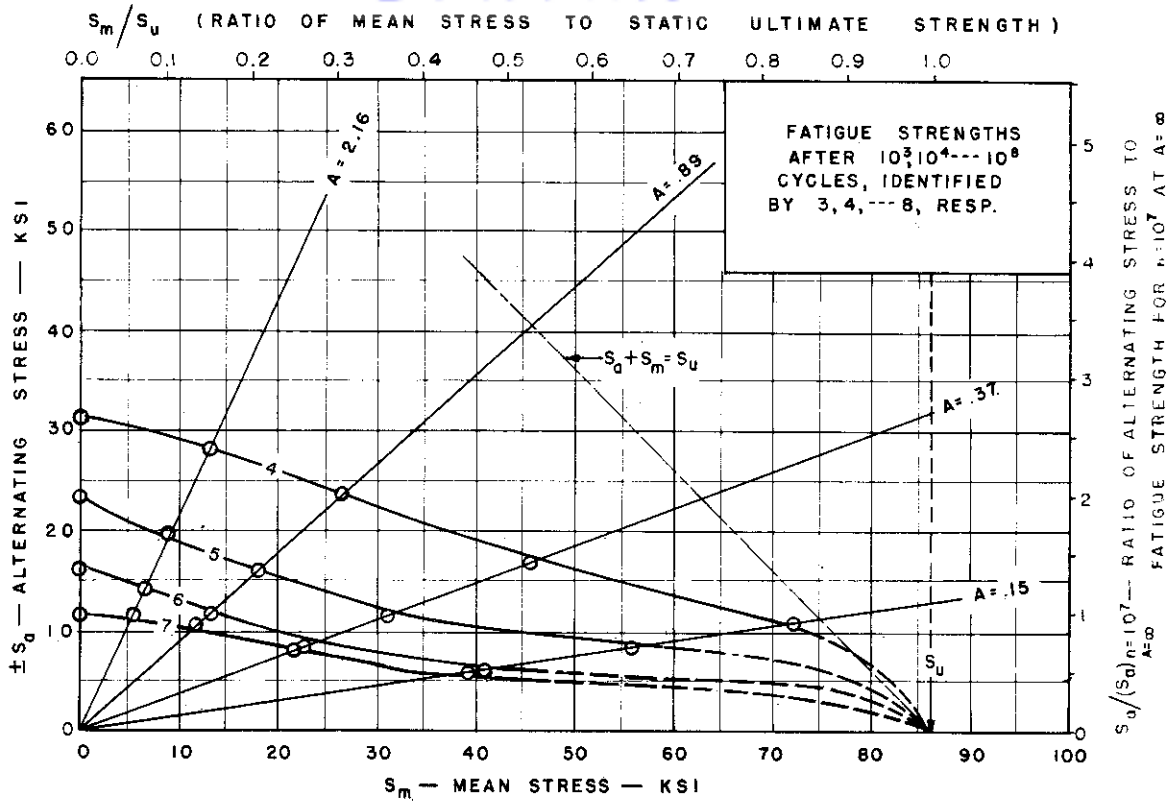

FIG. 36. — STRESS RANGE FATIGUE DIAGRAM FOR $K_t = 2.4$
SPECIMENS OF ALUMINUM ALLOY 24S — T4

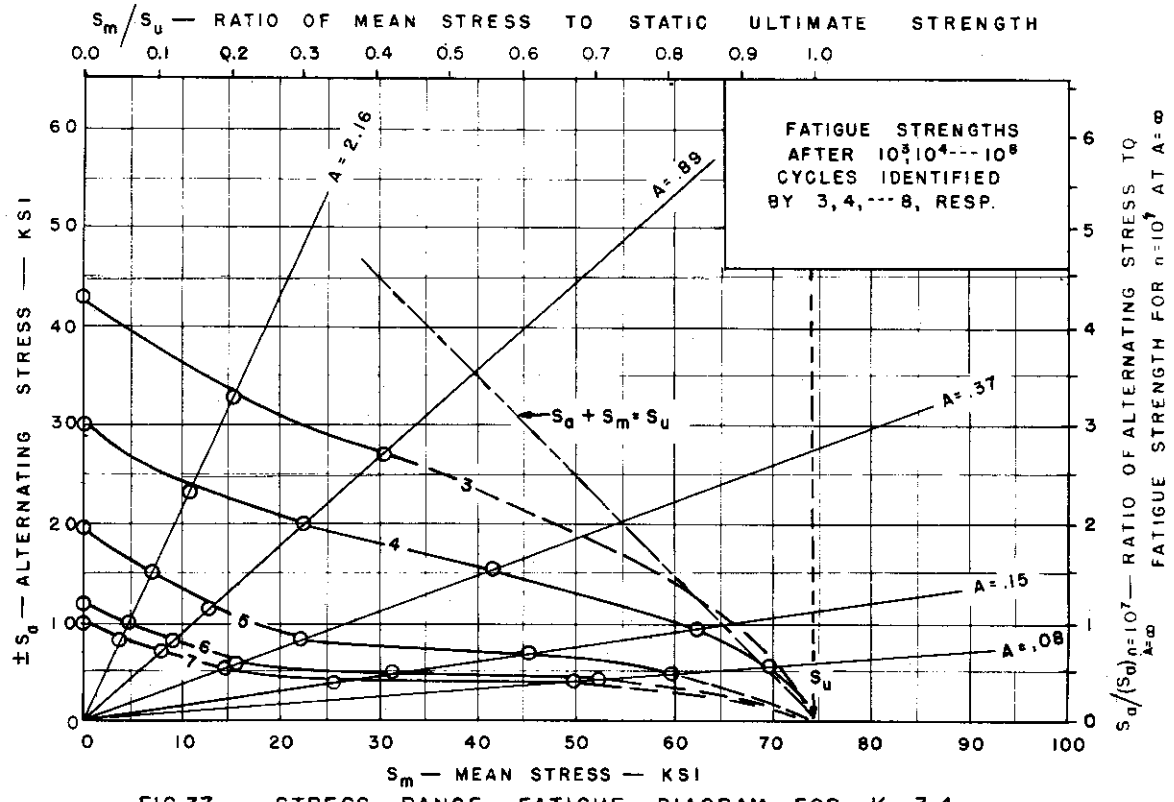

FIG. 37. — STRESS RANGE FATIGUE DIAGRAM FOR $K_t = 3.4$
SPECIMENS OF ALUMINUM ALLOY 24S-T4

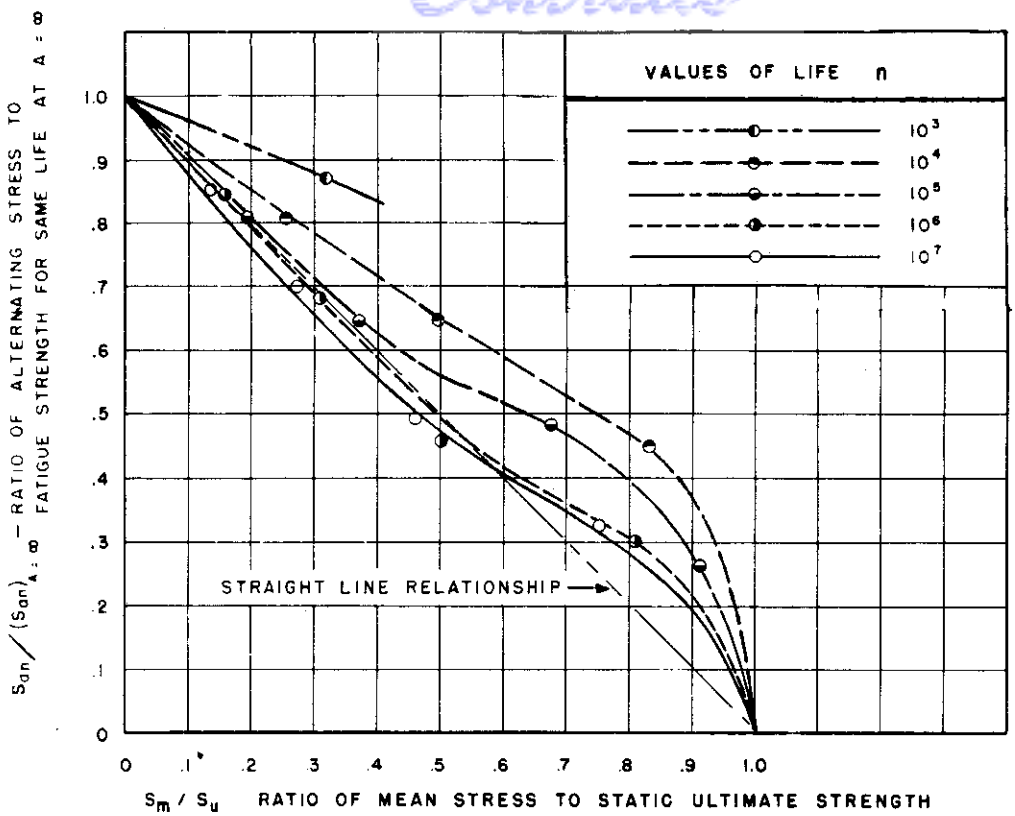

FIG.38. STRESS RANGE CURVES FOR K_t=1.0 SPECIMENS OF 24S-T4 ALUMINUM ALLOY USING DIMENSIONLESS RATIOS

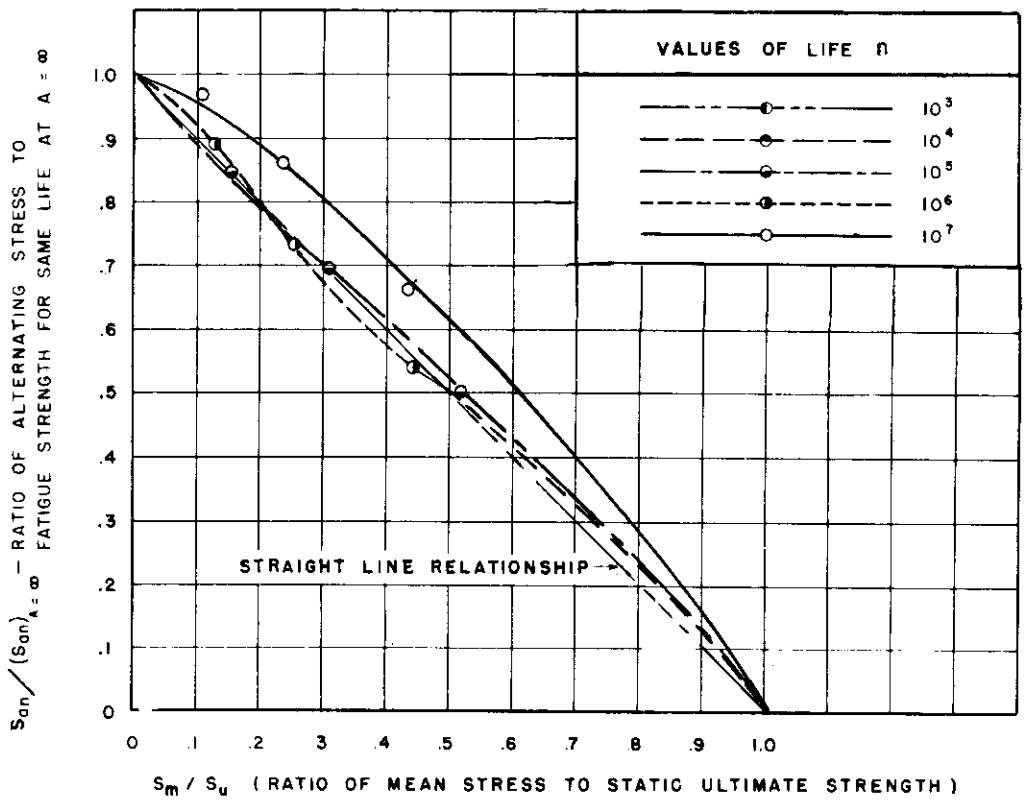

FIG.39. STRESS RANGE CURVES FOR K_t=1.6 SPECIMENS OF 24S-T4 ALUMINUM ALLOY USING DIMENSIONLESS RATIOS

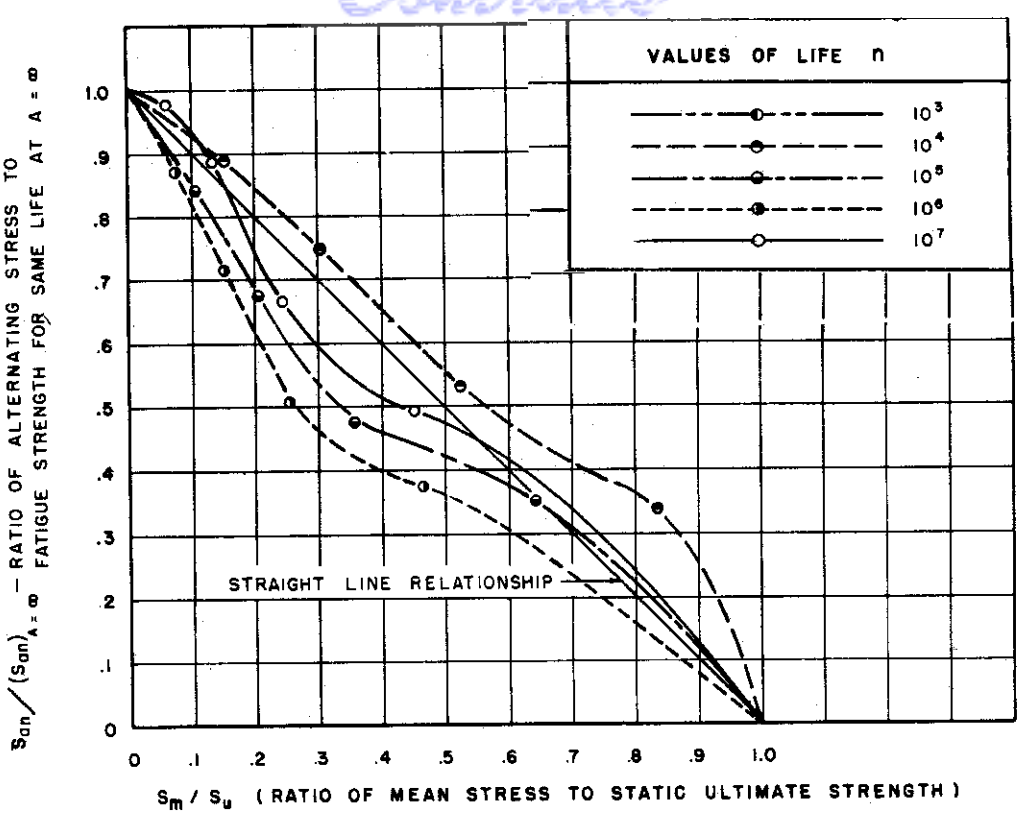

FIG.40. STRESS RANGE CURVES FOR $K_t = 2.4$ SPECIMENS OF 24S-T4 ALUMINUM ALLOY USING DIMENSIONLESS RATIOS

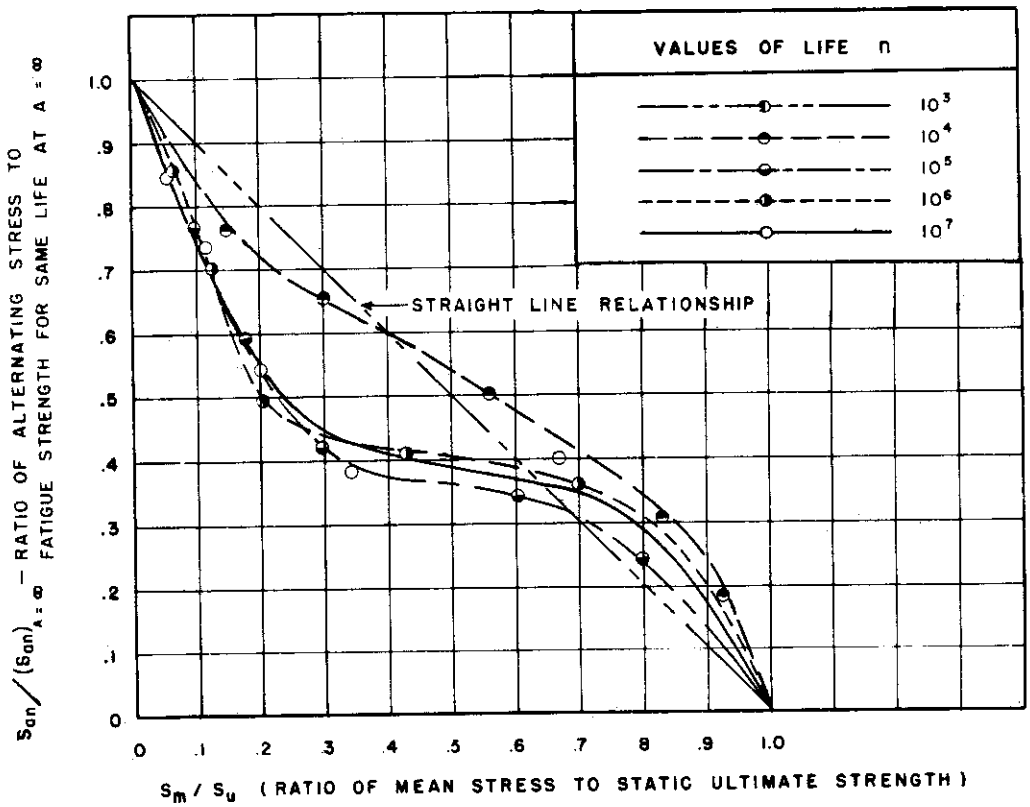

FIG.41. STRESS RANGE CURVES FOR $K_t = 3.4$ SPECIMENS OF 24S-T4 ALUMINUM ALLOY USING DIMENSIONLESS RATIOS

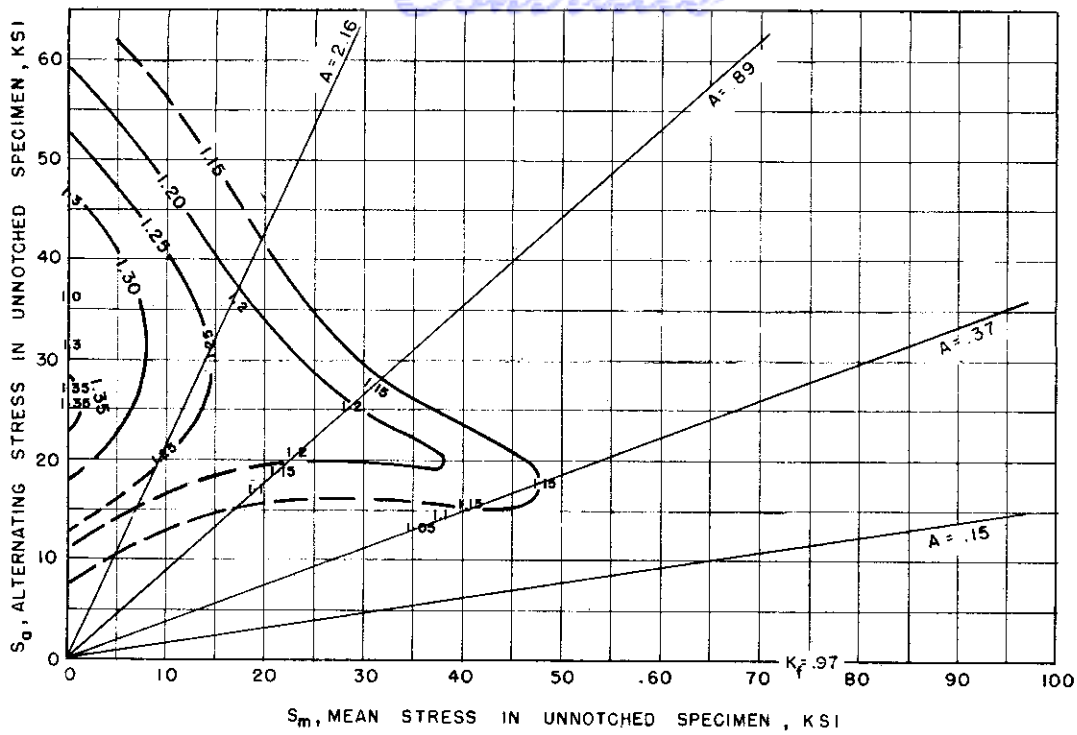

FIG. 42. FATIGUE STRENGTH - REDUCTION "CONTOUR" CURVES FOR K_t = 1.6 SPECIMENS OF ALUMINUM ALLOY 24S-T4 SHOWING K_f AS A FUNCTION OF S_a AND S_m OF THE UNNOTCHED SPECIMEN.

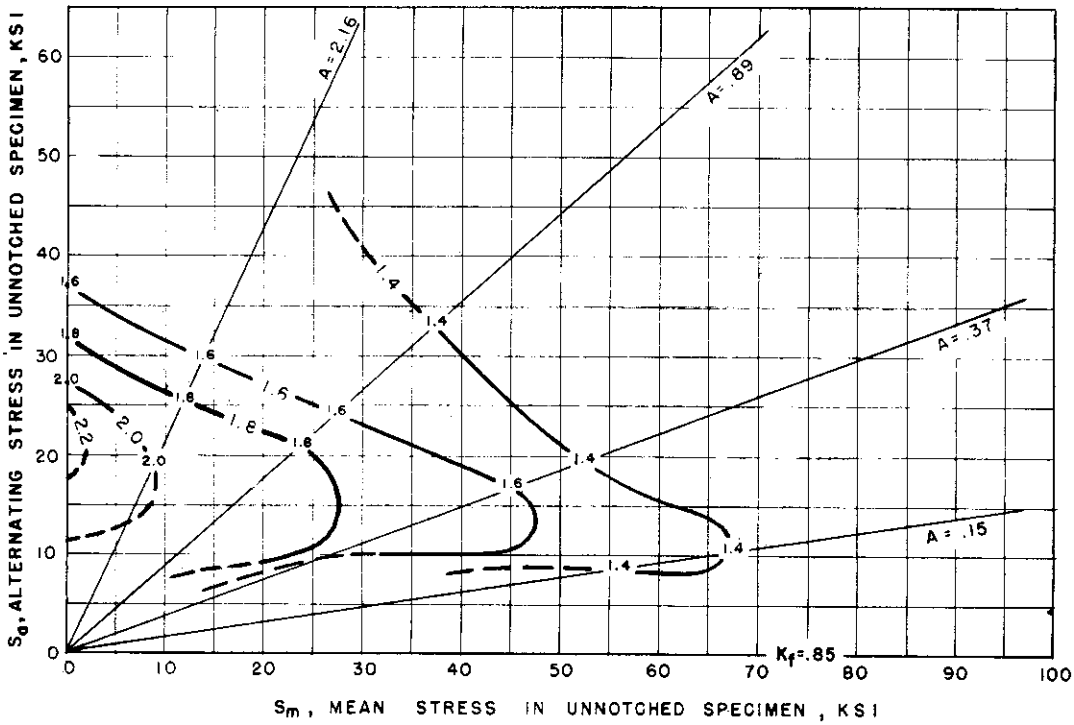

FIG. 43. FATIGUE STRENGTH - REDUCTION "CONTOUR" CURVES FOR K_t = 2.4 SPECIMENS OF ALUMINUM ALLOY 24S-T4 SHOWING K_f AS A FUNCTION OF S_a AND S_m OF THE UNNOTCHED SPECIMEN.

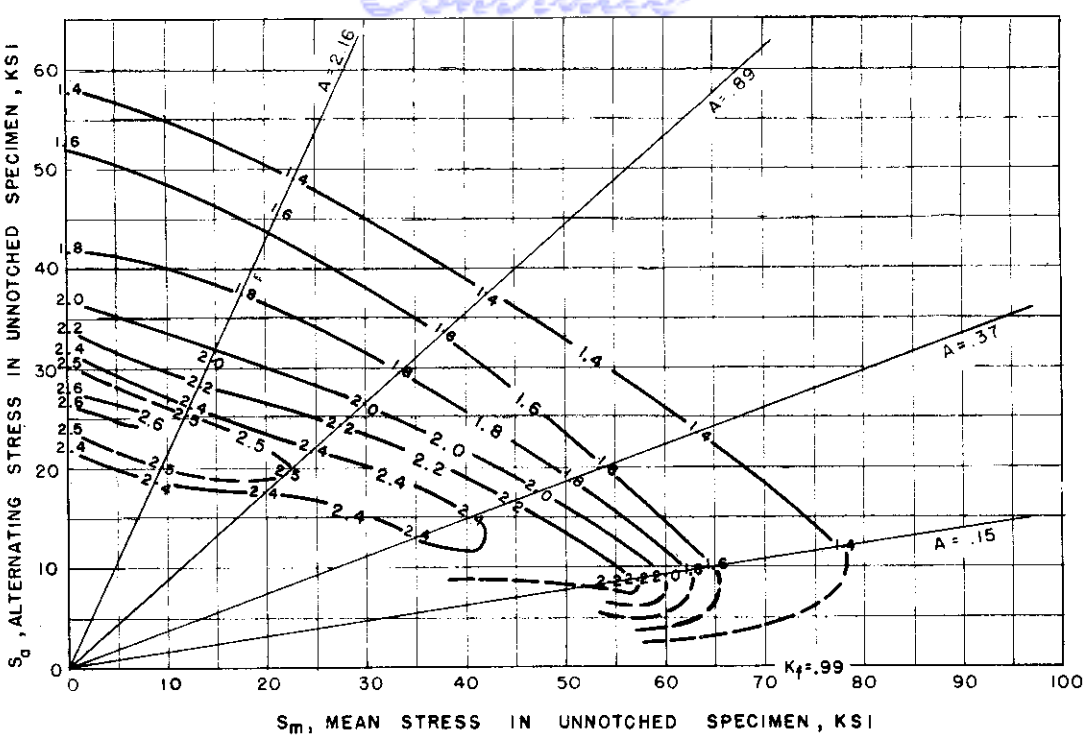

FIG. 44. FATIGUE STRENGTH - REDUCTION "CONTOUR" CURVES FOR K_t = 3.4 SPECIMENS OF ALUMINUM ALLOY 24S—T4 SHOWING K_f AS A FUNCTION OF S_a AND S_m OF THE UNNOTCHED SPECIMEN.

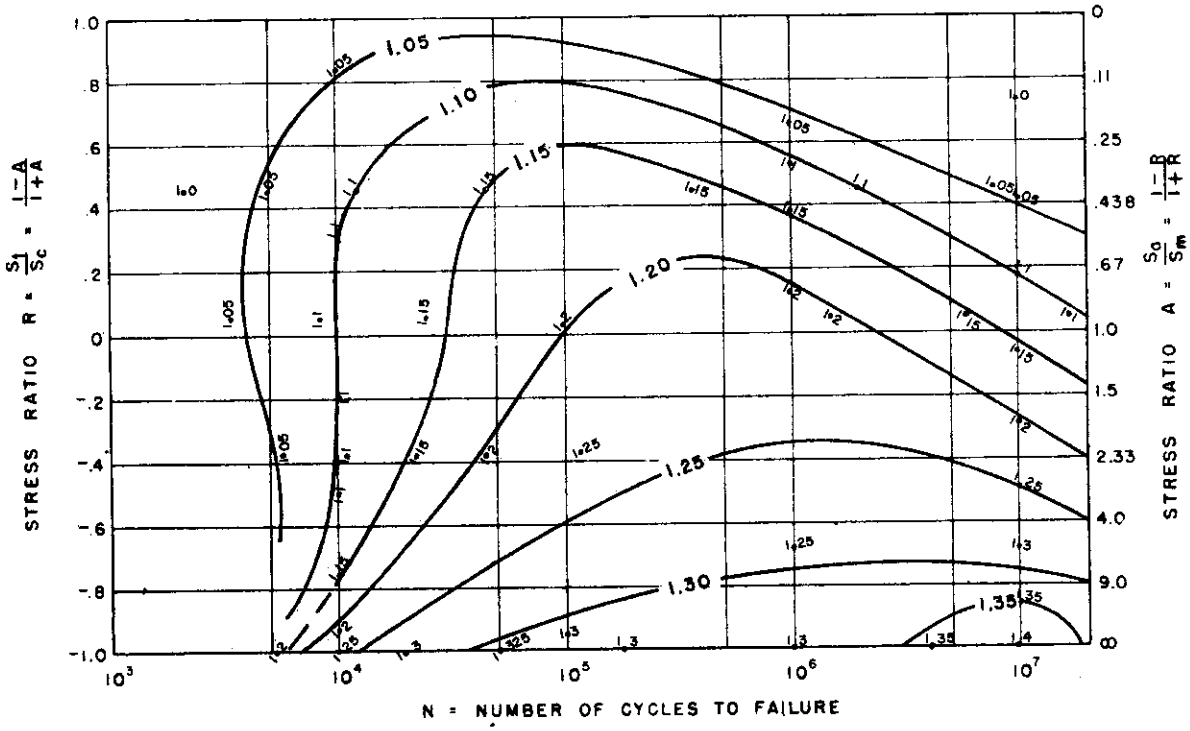

FIG. 45. FATIGUE STRENGTH - REDUCTION "CONTOUR" CURVES FOR K_t = 1.6 SPECIMENS OF ALUMINUM ALLOY 24S-T4 SHOWING K_f AS A FUNCTION OF N AND STRESS RATIO R

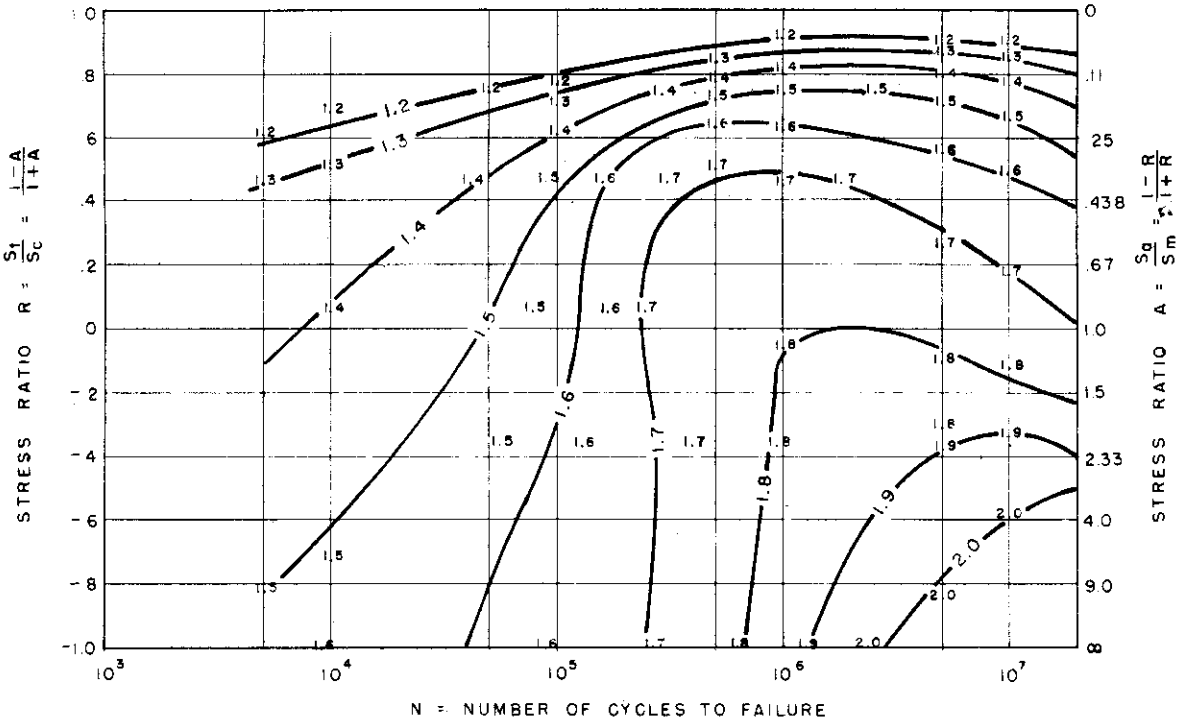

FIG. 46. FATIGUE STRENGTH REDUCTION "CONTOUR" CURVES FOR K_t = 2.4 SPECIMENS OF ALUMINUM ALLOY 24S-T4 SHOWING K_f AS A FUNCTION OF N AND STRESS RATIO R

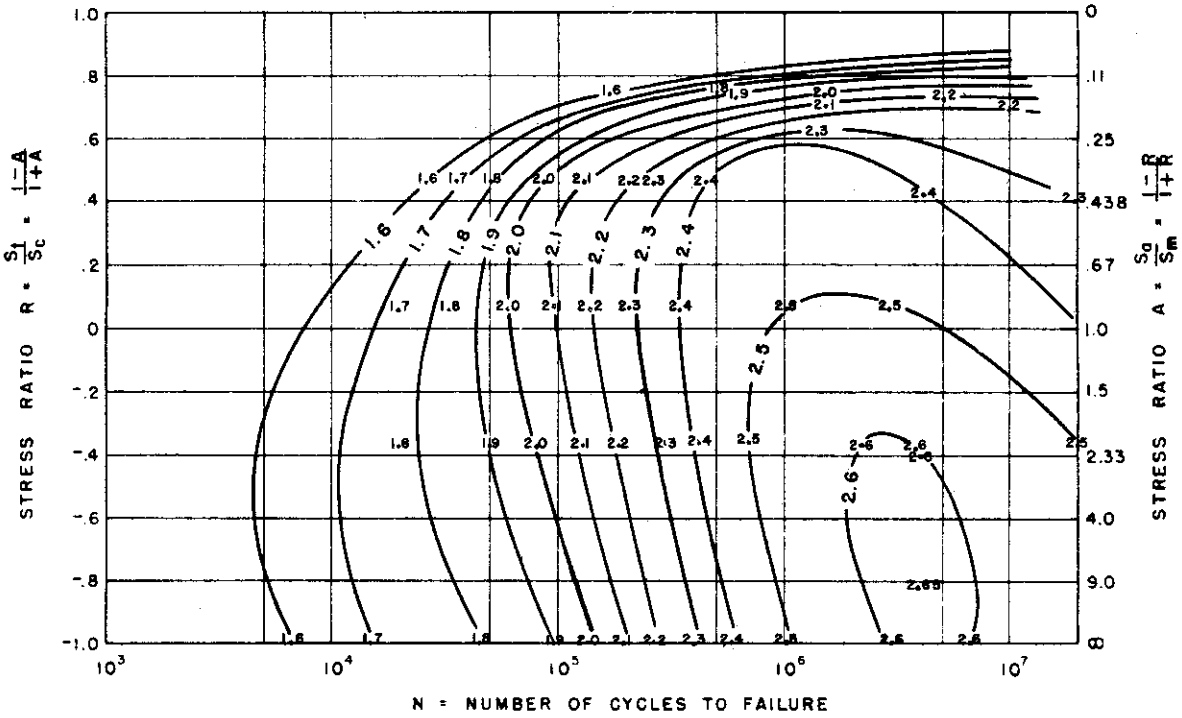

FIG. 47. FATIGUE STRENGTH - REDUCTION "CONTOUR" CURVES FOR K_t = 3.4 SPECIMENS OF ALUMINUM ALLOY 24S-T4 SHOWING K_f AS A FUNCTION OF N AND STRESS RATIO R

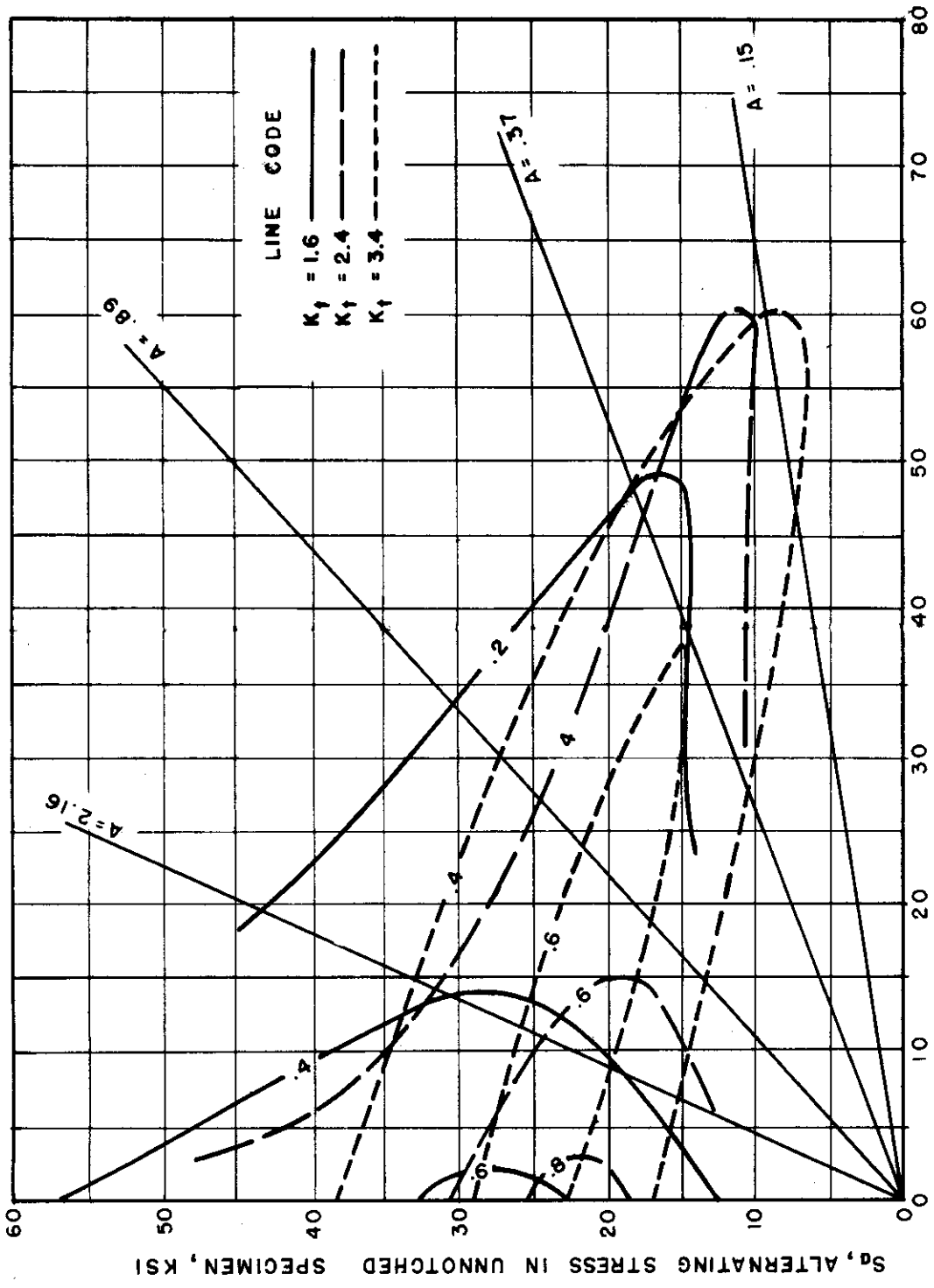

FIG. 48 NOTCH SENSITIVITY INDEX CURVES FOR K_t = 1.6, 2.4, AND 3.4 SPECIMENS OF ALUMINUM ALLOY 24S—T4 SHOWING q AS A FUNCTION OF S_a AND S_m OF THE UNNOTCHED SPECIMEN

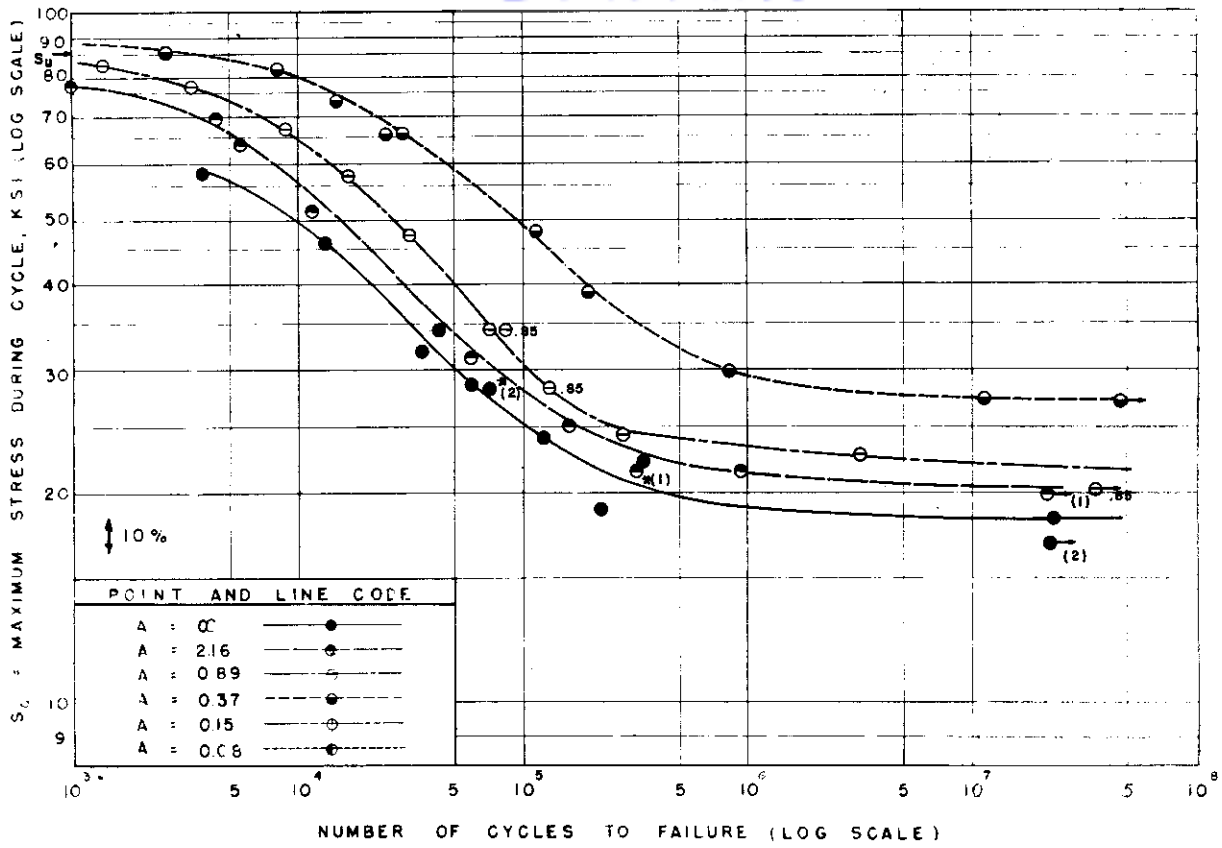

FIG.49. S-N FATIGUE DIAGRAMS AT VARIOUS STRESS RATIOS FOR $K_t = 1.0$ SPECIMENS OF ALUMINUM ALLOY 75S-T6.

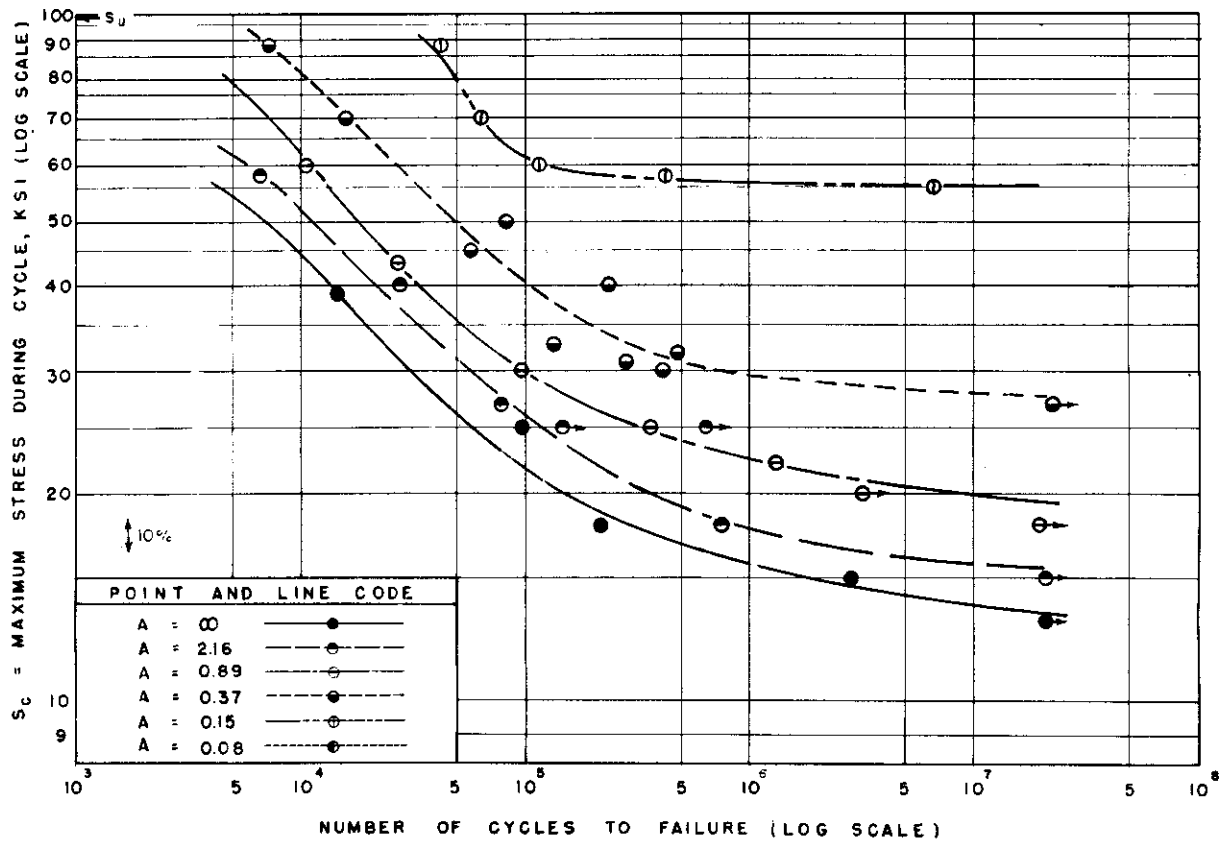

FIG.50. S-N FATIGUE DIAGRAMS AT VARIOUS STRESS RATIOS FOR $K_t = 1.6$ SPECIMENS OF ALUMINUM ALLOY 75S-T6

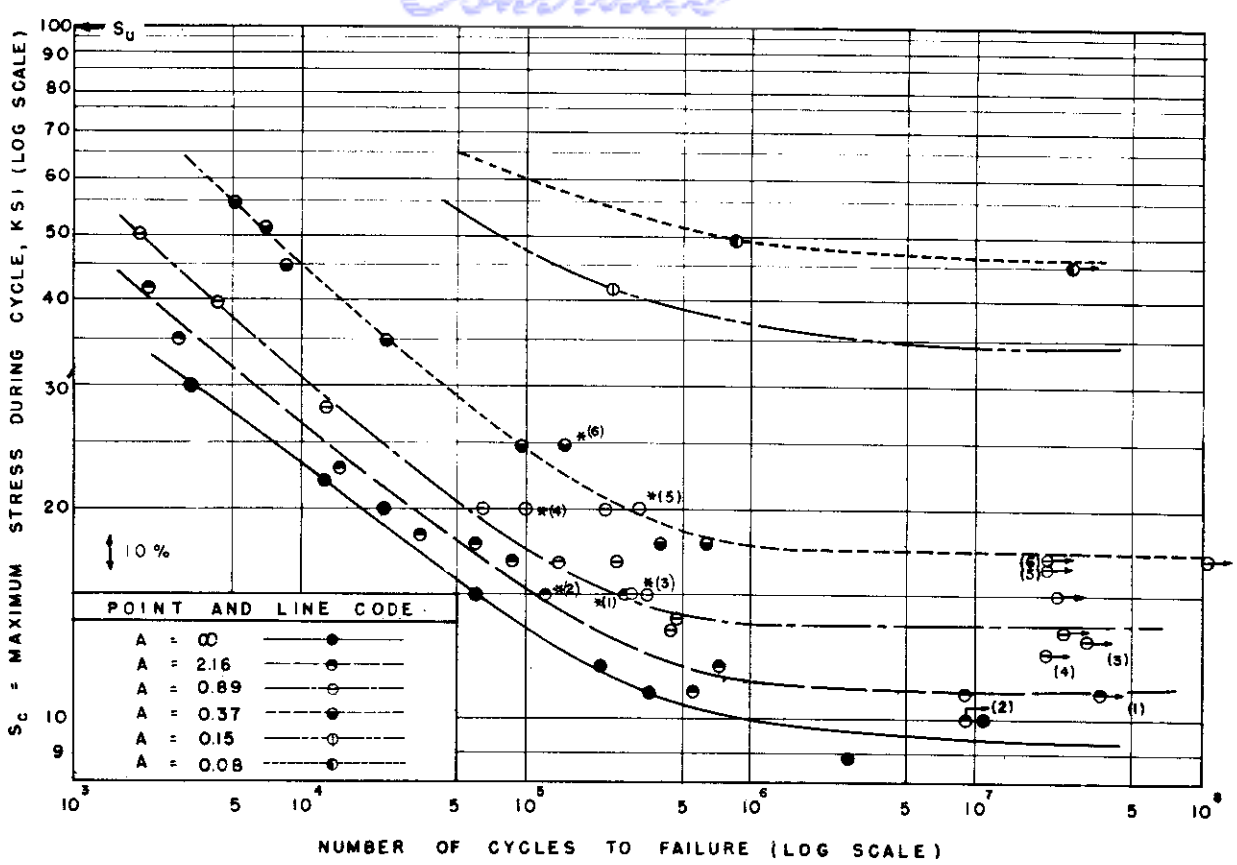

FIG.51 .S-N FATIGUE DIAGRAMS AT VARIOUS STRESS RATIOS FOR K_f= 3.4 SPECIMENS OF ALUMINUM ALLOY 75S-T6.

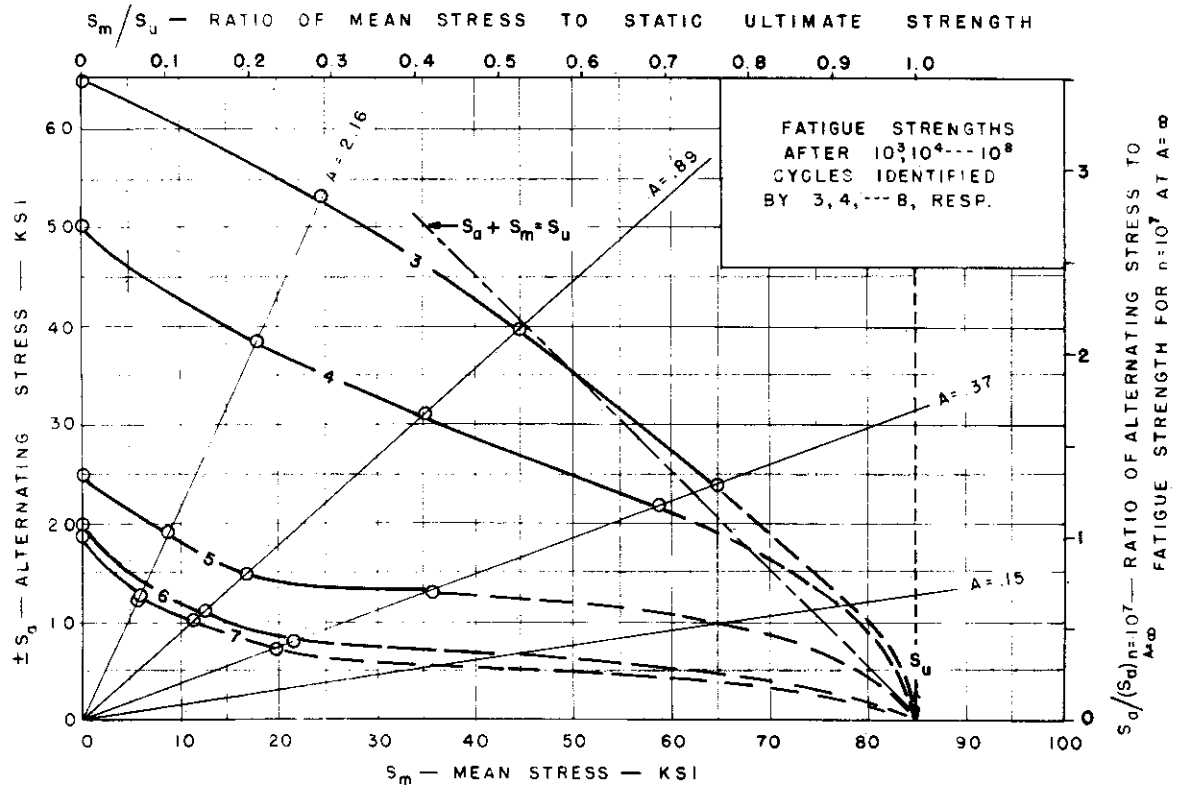

FIG.52. — STRESS RANGE FATIGUE DIAGRAM FOR K_f=1.0 SPECIMENS OF ALUMINUM ALLOY 75 S-T6.

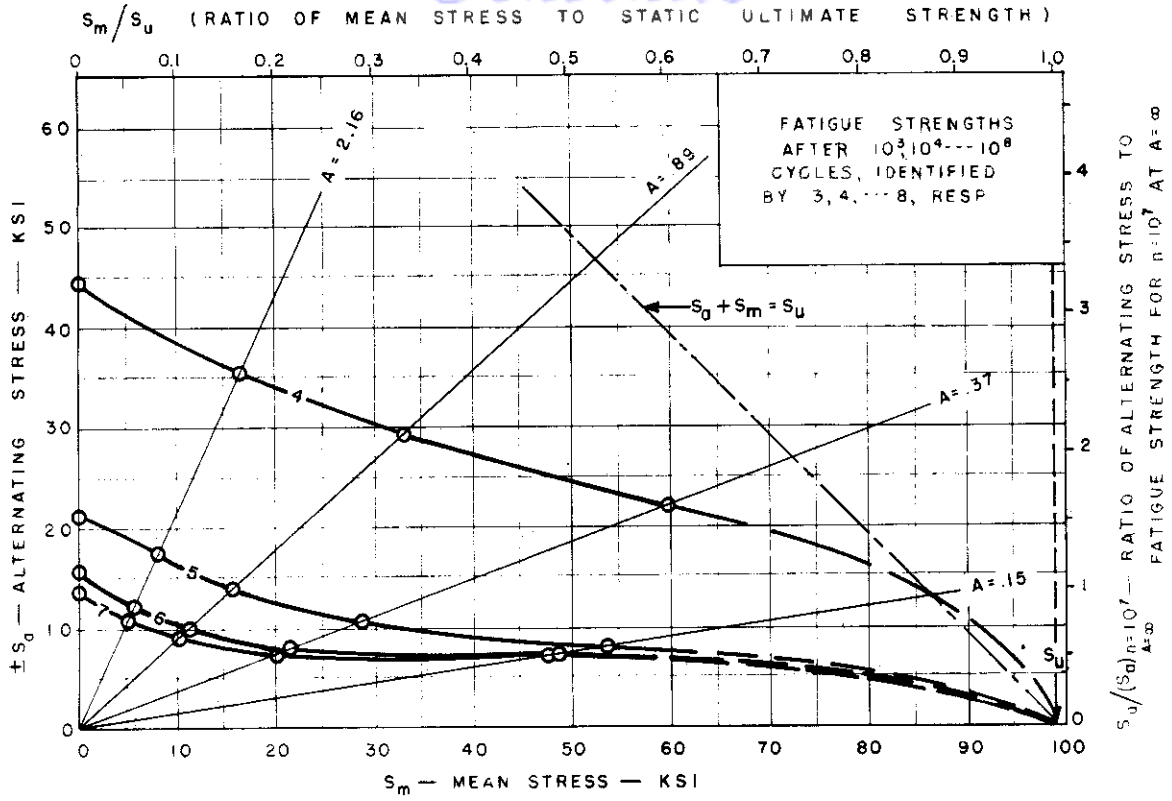

FIG. 53. — STRESS RANGE FATIGUE DIAGRAM FOR $K_t = 1.6$ SPECIMENS OF ALUMINUM ALLOY 75S-T6

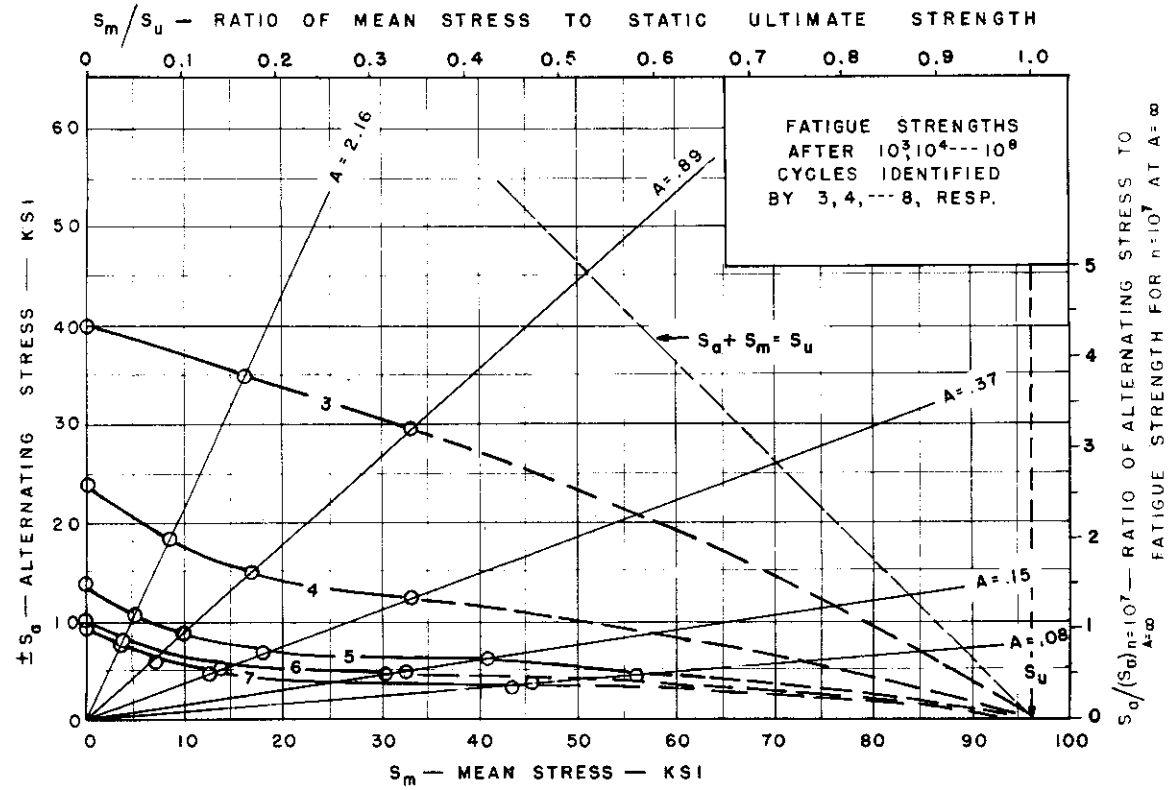

FIG. 54. — STRESS RANGE FATIGUE DIAGRAM FOR $K_t = 3.4$ SPECIMENS OF ALUMINUM ALLOY 75S-T6.

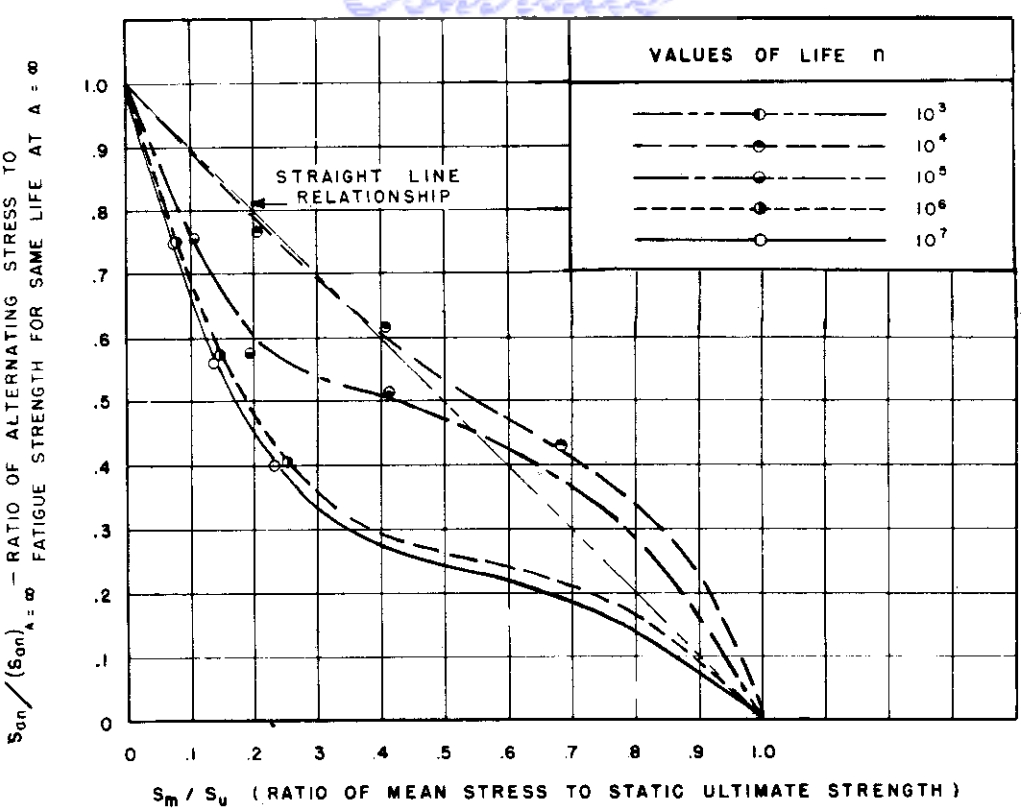

FIG.55 STRESS RANGE CURVES FOR K_t=1.0 SPECIMENS OF 75S-T6 ALUMINUM ALLOY USING DIMENSIONLESS RATIOS

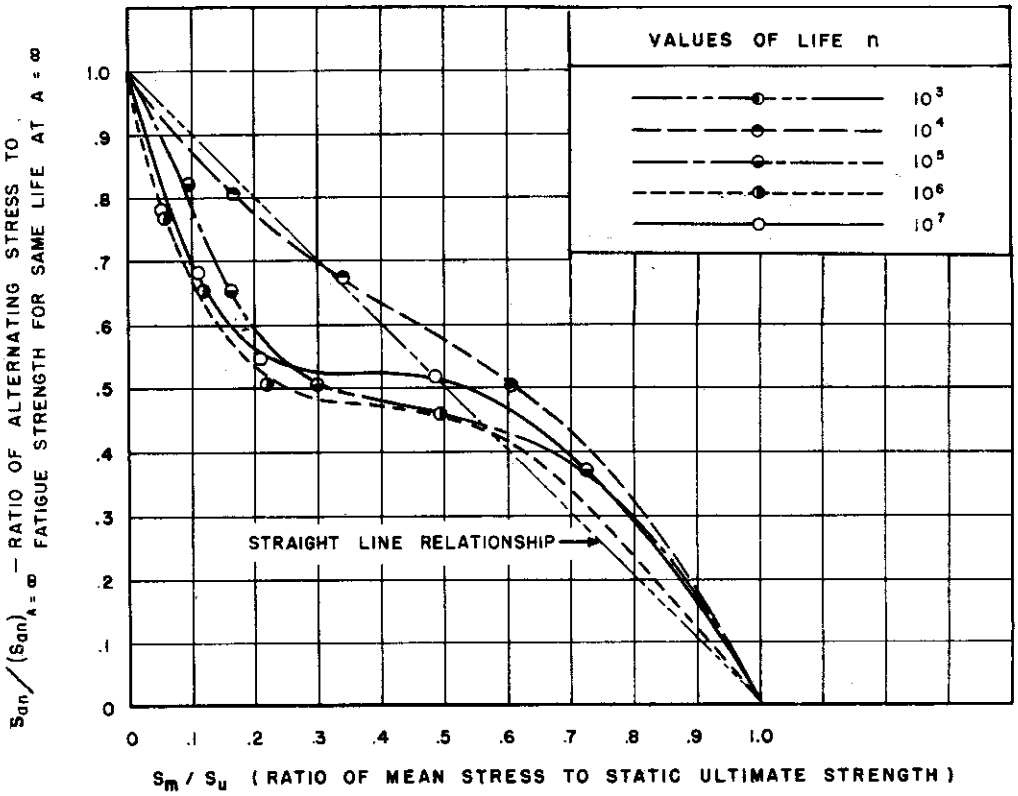

FIG.56. STRESS RANGE CURVES FOR K = 1.6 SPECIMENS OF 75S-T6 ALUMINUM ALLOY USING DIMENSIONLESS RATIOS

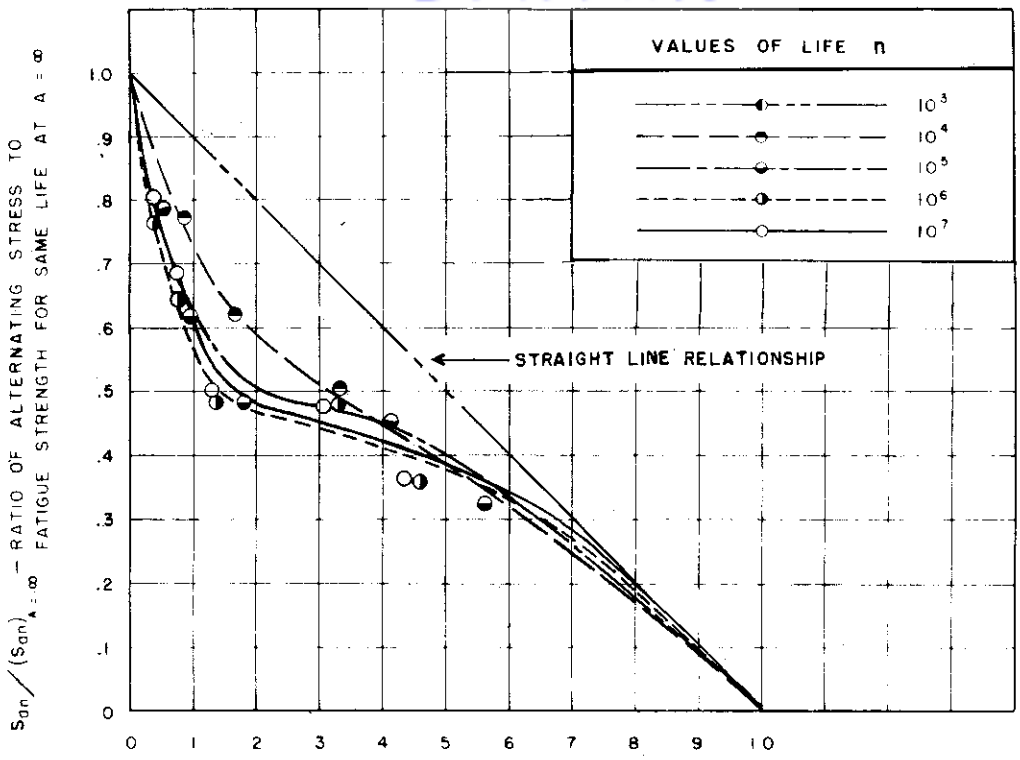

FIG 57. STRESS RANGE CURVES FOR $K_t = 3.4$ SPECIMENS OF 75S-T6 ALUMINUM ALLOY USING DIMENSIONLESS RATIOS

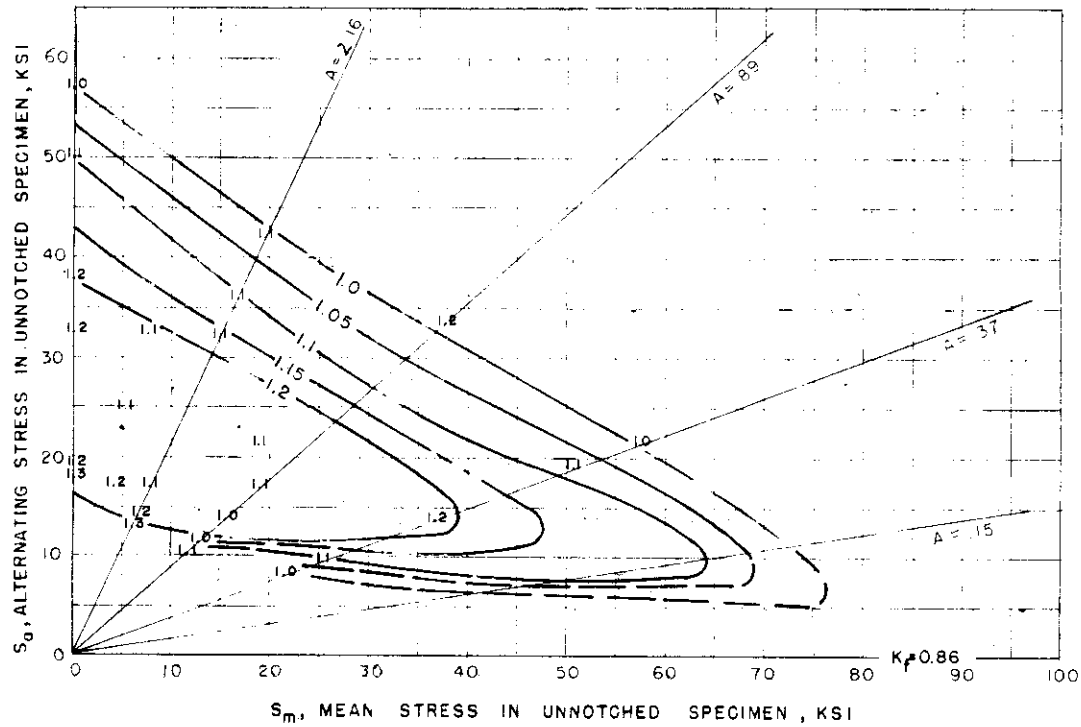

FIG. 58. FATIGUE STRENGTH - REDUCTION "CONTOUR" CURVES FOR $K_t = 1.6$ SPECIMENS OF ALUMINUM ALLOY 75S-T6 SHOWING K_f AS A FUNCTION OF S_a AND S_m OF THE UNNOTCHED SPECIMEN.

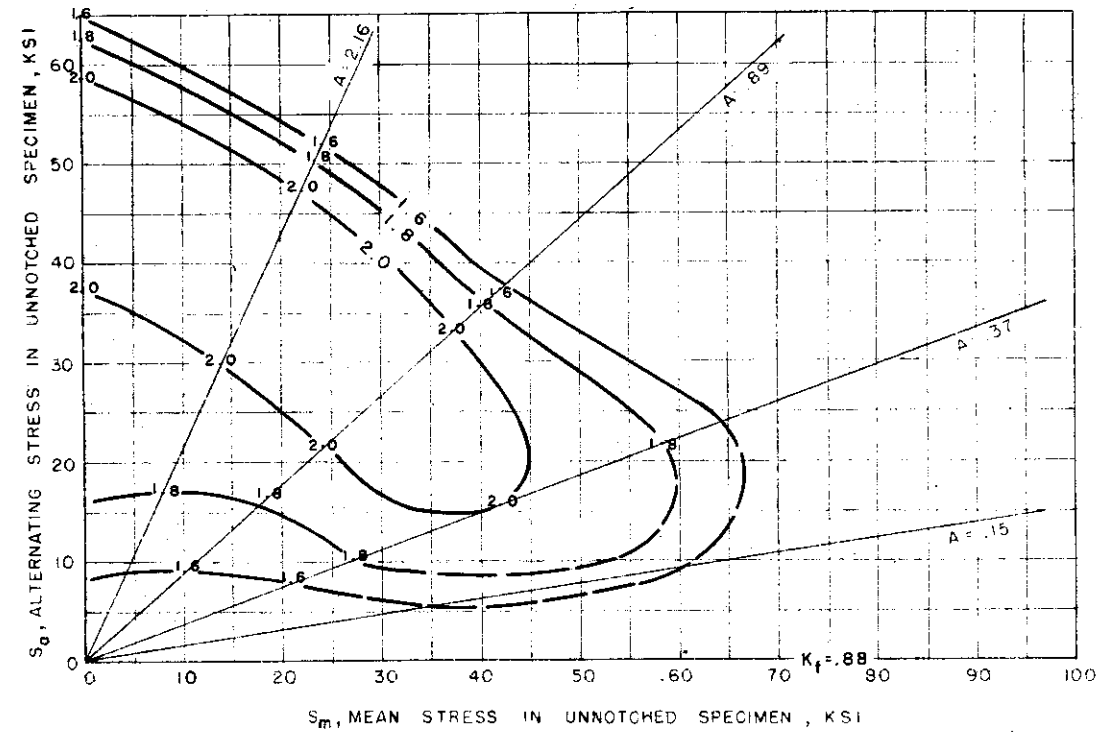

FIG. 59. FATIGUE STRENGTH - REDUCTION "CONTOUR" CURVES FOR $K_t = 3.4$ SPECIMENS OF ALUMINUM ALLOY 75S—T6 SHOWING K_f AS A FUNCTION OF S_a AND S_m OF THE UNNOTCHED SPECIMEN.

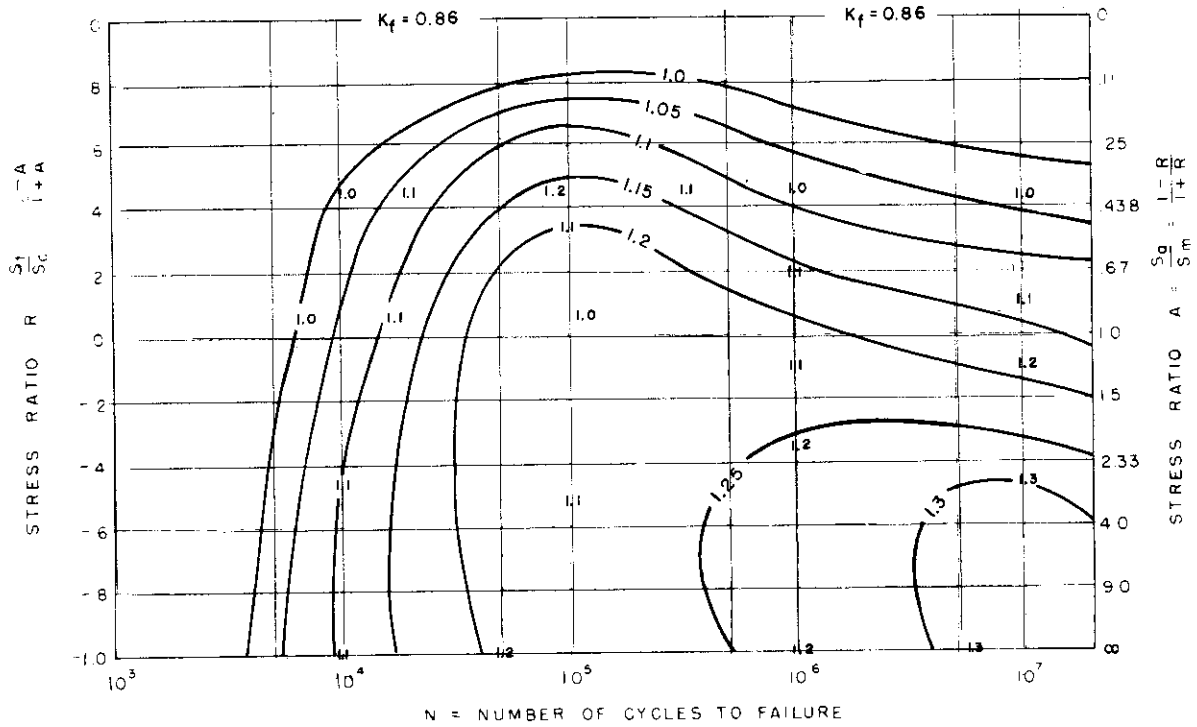

FIG 60. FATIGUE STRENGTH REDUCTION "CONTOUR" CURVES FOR $K_t = 1.6$ SPECIMENS OF ALUMINUM ALLOY 75S-T6 SHOWING K_f AS A FUNCTION OF N AND STRESS RATIO R

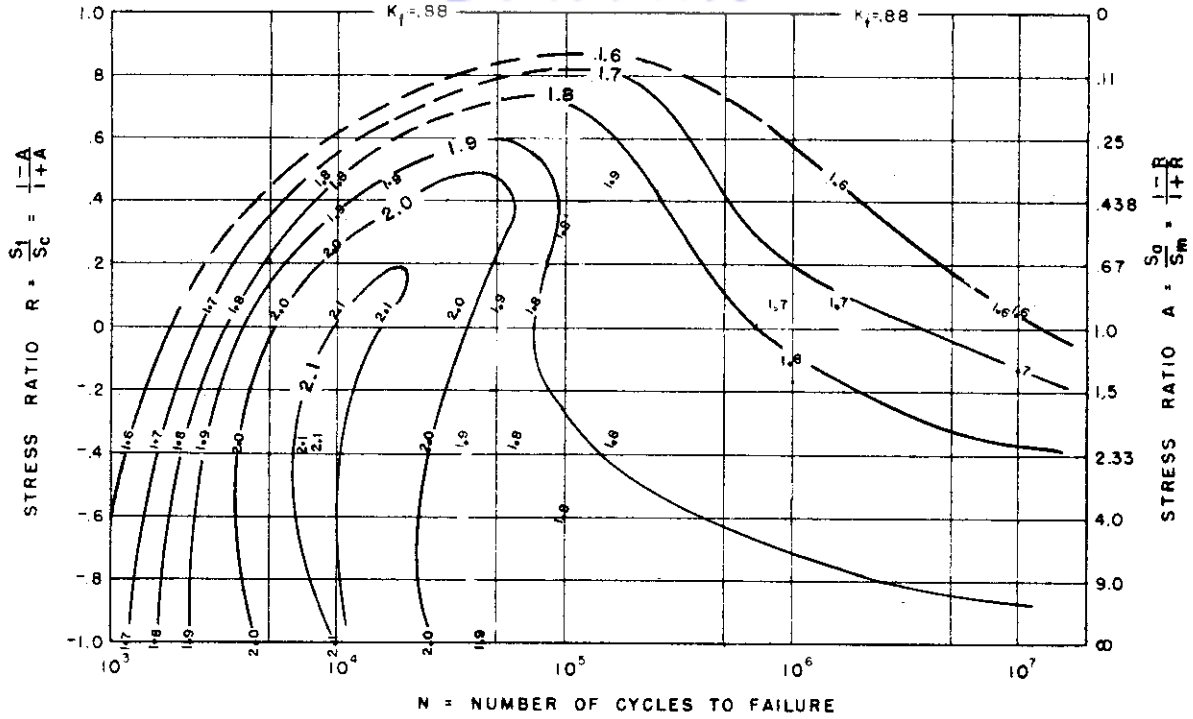

FIG. 61. FATIGUE STRENGTH - REDUCTION "CONTOUR" CURVES FOR K_t = 3.4 SPECIMENS OF ALUMINUM ALLOY 75S-T6 SHOWING K_f AS A FUNCTION OF N AND STRESS RATIO R

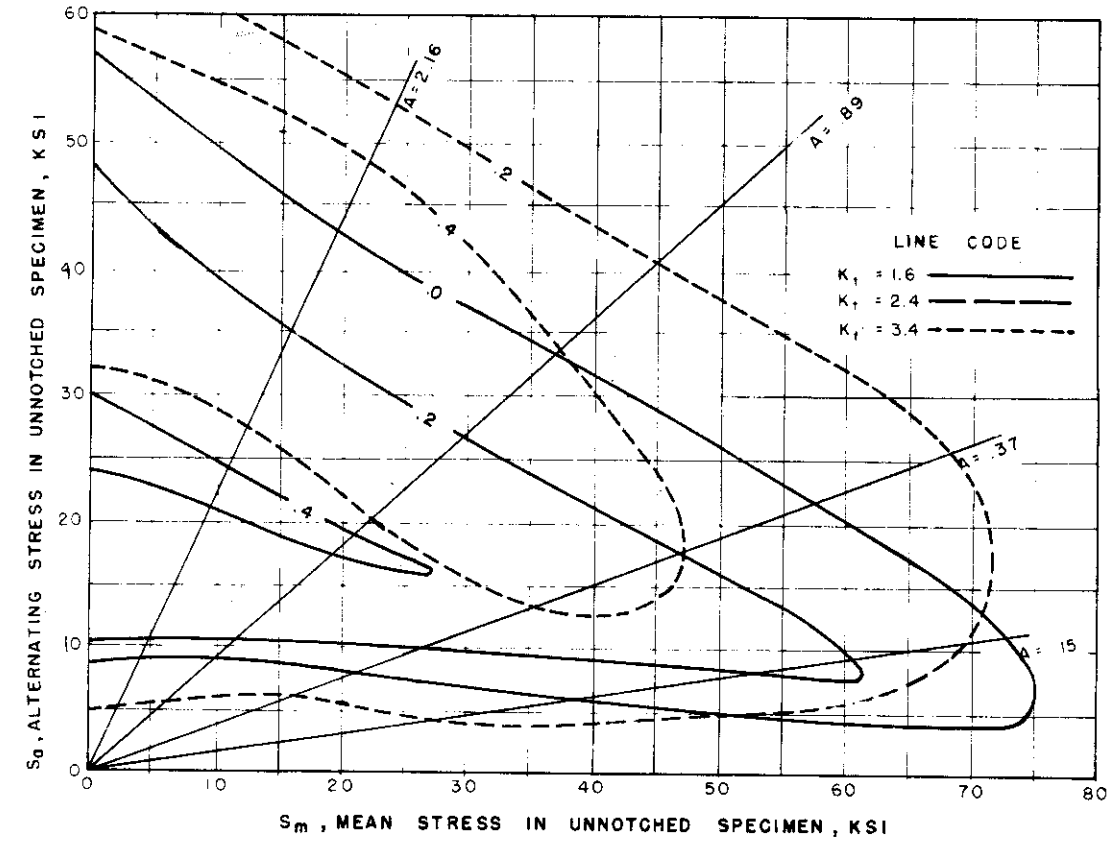

FIG. 62. NOTCH SENSITIVITY INDEX CURVES FOR K_t = 1.6, AND 3.4 SPECIMENS OF ALUMINUM ALLOY 75S-T6 SHOWING q AS A FUNCTION OF S_a AND S_m OF THE UNNOTCHED SPECIMEN

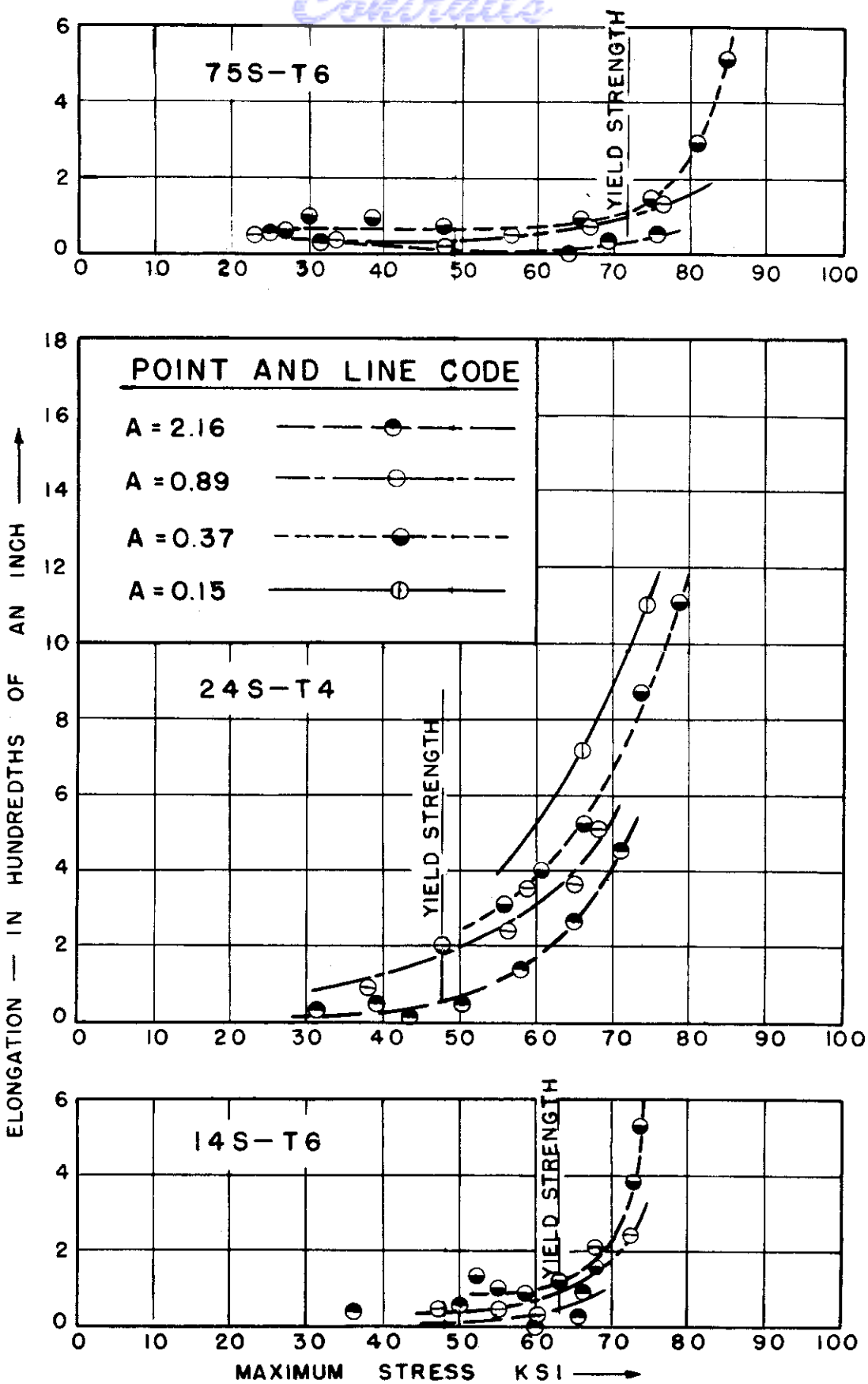

FIG.63. ELONGATION IN FATIGUE SPECIMENS AT VARIOUS STRESSES AND STRESS RATIOS.

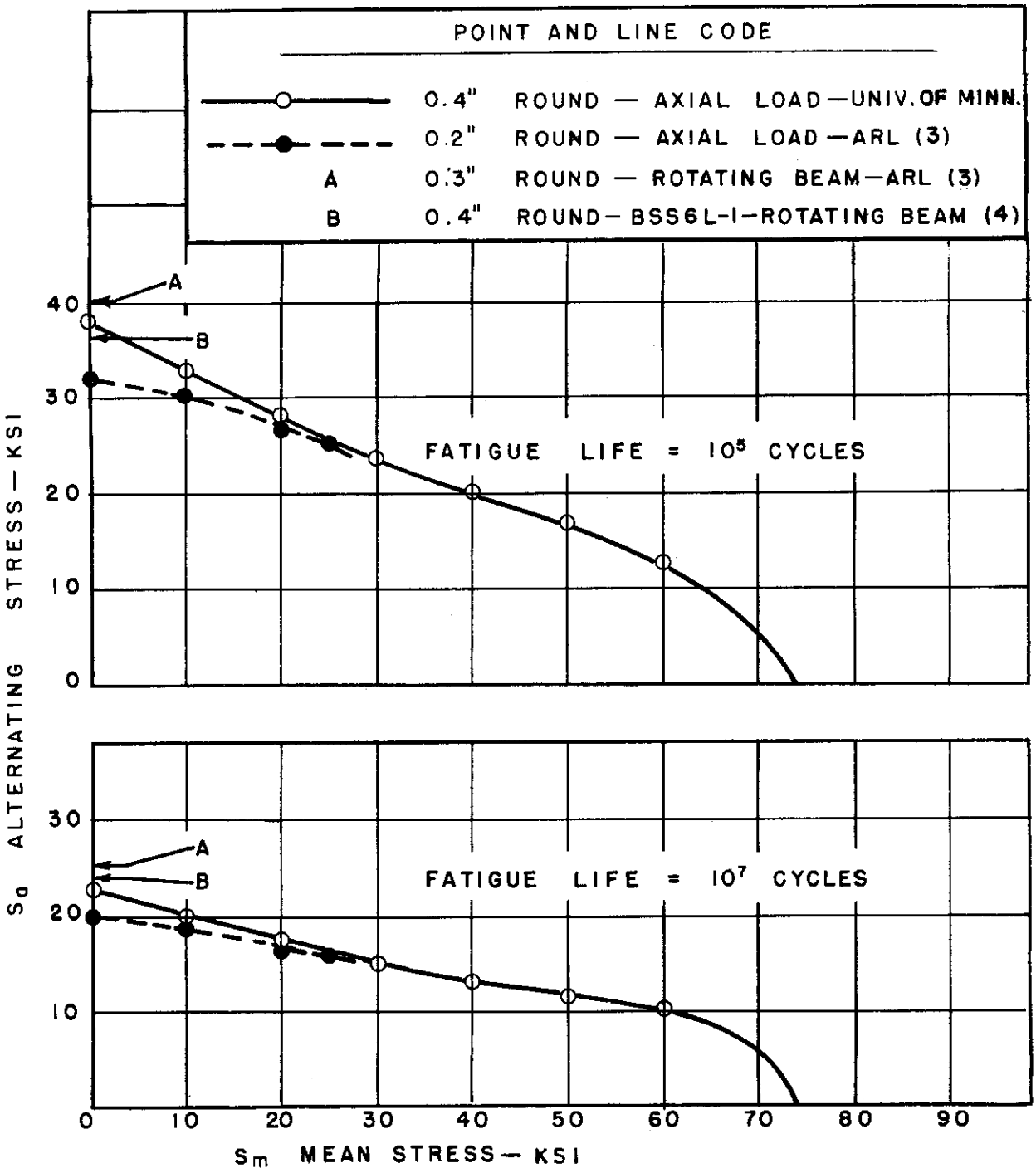

FIG. 64. COMPARISONS FROM VARIOUS SOURCES OF FATIGUE STRENGTHS OF UNNOTCHED SPECIMENS OF ALUMINUM ALLOY 14S—T6.

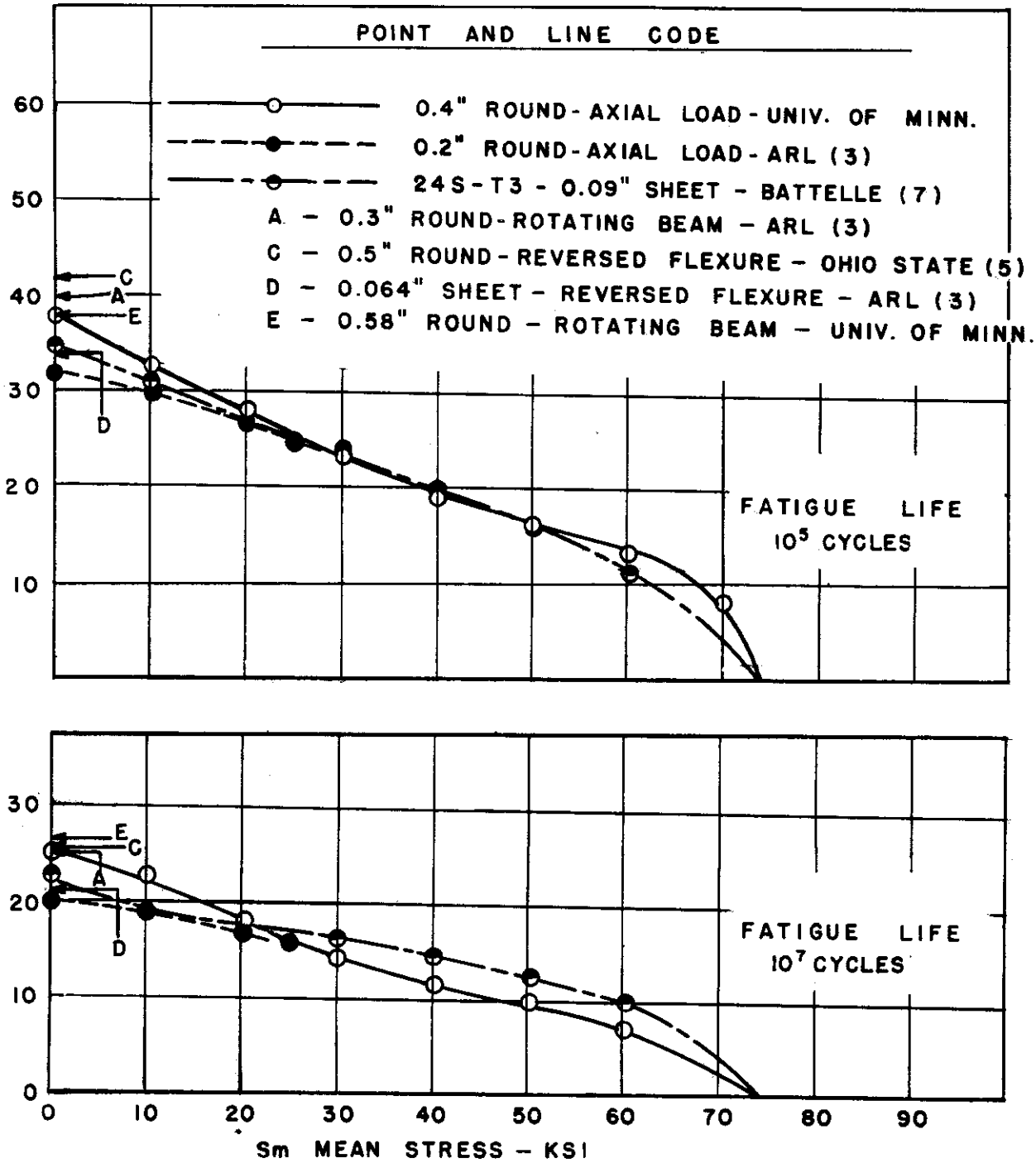

FIG. 65. COMPARISONS FROM VARIOUS SOURCES OF FATIGUE STRENGTHS OF UNNOTCHED SPECIMENS OF 24S-T4 ALUMINUM ALLOY

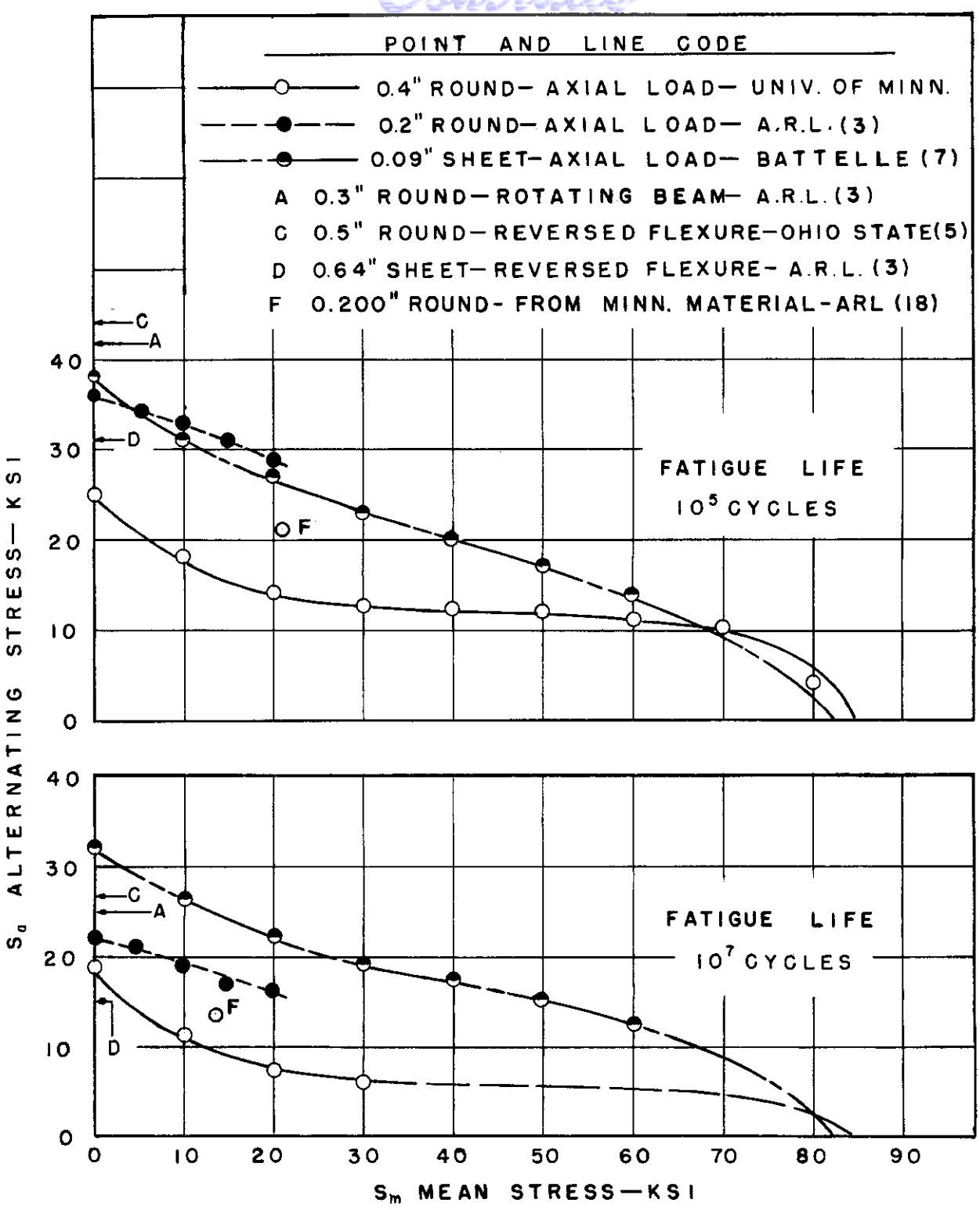

FIG. 66. COMPARISONS FROM VARIOUS SOURCES OF FATIGUE STRENGTHS OF UNNOTCHED SPECIMENS OF 75S-T6 ALUMINUM ALLOY.

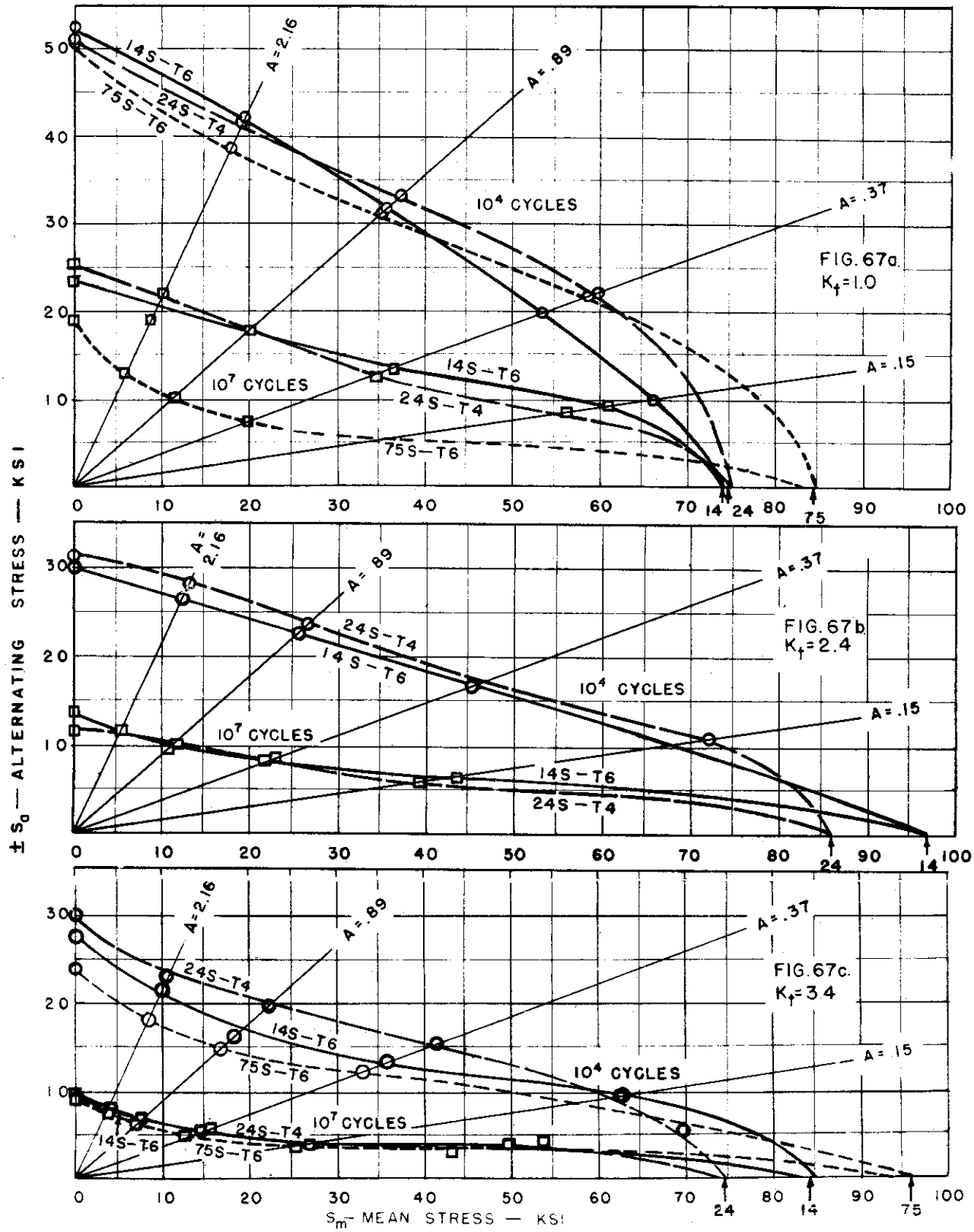

FIG. 67 — STRESS RANGE DIAGRAMS SHOWING COMPARATIVE FATIGUE STRENGTHS OF ALUMINUM ALLOYS 14S-T6, 24S-T4, AND 75S-T6

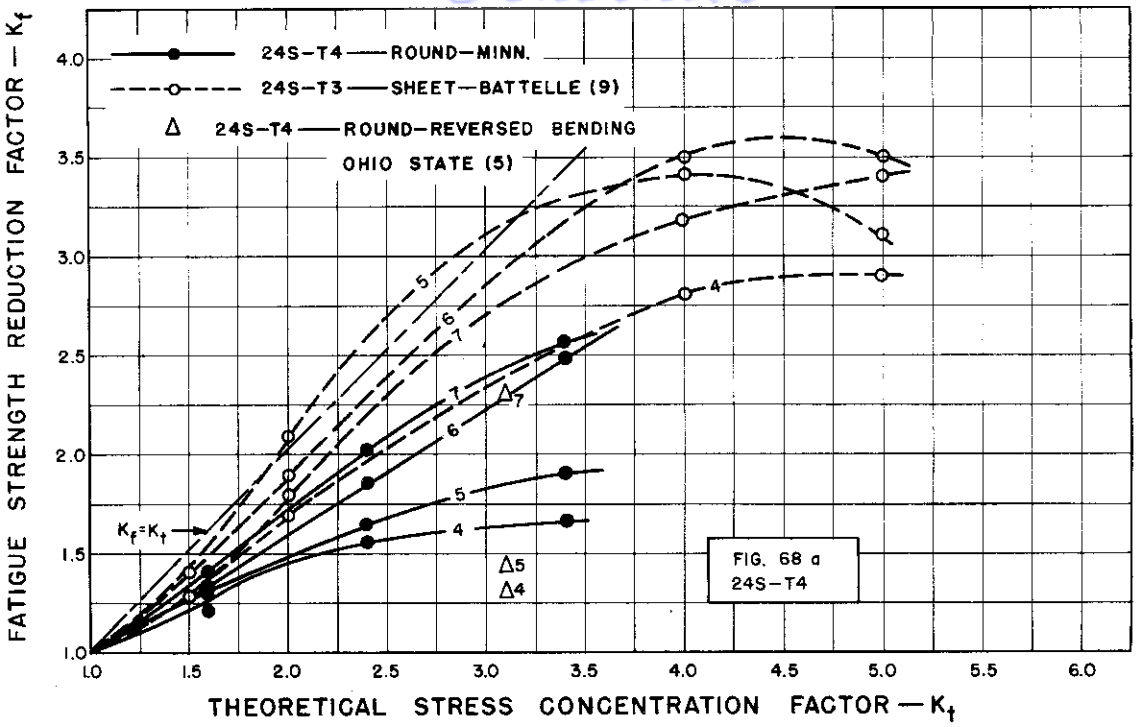

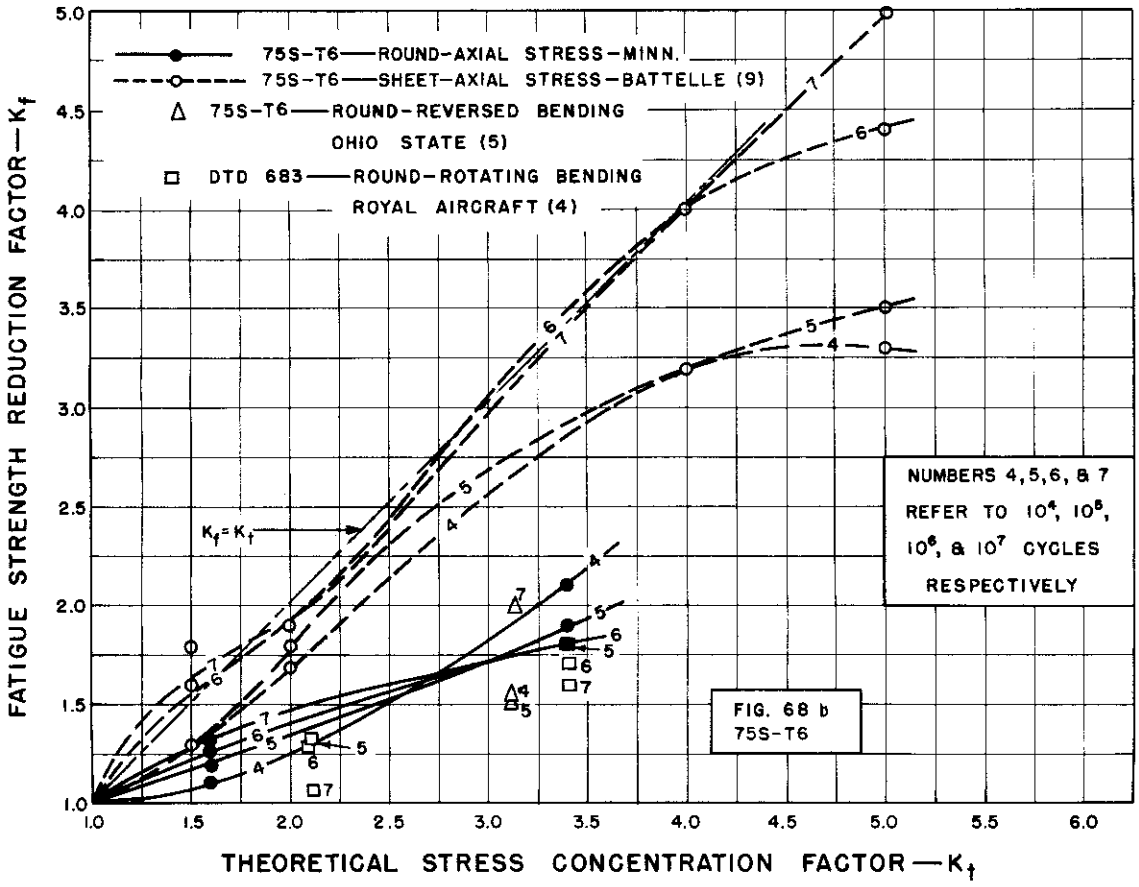

FIG. 68 COMPARISON CURVES OF K_f FOR 24S-T4 AND 75S-T6 FOR VARIOUS NUMBERS OF CYCLES OF REVERSED STRESS.